Liquid phase characterization of multicomponent gas hydrate systems

Francis Lang
Department of Chemical Engineering
McGill University, Montreal

May 2016

A thesis submitted to McGill in partial fulfillment of the requirements of the Degree of Doctor in Philosophy

Abstract

This thesis characterizes the liquid phase of several multicomponent gas hydrate systems during growth and equilibrium through mole fraction measurements. To demonstrate the importance of the liquid phase in gas hydrate equilibrium modeling, both liquid and gas phases of the CO_2+CH_4+H_2O system were modeled using various equation of states. It was found that the mole fraction where both liquid and gas fugacities met at equilibrium is highly dependent on the liquid phase when compared to the gas phase. Furthermore, liquid and gas phase compositions at three-phase equilibrium (hydrate-liquid-vapor) were generated using modified interaction parameters. If interaction parameters were optimized using only liquid mole fraction data, both gas and liquid equilibrium compositions were successfully generated. Conversely, both phases could not be adequately modeled when interaction parameters were optimized using only vapor data; successful results were limited to the vapor phase. These findings are likely due to non-ideal effects present in the liquid phase but absent in the gas phase.

Solubility isotherm trends for the N_2+CO_2+H_2O and CH_4+C_2H_6+H_2O systems were experimentally obtained. As simple nitrogen systems favor structure II and simple carbon dioxide systems structure I, their combination yields a system where a structure change transition occurs depending on the relative amount of gas. In the case of the methane and ethane mixture, both individual simple systems favor structure I while their mixture can form structure II under certain conditions. This phenomenon is the result of structure II offering a specific ratio of large and small cavities that is only favorable for specific ranges of methane and ethane concentrations. The solubility trends obtained of both multicomponent systems were found to shift where a structure change is reportedly occurring; a novel find. This can be explained by the fact that guest occupancies and hence solid phase mole fractions differ for each structure.

Replicates obtained near the conditions where a structure change is reportedly occurring were found to vary. This fluctuation was the consequence of both structures being present in various ratios during sampling, even if only one structure is thermodynamically favored.

Liquid and gas mole fractions were experimentally acquired during growth for the CH_4+CO_2+H_2O system. Constant gas phase compositions along with controlled pressure and temperature enabled a consistent differential pressure between operating conditions and the equilibrium plane during kinetic experiments. Similar to results obtained in literature for simple hydrate systems, both methane and carbon dioxide liquid mole fractions were found independent of time. Overall growth rates were obtained and had a linear relationship with time. Liquid mole fractions obtained during induction revealed that methane is consumed significantly more than carbon dioxide during the early stages of growth.

Résumé

Cette thèse a pour but d'étudier la phase liquide de systèmes d'hydrates gazeux comprenant plusieurs composants. À travers des mesures de fractions molaires, ces systèmes ont été étudiés sous équilibre thermodynamique ainsi qu'en période de croissance cristalline. L'importance des fractions liquides molaires par rapport aux modèles d'équilibre d'hydrates gazeux a été démontrée alors que les phases liquide et gazeuse du système CO_2+CH_4+H_2O ont été modélisées utilisant plusieurs équations d'états. Il a été démontré que les compositions molaires où les fugacités de la phase liquide et gazeuse se rencontrent, sont beaucoup plus dépendantes de la phase liquide que gazeuse. De plus, les compositions liquides et gazeuses d'équilibre à trois phases (hydrate-liquide-vapeur) ont été générées utilisant des paramètres d'interaction modifiés. Lorsque ces paramètres ont été optimisés utilisant uniquement des fractions molaires liquides, les deux phases (liquide et gazeuse) ont été modélisées avec succès. Inversement, l'optimisation des paramètres basée à partir de données molaires gazeuses n'a pu permettre une modélisation adéquate de la phase liquide. Ces résultats sont probablement dus aux effets non-idéaux présents dans la phase liquide, mais absents dans la phase gazeuse.

Les tendances d'isothermes de solubilité ont été obtenues pour les systèmes N_2+CO_2+H_2O et CH_4+C_2H_6+H_2O. Étant donné que le nitrogène favorise les hydrates de structure II et le dioxyde de carbone, la structure I, leur combinaison donne lieu à un système où un changement ou une transition de structure se manifeste dépendamment de la quantité relative des deux gaz. Dans le cas d'une mixture de méthane et d'éthane, tous deux favorisent les hydrates de structure I. Bien que leur combinaison favorise naturellement la structure I, elle peut aussi former la structure II sous certaines conditions. Ce phénomène est le résultat du fait que la structure II offre un ratio spécifique de grandes et de petites cavités qui est seulement favorable pour certaines concentrations d'éthane

et de méthane. Les tendances d'isothermes de solubilités obtenues pour chacun de ces systèmes à composants multiples ont été affectées par le changement de structure; une trouvaille novatrice. Cet effet peut être expliqué par le fait que chaque structure cristalline possède un différent taux d'occupation des cavités ce qui modifie les fractions molaires d'équilibre de toutes les phases. De leur côté, les répliques d'échantillons obtenues près de conditions où un changement de structure est reporté ont varié davantage. Cela est dû au divers ratio des structures, I et II, présents durant l'échantillonnage même si seulement une d'entre elles est thermodynamiquement favorisée.

Les fractions molaires liquides et gazeuses ont été déterminées expérimentalement durant la croissance cristalline du système CH_4+CO_2+H_2O. Une fraction molaire gazeuse constante ainsi qu'un contrôle de la pression et de la température ont ensemble permis le maintien d'un différentiel de pression constant entre les conditions d'opération et le plan d'équilibre. Tel que reporté en littérature pour des systèmes d'hydrates simples, il a été observé que les fractions molaires liquides de méthane et de dioxyde de carbone sont indépendantes du temps. Les taux de croissance obtenus ont démontré une relation linéaire avec le temps. Quant aux fractions molaires liquides obtenues durant la période d'induction, elles ont révélé une consommation de méthane beaucoup plus élevée que celle du dioxyde de carbone, et ce, durant les premiers stages de croissance cristalline.

Acknowledgments

I would like to thank first my supervisor, Dr. Phillip Servio, for believing in me and giving me a chance. My experience at McGill was truly special and I have only him to thank for welcoming me into his research group. He was and will always be more than a supervisor. His support, trust and humor will always be fondly remembered.

This journey would not have been the same without the other graduate students in the group. Every member contributed in making this a memorable degree. I would like to especially thank Jason and my officemate James. I consider myself very lucky to have shared with them the last four years. It just would not have been the same without the two of you. I would also like to thank Marina for her constant presence around the office.

This thesis would have been impossible without the technical staff at McGill. Their knowledge and experience was invaluable. I cannot count the number of times I had to rely on their technical expertise. For always being there and ready to help, I want to especially thank Frank Caporuscio and Andrew Golsztajn.

J'aimerais finalement remercier mes parents, François et Sylvie, de m'avoir toujours soutenu peu importe mes choix. Votre confiance inébranlable en moi sera quelque chose que je n'oublierai jamais. J'aimerais aussi remercier les autres membres de la gang, soit mon frère Alexandre et mes sœurs Valérie et Véronique, de faire partie de ma vie.

Contents

List of Figures

List of Tables

Contribution of Authors

The following thesis is a manuscript-based document containing three-peer reviewed articles published, as well as one article to be submitted. The author of this dissertation is the sole first author of all articles except one where the first authorship is shared. The author was responsible for the experimental work, data analysis and writing of all articles except one where, as previously mentioned, these duties where shared.

1. Lang, F. & Servio, P., *Liquid mole fractions during induction and growth for the CH_4+CO_2+H_2O system*, to be submitted

2. Lang, F. & Servio, P., *Solubility measurements for the CH_4+C_2H_6+H_2O system under hydrate-liquid-vapor equilibrium*, Journal of Natural Gas Science and Engineering, 26, 130-134, 2015

3. Lang, F. & Servio, P., *Solubility measurements for the N_2+CO_2+H_2O system under hydrate-liquid-vapor equilibrium*, Journal of Chemical & Engineering Data, 59 (8), 2547-2550, 2014

4. Renault-Crispo, J.-S.*, Lang, F.* & Servio P., *The importance of liquid phase compositions in gas hydrate modeling: Carbon dioxide-methane-water case study*, Journal of Chemical Thermodynamics, 68, 153-160, 2014
   * Co-first authors

Original Contributions

The following list represents original contributions made by this thesis:

- Development of sensitivity analyses on both liquid and gas phases of the $CH_4+CO_2+H_2O$ system through modeling. This demonstrated that experimental solubility data instead of experimental gas mole fractions should be used when evaluating gas hydrate equilibrium model.

- Experimentally obtained nitrogen and carbon dioxide solubility data for the $N_2+CO_2+H_2O$ system under H-Lw-V equilibrium. This is the first work to report experimentally obtained solubility for this binary system at three-phase equilibrium.

- Experimentally obtained methane and ethane solubility data for the $CH_4+C_2H_6+H_2O$ system under H-Lw-V equilibrium. This is the first work to report experimentally obtained solubility for this binary system at three-phase equilibrium.

- Established through two different studies that the type of hydrate structure present impacts solubility trends.

- Experimentally obtained bulk liquid mole fractions of methane and carbon dioxide during the early stages of growth for the $CH_4+CO_2+H_2O$ system. This is the first study to report bulk liquid mole fractions during growth of a binary hydrate system.

- Established that bulk liquid mole fractions for the $CH_4+CO_2+H_2O$ system are mostly independent of time during growth while the molar consumption rate is linear with respect to time.

- Established the preferential consumption of methane during the early stages of growth for the $CH_4+CO_2+H_2O$ system.

Chapter 1

Introduction

Gas hydrates, or clathrates, are crystalline compounds resulting from a phase change. Visually similar to ice, they however require in addition to water, a second component for its formation to be possible. This second component, often referred to as the “guest”, becomes enclosed in three-dimensional cages of water molecules. The size of the guest compared to the cavity is an important parameter determining cage stability. Examples of suitable components include methane, ethane, propane, carbon dioxide, nitrogen, oxygen and volatile liquids such as tetrahydrofuran and neohexane. Due to the fact that guest molecules are compactly ordered in a solid phase, gas hydrates have the ability to store a significant amount of gas. Thermodynamic conditions favoring gas hydrate formation consist of temperatures typically above the freezing point of water and pressures an order of magnitude greater than atmospheric pressure.

These specific combinations of water, suitable guest molecules and appropriate thermodynamic conditions can arise in nature and in man-made environments. The latter is an example where gas hydrate formation is undesirable as they can form and plug natural gas pipelines. Due the potential disastrous outcomes of a clogged hydrocarbon pipeline, these crystal clusters pose a major issue to flow assurance. During the infamous BP oil spill, for instance, a leak containment operation failed due to hydrate formation, resulting in greater environmental and economical impacts. Pipeline additives capable of preventing gas hydrate occurrences and/or growth are thus an important and growing field of hydrate research.

Conversely, these crystalline compounds are also widely regarded as a potential energy resource. Naturally occurring gas hydrate deposits in ocean floors and permafrost regions represent a huge untapped energy reservoir as guests are predominantly methane; originating either from thermogenic or biogenic processes. Recent estimates claim that more carbon-based resources exist as hydrates than all other fossil fuels combined. These evaluations led to significant efforts in academia and industry to render gas hydrate exploitation economically viable. Carbon dioxide sequestration through hydrate technologies serves as a potential but polarizing solution. While exchanging captured anthropogenic carbon dioxide emanations with enclathrated methane gas offers a two for one solution in theory (reduction of CO_2 emissions and extraction of methane gas), its efficiency and environmental side effects need to be clearly understood. The selective nature of gas hydrate formation (favorable thermodynamic conditions vary for every suitable guest) is currently being studied for other novel applications such as flue gas separation and seawater desalination. Furthermore, its unique gas storage capabilities could be used to transport natural gas. This could serve as a more safe and economical process than Liquefied Natural Gas (LNG).

A minimum of one suitable gas or volatile liquid component is required for hydrate formation. For this reason, experimental systems often study simple hydrate systems that are made of one guest component. Real systems however, whether natural or man-made, comprise of not one, but multiple gas components. Hence multicomponent hydrate systems are of crucial importance in order for novel gas hydrate technologies to be successful. As a crystallization process, gas hydrate formation always stems from the liquid phase. Therefore, characterizing this phase is an essential element that provides insights into gas hydrate formation and growth. It can now be understood why combining these two aforementioned concepts yields a relevant subject for this thesis: liquid phase characterization of multicomponent gas hydrate systems. Liquid phase

compositions at equilibrium and during growth were experimentally obtained for various multicomponent systems. Furthermore, the importance of experimental solubilities was highlighted through a modeling study.

Chapter 2

Background

2.1 History

Sir Humphry Davy first discovered gas hydrates in 1811 as he made the observation that a solution of water and chlorine gas crystallized at temperatures higher than the freezing point of water (Davy, 1811). For the next century, the discovery remained only an academic interest as research focused on finding components that allow gas hydrates to occur as well as the ratio of water to gas in the hydrate phase. During that period, Cailletet and Bordet were the first to study, in 1882, gas hydrates with mixtures of two components (Sloan and Koh, 2008). The first industrial application of Davy's find was published by Hammerschmidt who proved in the mid-1930's that these crystalline structures formed inside natural gas pipelines (Hammerschmidt, 1934). As a newly found nuisance to flow assurance, research was consequently intensified to minimize the risks associated with gas hydrate formation. This can be accomplished through additives that either modify the thermodynamic equilibrium, making clathrate formation unfavorable or modify the kinetics, reducing crystal growth rates within transmission lines. Following this, Deaton and Frost obtained state-of-the-art experimental equilibrium data on several hydrocarbon gas hydrate systems such as methane and ethane (Deaton and Frost, 1946). Three decades after Hammerschmidt's breakthrough, *in situ* gas hydrates were discovered by Makogon (Makogon, 1965). These deposits located in both permafrost regions and ocean floors contain hydrocarbons, predominantly methane. As such, gas hydrates were for the first time considered an energy resource. Both Makogon and Kvenvolden separately quantified the extent of gas hydrate reserves to be

twice as great as all fossil fuels reserves combined (Kvenvolden, 1988; Makogon, 1988).

2.1.1 Pipeline blockages

Hydrate formation in pipelines have the potential to grow and completely stop flow, resulting in month-long stoppages to ensure their full dissociation (Sloan and Koh, 2008). This process itself is also a concern: local pressure build-ups have the potential of creating high velocity projectiles as clusters decompose. As such, the conception of chemical hydrate inhibitors capable of reducing these risks is one of the core fields of hydrate research. They can be classified as either thermodynamic or kinetic. Thermodynamic inhibitors modify the necessary conditions for hydrate formation in such a way that the phase change is impossible (by decreasing equilibrium temperatures and increasing equilibrium pressures). Such inhibitors (methanol, glycols) are required in great quantities (~60 %) and are difficult to recover (Koh et al., 2002). On the other hand, kinetic inhibitors and antiagglomerants do not prevent hydrate formation but rather reduce their growth rates. This is accomplished by increasing the time required to form hazardous crystal masses up to a point where the residence time of the fluid in the pipeline is small in comparison. Low dosage kinetic inhibitors operational between 0.1 and 1 % are another interesting proposition due to their environmentally friendly impacts and cost effectiveness (Karaaslan and Parlaktuna, 2002; Koh et al., 2002).

2.1.2 *In situ* deposits

The discovery of in situ gas hydrate deposits in ocean floors and permafrost regions forever changed the perception of gas hydrate in the scientific community. They are now widely considered an energy resource as these deposits contain mostly methane, the main component of natural gas. Due to enormous natural reserves, significant efforts from various countries are being

deployed to establish an economically viable gas hydrate extraction process; a feat yet to be accomplished. *In situ* gas hydrate deposits also pose an environmental threat due to a possible contribution to global warming. As global temperature increases, marine and permafrost hydrates dissociate, leading to significant releases of methane gas. Being twenty one times more harmful to the ozone layer than carbon dioxide (Taylor, 1991), this could in turn increase global warming thus creating a vicious circle called the runaway greenhouse effect (Englezos, 1993).

2.1.3 Carbon dioxide sequestration

Extracting natural resources always pose environmental risks; gas hydrates are no exception. Harvesting marine seafloors for enclathrated methane could trigger slope failures, a potential precursor of tsunamis (Maslin et al., 2010). Because of this, extraction methods that would not disrupt geographical infrastructure are investigated. A solid-state replacement is a suggested solution where injections of captured carbon dioxide emissions in marine methane hydrate deposits would displace methane leading to its release. However, this large addition of carbon dioxide in ocean seafloors could severely affect marine wildlife (Harrison et al., 1995). While this exchange phenomenon was proved experimentally possible (Lee et al., 2003; Park et al., 2006b), the stability of such marine carbon dioxide hydrates are uncertain. Brewer, who conducted several field studies, concluded that permanent carbon dioxide hydrates in marine seafloors is not realistic (Brewer et al., 1999). This is explained by the fact that equal chemical potential across all phases (the criteria for stability) cannot be maintained due to the absence of a natural source of carbon dioxide (Brewer et al., 1999).

2.1.4 Transportation of natural gas

Conventional methods of transporting natural gas include compressed natural gas (CNG) and liquefied natural gas (LNG). These techniques require very low temperatures (-160°C) and high pressures (20 MPa) (Thomas and Dawe, 2003). Transportation of natural gas in hydrate form was first suggested by Benesh (Benesh, 1942) and can be accomplished at milder conditions (-5°C and atmospheric pressure), making this process a safer and more economical alternative. However, CNG and LNG are more compact as each can respectively store 200 and 637 m^3 of gas at standard room temperature and pressure in a volume of 1 m^3, compared to 160 m^3 for gas hydrates (Thomas and Dawe, 2003). Even with this drawback taken in consideration, it was calculated to be a more economical process than LNG (Gudmundsson and Borrehang, 1996).

2.1.5 Separation process

As greenhouse gas emissions are an ever-growing concern, capturing CO_2 emissions for subsequent use in another process is a practical venue to explore. As hydrate formation selectively crystallizes gas molecules, the process has potential to separate gas mixtures. The concept was demonstrated by Kang and Lee as hydrate formation was used to isolate carbon dioxide from flue gas (Kang and Lee, 2000). Small additions of tetrahydrofuran (THF) have also proven to increase significantly the conversion of carbon dioxide gas to hydrate (Kang and Lee, 2000). Desalination of water was also targeted as a possible gas hydrate application but was deemed unfavourable economically when compared to current alternative methods (Eslamimanesh et al., 2012b). While more-in depth studies are required to correctly assess gas hydrate separation processes, the concept has been proven experimentally and may find a future application in different economical and technological context. (Aaron and Tsouris, 2005; Eslamimanesh et al., 2012b).

2.2 Structures

Gas hydrates are a solid phase obtained from the crystallization of a water-based solution with a guest gas or volatile liquid as the solute. As a phase transition, thermodynamics dictate when conditions are favorable to its formation. These are typically above the freezing point of water and at pressures generally an order of magnitude greater than atmospheric pressure. Under these environments, water molecules reorient themselves through hydrogen bonding to form three-dimensional cages termed "cavities" around guest molecules which stabilize the structure. There is no interaction between the guest and the cavity, just weak Van der Waals force and as such, no chemical bonds are formed or broken in the process. Not every cavity is necessarily filled with a guest molecule, which explains the non-stoichiometric nature of gas hydrates. On the other hand, it is possible for a cavity to host more than in a single molecule under extreme pressures (Chazallon and Kuhs, 2002).

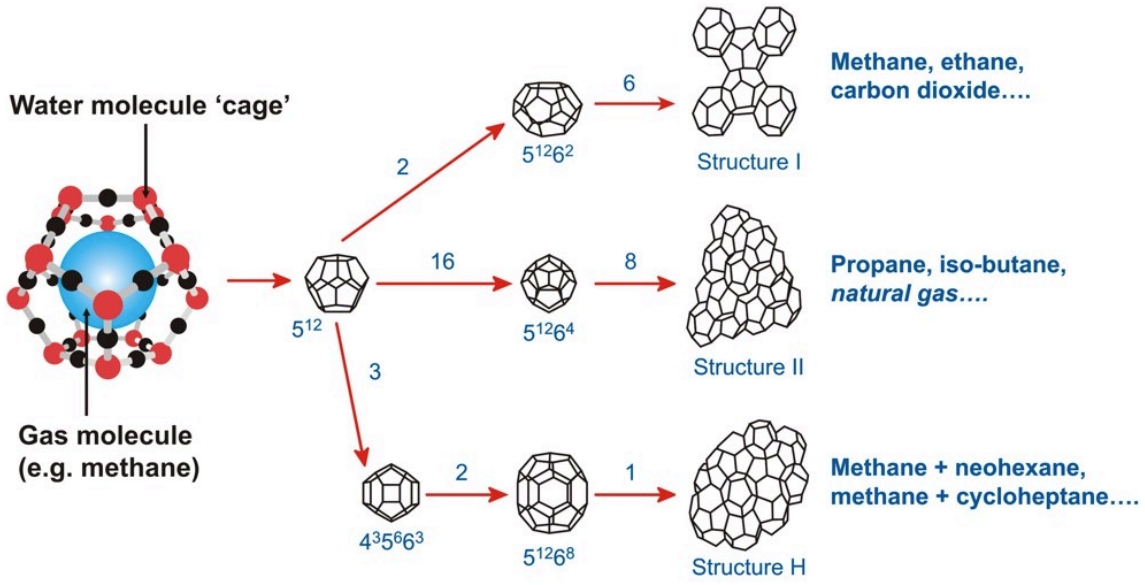

Figure 2.1: Three most common hydrate structures (Heriot Watt Institute of Petroleum Engineering).

As various size of cavity exist, their different combinations naturally yields different structure types, the most common being structure I (sI), structure II (sII) and structure H (sH) represented above. The size of the guest molecule is a predominant factor that dictates the structure type. To determine if a certain molecule can stabilize a cavity, the ratio of the molecular diameter to the cavity diameter is often referred to. A ratio above 1 signifies the guest is too big, while ratios too low aren't viable either as molecular attractive forces aren't significant enough (Sloan and Koh, 2008). It is however possible that the guest molecule becomes part of the cavity structure. In such cases, these structures are referred to as semi-clathrates.

Established by Jeffrey (Jeffrey, 1984), cavity nomenclature makes use of base numbers to represent the amount of vertices a face has, while its exponent represent how often the face is repeated throughout the cavity. Hence, a 5^{12} cavity has twelve pentagonal faces. One unit cell of structure I, for instance, contains two 5^{12} cavities and six $5^{12}6^2$ cavities for a total of 46 water molecules. These cavities host small molecules (0.4 - 0.55 nm) such as methane, ethane and carbon dioxide (Sloan, 2003). Mixtures of these gases also form sI such as methane and carbon dioxide, while some have the ability to form either sI or sII depending on the molar ratio of the two gas components. The combination of methane and ethane (Subramanian et al., 2000) and of nitrogen and carbon dioxide (Diamond, 1994) are examples of such cases.

Structure II hydrate is formed by sixteen 5^{12} cavities and eight $5^{12}6^4$ cavities for a total of 136 water molecules (Sloan and Koh, 2008). Due to the larger cavity of sII being bigger than the larger cavity in sI, guest molecules favoring structure II are typically larger (0.6 – 0.7 nm) such as propane (Sloan, 2003). However, the presence of a high small cavity/large cavity ratio (ratio of 2 for sII versus 0.33 for sI) and the fact the 5^{12} cavity in sII is slightly smaller than 5^{12} cavity in sI explains why smaller (less than 0.4 nm) (Sloan, 2003) molecules

such as nitrogen, argon and krypton favor sII (Davidson et al., 1984; Holder and Manganiello, 1982; Sloan and Koh, 2008).

Discovered by Ripmeester (Ripmeester et al., 1987), structure H is a combination of three different cavities; 5^{12}, $4^3 5^6 6^3$ and $5^{12} 6^8$ which are present in a 3:2:1 ratio per unit cell for a total of 34 water molecules (Sloan and Koh, 2008). Unlike the two previous structure types, sH cannot form with only one guest. It requires a small and large guest; the latter between 0.8 and 0.9 nm (Sloan, 2003). An example of a suitable combination includes methane and neohexane.

2.3 Phase equilibrium

As each guest molecule crystallizes in the presence of water under different thermodynamic conditions, the discovery of hydrates gave rise to more than a century of research dedicated to finding suitable guest molecules along with their respective equilibrium conditions. Thermodynamic equilibrium is achieved when thermal, mechanical and chemical equilibrium coexist. This occurs when temperature, pressure and chemical potential are independent of time. While molecules always continuously change phases, equilibrium is a state where there is no net global conversion rate. Gas hydrate equilibrium is simply defined as a system in the presence of gas hydrates in thermodynamic equilibrium. Common systems have either three phases such as hydrate-liquid water-vapor (H-Lw-V) or two phases (H-Lw or H-V). Other phases like ice or liquefied guest gases can also be present depending on thermodynamic conditions.

Traditionally, thermodynamic equilibrium is experimentally determined through isothermal pressure-search or isobaric temperature-search methods pioneered by Deaton and Frost (1946). The presence of hydrates is monitored through windows mounted on an isochoric reactor while either pressure or temperature is altered. Through several iterations, partial phase diagrams are mapped, thus determining both favorable and unfavorable conditions for hydrate

formation as illustrated by Fig 2.2. As the change from liquid to solid results in a lower energy state, energy must be released. As such, gas hydrate formation is accompanied by a sudden temperature increase; an event commonly used to confirm their presence. An extensive compilation of experimentally obtained equilibrium conditions for various systems is reported by Sloan (Sloan and Koh, 2008).

The natural evolution of gas hydrate academia led to the development of models capable of predicting hydrate equilibrium conditions. This can be undertaken through sets of calculations that simultaneously solve mass balances and equilibrium equations for all three phases. Bishnoi (Bishnoi et al., 1989) and Gupta (Gupta et al., 1991) were the first to accomplish the feat. Both the liquid and gas phase are described by an equation of state (EOS) such as Peng-Robinson (Peng and Robinson, 1976), Soave-Redlich-Kwong (Soave, 1972) or Trebble-Bishnoi (Trebble and Bishnoi, 1987, 1988). On the hand, the hydrate phase is described by a statistical thermodynamic model developed by van der Waals and Plawtteeuw (van der Waals and Plawtteeuw, 1959).

2.3.1 Partial phase diagram

Gas hydrate equilibrium data obtained either experimentally or computationally can be compiled to create phase diagrams as shown by Fig. 2.2. Describing which combination of phases can be present under certain conditions, phase diagrams are used to determine thermodynamic regions where hydrate formation is favorable and unfavorable. The equilibrium line of interest lies past Q_1, which is typically near 273 K as it describes the three-phase hydrate-liquid water-vapor (H-Lw-V) equilibrium. Q_1 represents a quadruple point where four phases are present: hydrate-liquid water-vapor-ice (H-Lw-V-I). The existence of a second quadruple point depends on the critical properties of the guest molecule. As the dotted line in Fig 2.2 represents the conditions where the guest

gas can be liquefied, the line is only valid for gases that have the ability to do so. Not matter how high pressure is, gases with critical temperatures lower than Q_1 will not liquefy and thereby will not create a second quadruple point as they will either retain their gaseous form or become supercritical. Because of this, gases with higher supercritical temperatures like carbon dioxide and ethane will have a second quadruple point past Q_1 where hydrate-liquid water-vapor-liquefied guest (H-Lw-V-L) coexist while methane and nitrogen do not.

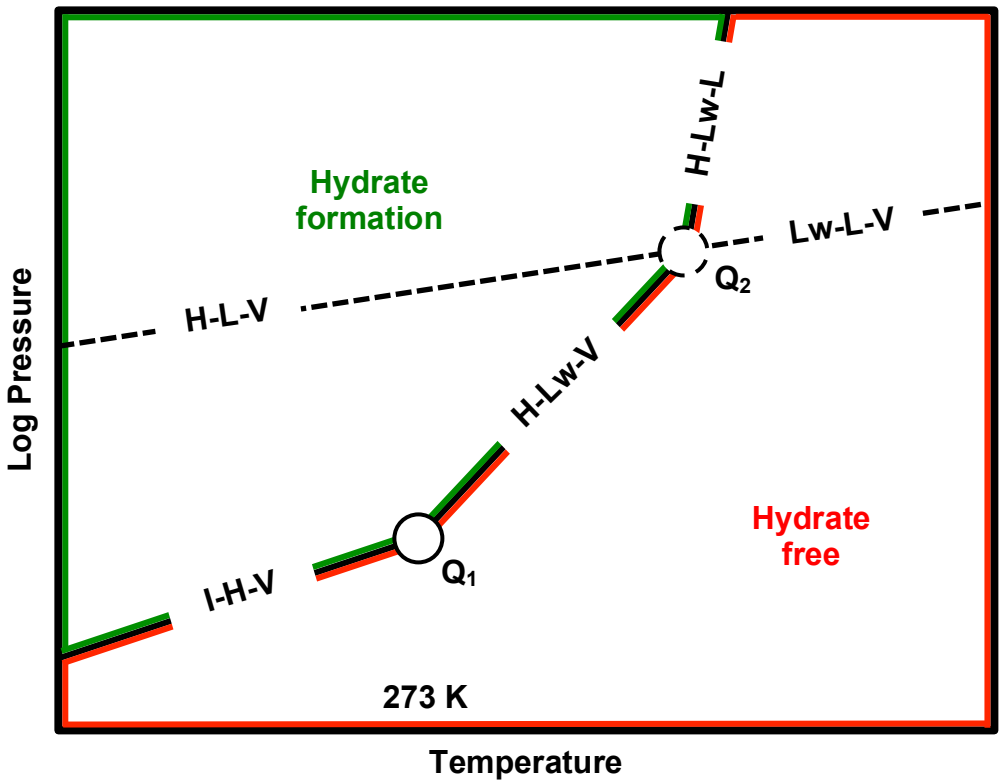

Figure 2.2: Partial phase diagram for simple gas hydrate systems where four phases are possible: hydrate (H), liquid water (Lw), vapor (V), ice (I) and liquefied guest (L). Q_1 is a quadruple point where four phases co-exist: H-Lw-V-I. The dotted line and the existence of Q_2, are dependent on the thermodynamic conditions allowing the guest to liquefy. Hence, Q_2 is a possible second quadruple point where four phases co-exist: H-Lw-V-L. The green and red regions depict the favorable and unfavorable conditions for hydrate formation, respectively.

2.3.2 Gibb's Phase rule

As gas hydrate formation is a phase change and thus a non-reacting process, Gibb's phase rule can be applied to describe the degree of freedom of system at equilibrium. The degree of freedom specifies the amount independent intensive properties characterizing a system and is defined as:

$$F = N - \pi + 2$$

where F, N and π each represents the degree of freedom, the number of components and the number of phases, respectively. Graphically, a system with zero degrees of freedom is represented by a point; one single degree of freedom is represented by a line and two degrees of freedom are represented by a three dimensional plane. Experimentally, the system properties are manipulated by controlling F intensive properties. For a system at equilibrium to be completely specified, F + 1 intensive properties have to be reported (Beltran et al., 2012).

A simple hydrate system at H-Lw-V equilibrium has one degree of freedom and is often specified using temperature and pressure. Binary gas hydrate systems at three-phase equilibrium on the other hand have two degrees of freedom. In this case, pressure and temperature are controlled and typically gas phase compositions are reported.

2.3.3 Solubility of gas hydrate former

Solubility is an equilibrium property between a solute and a solvent. In the case of gas hydrates, the role of the solvent is always taken by water while a gas typically represents the solute. As the reorganization of molecules resulting in a solid phase begins in the liquid phase, solubility is a determining factor in the crystallization process. If the amount of gas present in the liquid phase exceeds

the solubility, which is the maximum allowable gas content at equilibrium, the solution enters a metastable state called supersaturation. This regime is essential for gas hydrate formation as it is this surplus that enables the transition from the liquid to a solid phase. More specifically, the difference between the bulk liquid mole fraction and solubility, which can be referred to as the degree of supersaturation, is used to describe the driving force for hydrate formation. More details on gas hydrate kinetics will be discussed in the following sections.

An isobaric solubility trend as a function of temperature is demonstrated by Figure 2.3 where three different equilibrium systems are displayed by the solid black lines (H-Lw, Lw-V, H-Lw-V) while a supersaturated or metastable system is defined by the dashed line. It can be observed that the solubility trends under Lw-V and H-Lw intersect at the point where all liquid, hydrate and vapor phase coexist at one specific temperature. Figure 2.3 could also be represented as a three-dimensional plot, where pressure would be present on the axis in and out of the page. In this scenario, the H-Lw-V point in Figure 2.3 would transition into a line; one that can be found in Figure 2.2, between Q_1 and Q_2.

As the temperature increases in Figure 2.3, the solubility under H-Lw equilibrium increases as well due to the hydrate phase decomposition, which releases previously enclathrated gas molecules into the liquid phase. This release of gas molecules will eventually warrant the presence of a gas phase, at a specific temperature. At this point, raising the temperature will result in complete hydrate dissociation, leaving only liquid and gas phases. The behavior of this other two-phase system mirrors the H-Lw equilibrium trend, as temperature increases will result in gas molecules leaving the liquid phase, a well-known phenomenon. These trends were found valid through the work of Gaudette and Servio (Gaudette and Servio, 2007), Hashemi et al. (Hashemi et al., 2006), Yang et al. (Yang et al., 2001; Yang et al., 2000) and Kim et al. (Kim et al., 2003).

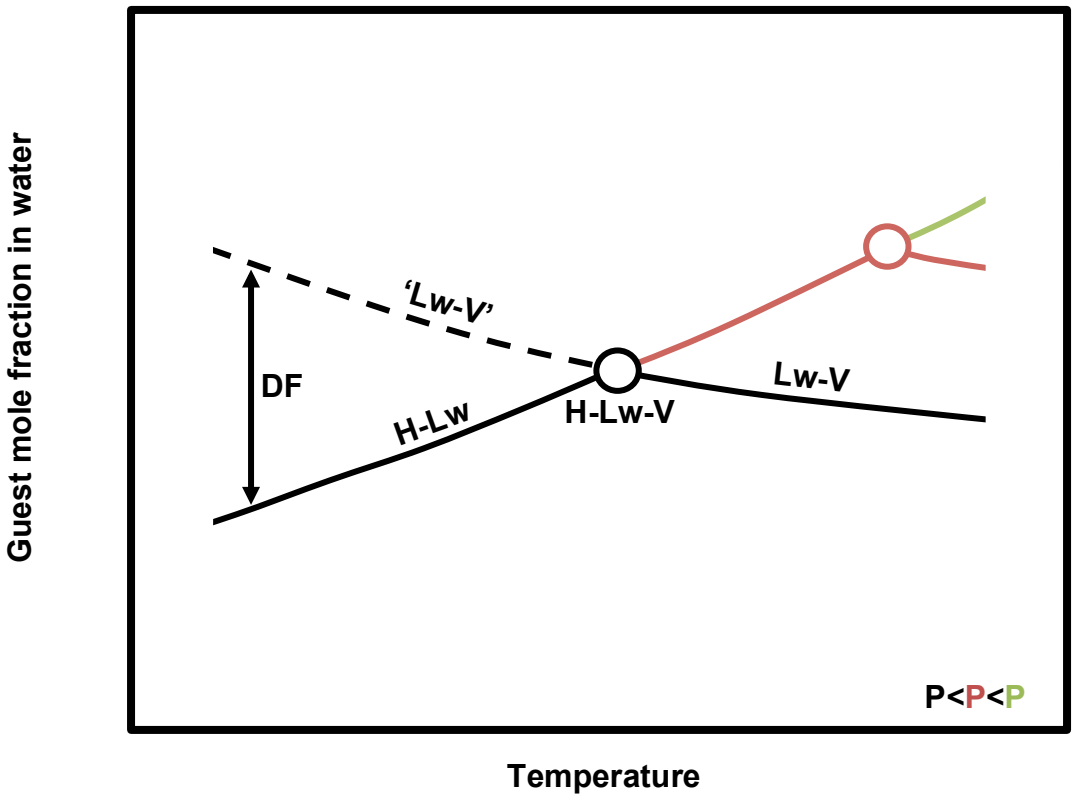

Figure 2.3: Isobaric solubility trend adapted from Hashemi et al. (Hashemi et al., 2007). The driving force is defined here as the difference between the hypothetical Lw-V solubility and the solubility under H-Lw equilibrium both at the experimental temperature and pressure.

Pressure effects on solubility under H-Lw equilibrium are, on the other hand, not as apparent to establish. Servio and Englezos (Servio and Englezos, 2001, 2002), Yang et al. (Yang et al., 2001; Yang et al., 2000) and Kim et al. (Kim et al., 2003) did however determine the weak relationship between methane solubility and pressure under this two-phase system. This is likely due to the incompressibility of the liquid phase. Conversely, Handa modeled H-Lw equilibrium using the work of van der Waals and Platteeuw and found that methane solubility decreases with increasing pressures (Handa, 1990). This trend was also obtained experimentally by Seo et al. (Seo et al., 2002) and Lu et al. (Lu et al., 2008). Carbon dioxide solubility under H-Lw has not been as extensively studied but was found to increase with increasing pressures under a specific temperature range (Someya et al., 2005); a similar find proven theoretically by Bergeron et al. (Bergeron et al., 2010).

2.4 Kinetics

In order for a two-phase Lw-V system to induce hydrate growth, thermodynamic conditions must be set above equilibrium as depicted by the green region in Figure 2.2. To study their effects, these conditions are typically maintained throughout the experiment. For these cases, isothermal and isobaric environments are required during gas hydrate kinetic investigations. Similar to crystallization, the gas hydrate formation process can be divided into two steps: nucleation and growth, which are separated from each other by the turbidity point.

2.4.1 Nucleation

Nucleation is the result of a constant formation and decomposition of hydrate precursor structures due to local concentration fluctuations in a supersaturated regime depicted by the dotted line in Figure 2.3 (Natarajan et al., 1994). This ongoing process continues until the achievement of a stable critical

size cluster, one with an equal probability of either decomposing or growing (Natarajan et al., 1994). If the cluster size increases past this critical value, spontaneous crystal growth will follow, thereby terminating the nucleation phase (Natarajan et al., 1994). The induction period represents the time required to reach this event, called the turbidity point. Its duration, stochastic in nature, was found to be inversely proportional to supersaturation levels (Bishnoi and Natarajan, 1996). Furthermore, systems with water that had previously formed hydrates manifested shorter induction times compared to water with no such history (Vysniauskas and Bishnoi, 1983). Surfaces prone to heterogeneous nucleation in contact with the liquid phase were also shown to reduce induction times (Natarajan et al., 1994). In summary, induction time measurements are sensible to many parameters including the water itself (history, presence of foreign particles) and the experimental setup (surface area for mass transfer, stir rates) (Sloan and Koh, 2008).

2.4.2 Growth

The growth phase begins with the formation of the first stable hydrate crystal, accompanied by a temperature increase as the phase change from liquid to solid is exothermic. Due to the fact the hydrate phase contains up to 15 mol % of gas (which is more than two orders of magnitude greater than methane solubility), a significant amount of gas molecules is required to cross multiple phases and interphases to reach the hydrate surface (Sloan and Koh, 2008). Figure 2.4 below illustrates this path. Hence, both heat and mass transfer are integral processes that affect gas hydrate growth. To ensure these parameters do not limit the growth, gas hydrate kinetics are often studied in a stirred batch crystallizer. These studies resulted in numerous hypothesized driving forces for hydrate formation.

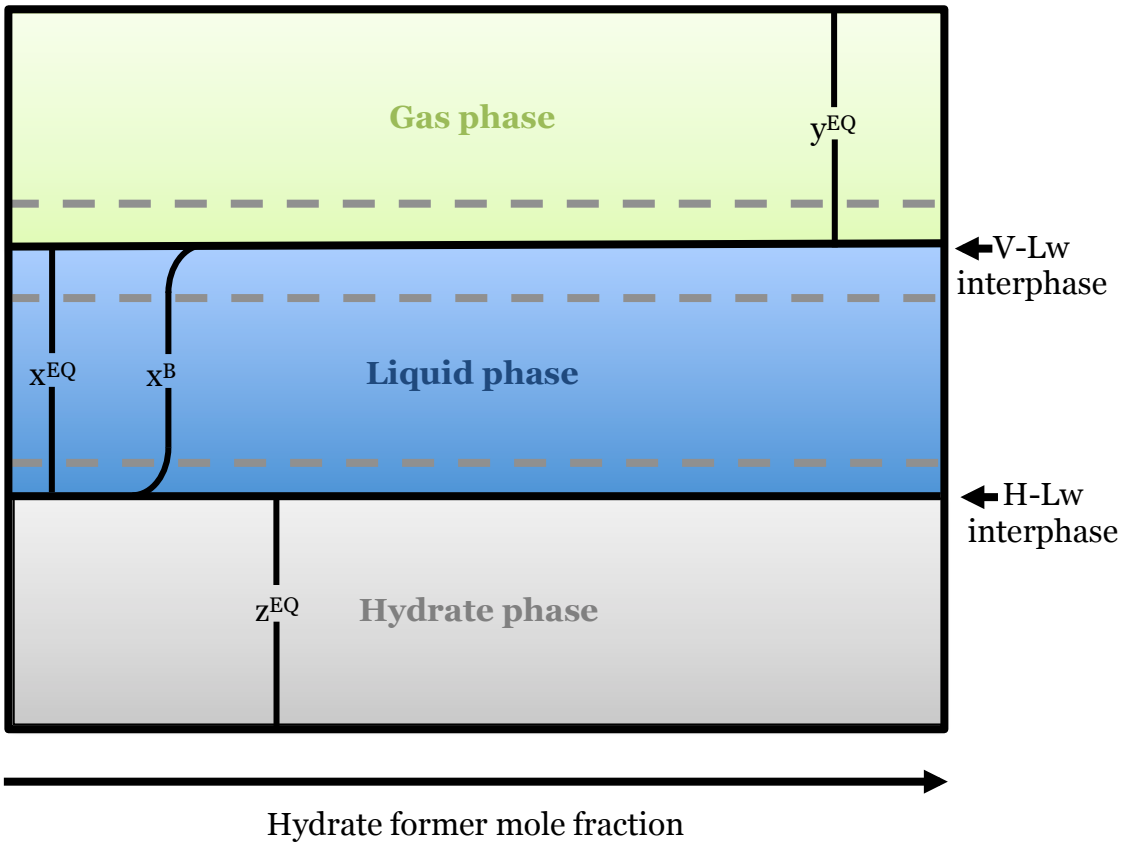

Figure 2.4: Example of a possible mole fraction profile in the hydrate, liquid and vapor phase under equilibrium (superscript EQ) as well as the bulk (superscript B) liquid mole fraction during growth.

Vysniauskas and Bishnoi were the first to investigate gas hydrate kinetics and theorized that rates of formation were a function of interfacial area, pressure, temperature and degree of subcooling while also presenting a semi-empirical model (Vysniauskas and Bishnoi, 1983). A fugacity-based model was proposed by Englezos where the driving force was defined as the difference between the fugacity of the dissolved gas at experimental temperature and pressure and that of the fugacity of the dissolved gas at experimental temperature and the corresponding three-phase equilibrium pressure (Englezos et al., 1987). In their work, Skovborg and Rasmussen formulated the driving force to be the difference between the mole fraction of the guest at the vapor-liquid water interface and that of the guest bulk liquid mole fraction (Skovborg and Rasmussen, 1994). Conversely, Mork and Gudmundsson suggested to the driving force to be the difference between the mole fraction of the guest at the vapor-liquid interface under H-Lw equilibrium and that of the guest at the hydrate surface at experimental temperature and corresponding three-phase equilibrium pressure (Mork and Gudmundsson, 2002).

A more recent form of the gas hydrate driving force is suggested by Hashemi where it is defined as the difference between the guest mole fraction at the vapor-liquid interface and that at the hydrate-liquid water interface, both at experimental temperature and pressure (Hashemi et al., 2007). Since interfaces are theoretically infinitely small, they are always at equilibrium. Hence, Figure 2.3 can visually describe Hashemi's model. Based on Hashemi's work, Bergeron and Servio proposed a more practical model. Instead of using the guest mole fraction at the vapor-liquid interface, the bulk liquid mole fraction is directly used (Bergeron and Servio, 2009). Hence, the model does not have to account for the resistance at vapor-liquid interface and makes use of a parameter obtainable experimentally.

Chapter 3

The importance of liquid phase compositions in gas hydrate modeling: carbon dioxide-methane-water case study[1]

3.1 Preface

In order to first establish the importance of solubility measurements in gas hydrate academic research, a modeling study using the CO_2-CH_4-H_2O mixture is undertaken. Two-phase fugacity calculations using a wide range of gas and liquid mole fractions illustrated the sensitivity of the computed equilibrium. Furthermore, the sensitivity of the results obtained was examined as interaction parameter modifications were made. These parameters, optimized based on vapor-liquid equilibrium (VLE) data, were then utilized to make three-phase H-Lw-V equilibrium gas and liquid mole fractions predictions. Two other cases are presented; one where interactions parameters were regressed only based on vapor equilibrium data only and conversely another where only liquid equilibrium data was used. These exercises demonstrate how two and three-phase equilibrium computations heavily relies on accurate modeling of the liquid phase. Hence, the validation of these models requires experimental solubility measurements.

[1]Reproduced in part with permission from Renault-Crispo J.-S.*, Lang, F.* & Servio P., *The importance of liquid phase compositions in gas hydrate modeling: Carbon dioxide-methane-water case study*, Journal of Chemical Thermodynamics, 68, 153-160, 2014. DOI: 10.1016/j.jct.2013.09.011

* The authors contributed equally to the work

3.2 Abstract

Liquid compositions obtained through vapor-liquid-hydrate equilibrium modeling are often neglected and not reported in literature. This work demonstrates the sensitivity and importance of the liquid phase compositions on selected models and parameters. In order to model two-phase systems, the Soave-Redlich-Kwong, the Valderrama-Patel-Teja and the Trebble-Bishnoi equations of state are used. The modelling analysis for three-phase systems is based on the Trebble-Bishnoi equation of state along with the model by van der Waals and Platteeuw. The vapor-liquid equilibrium model predictions at gas hydrate formation conditions were found to be greatly dependent on the liquid phase compositions. At the three-phase equilibrium, small modifications in the equation of state's interaction parameters significantly affected the liquid composition predictions while leaving the vapor compositions mostly unchanged. Lastly, the interaction parameters were optimized for the two phases separately using vapor-liquid equilibrium data. When optimized only for liquid, vapor and liquid compositions were predicted correctly. However, when optimized only for vapor, liquid compositions failed to fit experimental data.

3.3 Introduction

Gas hydrates, or clathrate hydrates, are nonstoichiometric crystalline compounds that arise from a gas or volatile liquid being encapsulated by water molecules. The guest molecules must be of correct size to fit inside and stabilize the crystal lattice via weak van der Waals forces with the host water molecules (Sloan and Koh, 2008). Gas hydrates usually form at moderate temperatures (0 °C - 25 °C) and high pressures (above 1 MPa). There are over 180 different molecules that form gas hydrates, the most notable being methane, ethane and carbon dioxide which are of particular interest for industrial applications

(Englezos, 1993). Gas hydrates were first documented in 1810 by Sir Humphry Davy and became relevant for the oil and gas industry in the 1930s as they were found to cause blockages in natural gas transmission lines (Hammerschmidt, 1934). Subsequently, academic interest in the field increased significantly and focused mainly on predicting hydrate formation conditions and inhibiting hydrate formation. The discovery during the 1960s of *in situ* natural gas hydrates in the Siberian permafrost (Makogon, 1965), expanded research to include gas hydrates as a potential energy resource. Current conservative estimates propose that the amount of energy stored in natural gas hydrate deposits, which predominantly consist of methane gas, is double the amount of all the other fossil fuel combined (Pellenbarg and Max, 2000). The enormous quantities of methane stored as metastable hydrates also pose an environmental issue as methane is a strong greenhouse gas (Taylor, 1991). Hydrates are also being investigated as an alternative to liquefied natural gas for transportation and storage purposes (Thomas, 2003).

The accurate prediction of gas hydrate formation conditions is vital to industrial applications as hydrates can form inside pipelines thereby creating a hazard to flow assurance. Equilibrium data is available but it is experimentally time-intensive to acquire and limited to very specific conditions and components. Moreover, liquid compositions in hydrate systems are difficult measurements to obtain and are consequently scarce in literature. Due to these limitations, modeling from a thermodynamic perspective, is essential to rapid and accessible determination of equilibrium conditions (Koh et al., 2011). Gas hydrate phase equilibria temperatures, pressures and compositions can be predicted using van der Waals and Platteeuw's model to incorporate the hydrate phase and any typical thermodynamic method to model the vapor and liquid phases (van der Waals and Plawtteeuw, 1959). The vapor and liquid phases are most often represented by an equation of state (EoS) model, of which there are hundreds, each with its own advantages and disadvantages (Tester, 1997). Classical cubic

equations of state for gas hydrate modeling include the Soave-Redlich-Kwong (Soave, 1972) and Peng-Robinson EoS (Peng and Robinson, 1976). These models make use of pure components' parameters regressed from experimental data of vapor pressure and liquid density. As mixtures are always present at the three-phase equilibrium (water and a minimum of one gas hydrate former), binary interactions parameters (IPs) need to be included in the equation of state model to account for the interactions between different molecules. Using a two-phase flash algorithm, these parameters are regressed from vapor-liquid equilibrium (VLE) data for each specific mixture. This demonstrates the strength of this method as it utilizes binary vapor-liquid equilibrium data to predict multi-component vapor-liquid-hydrate equilibrium. The authors use the Trebble-Bishnoi EoS (Trebble and Bishnoi, 1987, 1988) as it contains four binary interaction parameters (k_a, k_b, k_c, k_d) which is more than classical EoSs and therefore is better suited to predict the non-ideal behaviour when polar compounds such as water are present. The Soave-Redlich-Kwong (Soave, 1972) and the Valderrama-Patel-Teja EoS with NDD mixing rules (Avlonitis et al., 1994; Patel and Teja, 1982; Teja and Patel, 1981; Valderrama, 1990) are used for one exercise in order to demonstrate that the choice of EoS had no consequence on the results obtained in this case study.

Gas hydrate systems always consist of water in combination with one or more gas molecules. Condensed phases, like liquid water, contain non-ideal effects as a result of the interaction between different molecules. Under vapor-liquid-hydrate forming conditions, the liquid phase is far less ideal than the vapor phase, which results in liquid compositions being more complex to model. The liquid phase is the reason why binary interaction parameters have a significant role in gas hydrate modeling. These parameters facilitate the fit of the liquid phase composition and ultimately dictate the equilibrium. Consequently, it is critical to show that liquid phase compositions fit experimental data to confirm a model's validity. The motivation behind this paper is that several gas hydrate

modeling papers only report equilibrium conditions (temperature and pressure) and the vapor phase compositions but do not report the liquid phase compositions (Eslamimanesh et al., 2013; Eslamimanesh et al., 2012a; Herri et al., 2011; Holder and Hand, 1982; Kontogeorgis et al., 2007; Li et al., 2007; Nagata and Kobayashi, 1966; Seo et al., 2000). It is assumed that the lack of experimental solubility data is the main reason for this although other reasons are possible such as a poor fit of the liquid phase. The objective of this paper is to demonstrate the importance of considering the liquid phase composition when modeling gas hydrates equilibrium. The sensitivity of the different phases is analyzed with respect to different input parameters and it is shown that the predicted liquid phase composition can sometimes be erroneous while the predicted vapor phase composition and equilibrium temperature and pressure are correct. In gas hydrate applications, liquid compositions are more important than vapor compositions since they define the driving force for hydrate growth (Bergeron et al., 2009; Bergeron and Servio, 2008). In general, crystallization processes use liquid compositions to define crystal growth (Mullin, 2001). The liquid compositions are also a very important parameter of gas hydrate formation in sediments (Clennell et al., 1999; Henry et al., 1999). When assessing the exact amount of gas stored in hydrate deposits, the gas solubility is a crucial factor in the calculations. Lundgaard and Mollerup (Lundgaard and Mollerup, 1991) demonstrated that the solubility of the guest molecule significantly influenced the gas hydrate dissociation pressure. To show the significance of modeling using the liquid phase, the system selected in this study is the carbon dioxide-methane-water vapor-liquid-hydrate system. Applications of this hydrate system include flue gas separation and carbon dioxide sequestration (Linga et al., 2007; Van Denderen et al., 2009). In this paper the technique of modeling three-phase gas hydrate equilibrium is first explained. Following this, the sensitivity and importance of the liquid phase compositions are evaluated for several cases studied.

3.4 Theory

For the three-phase, vapor-liquid-hydrate equilibria, the basic thermodynamic equations for the equilibrium condition are the equality of chemical potentials, μ_i^π, in all phases π:

$$\mu_i^L = \mu_i^V = \mu_i^H \quad (i = 1, \dots, N) \tag{3.1}$$

where N is the total number of components in the system and μ is the chemical potential.

The fugacity and chemical potential of a component in the liquid and vapor phase can be calculated from a suitable equation of state. In this study the Trebble-Bishnoi equation of state is used (Trebble and Bishnoi, 1987, 1988). For the chemical potential of water in the hydrate phase, van der Waals and Platteeuw (van der Waals and Plawtteeuw, 1959) proposed a model that has been modified by Parrish and Prausnitz (Parrish and Prausnitz, 1972) to make it computationally efficient. The equation for the chemical potential of water in the hydrate phase is:

$$\mu_w^H = \mu_w^{MT} - RT \sum_{m=1} \nu_m \ln\left(1 + \sum_{j=1}^{NH} C_{mj} \hat{f}_j\right) \tag{3.2}$$

where $\hat{f}_j$ is the fugacity of hydrate former j, μ_w^{MT} is the chemical potential of water in the empty hydrate lattice, ν_m is the number of cavities of type m per water molecule. C_{mj} is the Langmuir constant which is a function of temperature given by a correlation proposed by Parrish and Prausnitz (Parrish and Prausnitz, 1972) that is valid in the range 260 K to 300 K.

The chemical potential difference of water in the empty hydrate lattice and the pure liquid state is:

$$\mu_w^{MT} - \mu_w^{L_o} = \Delta\mu_w^{MT-L_0} \tag{3.3}$$

The right hand side of equation (3.3) is represented by the following equation from Holder et al. (Holder et al., 1980):

$$\frac{\Delta\mu_w^{MT-L_o}}{RT} = \frac{\Delta\mu_w^0}{\mathrm{RT_0}} + \int_{P_0}^{P} \frac{\Delta V_w^{MT-L_o}}{\mathrm{RT}}\,\mathrm{dP} - \int_{T_0}^{T} \frac{\Delta h_w^{MT-L_o}}{\mathrm{RT^2}}\,\mathrm{dT} \tag{3.4}$$

The temperature dependent equation of the enthalpy is given below:

$$\Delta h_w^{MT-L_o} = \Delta h_w^0(T_0) + \int_{T_0}^{T} \Delta \mathrm{C_{Pw}}\,\mathrm{dT} \tag{3.5}$$

The last equation required is for the chemical potential of water in the liquid solution phase:

$$\mu_w^{sol} = \mu_w^{L_o} + RT\ln(a_w) \tag{3.6}$$

Combining equations (3.1) through (3.6) gives the following expression that is used to solve the hydrate chemical potential as shown by Bruusgaard et al. (Bruusgaard and Servio, 2011):

$$\begin{aligned} \frac{\Delta\mu_w^{MT-L_o}}{R\mathrm{T_0}} + \int_{P_0}^{P} \frac{\Delta V_w^{MT-L_o}}{\mathrm{RT}}\,\mathrm{dP} - \int_{T_0}^{T} \frac{\Delta h_w^{MT-L_o}}{\mathrm{RT^2}}\,\mathrm{dT} + ln a_w \\ = -RT \sum_{m=1} \nu_m \ln\left(1 + \sum_{j=1}^{NH} C_{mj}\hat{f}_j\right) \end{aligned} \tag{3.7}$$

The parameters for the above equations are taken from the work of Holder et al. (Holder et al., 1980) except for a re-optimized value of $\Delta h_w^{MT-L_0}$ which was taken from Hashemi et al. (Hashemi et al., 2006).

For the equilibrium criteria to be respected, the component fugacities must be equal in all three phases. All components must be distributed in the system phases such that the total Gibbs energy is at a minimum. From thermodynamics, the total Gibbs energy is given by the following equation:

$$\underline{G} = \sum_{\pi} \sum_{i} n_i^{\pi} \mu_i^{\pi} \tag{3.8}$$

where n_i^{π} is the molar amount of component i in phase π.

The system conditions are predicted by the minimization of energy using a flash technique. The temperature is initially fixed. Then, a pressure-search method is used to solve for the three-phase equilibrium condition. At each pressure, the two-phase flash is first solved (the requirement being equal component fugacities in liquid and vapor phases). The two-phase flash algorithm can be found in most thermodynamic textbooks (Michelsen and Mollerup, 2007; Tester, 1997). These fugacities are then plugged into equation (3.7) along with all the required parameters. If both sides of the expression are equal then the pressure is correct and if not the pressure is updated to a new value and the process repeated. The full hydrate equilibrium algorithm can be found in the work of Parrish and Prausnitz (Parrish and Prausnitz, 1972).

3.5 Discussion

3.5.1 Two-phase systems

Modeling and reporting vapor-liquid-hydrate equilibrium pressures, temperatures and vapor compositions is common in literature. However, it is not common to report liquid composition predictions because the liquid phase is much less ideal than the vapor phase at gas hydrate formation conditions. Thus obtaining liquid phase composition predictions poses a greater challenge due to its sensitivity while being essential for many hydrate applications. As a first step to verify that the liquid phase compositions are more sensitive than the gas phase compositions, a two-phase flash is used to calculate the methane partial fugacity in both liquid and vapor phases of a vapor-liquid water-methane system for different mole fractions. From the results shown in Figure 3.1, the slopes of both liquid and vapor methane partial fugacity illustrate the relative sensitivity of both phases to a small change in mole fraction. While Figure 3.1 results are obtained using the Trebble-Bishnoi (TB) and Valderrama-Patel-Teja (VPT) EoS, Figure 3.2 shows the results for the same exercise using the Soave-Redlich-Kwong EoS. Since the results obtained from the Soave-Redlich-Kwong (SRK) EoS are two orders of magnitude different than those obtained in Figure 3.1, they are displayed in a separate figure. By repeating the exercise with several EoS, the authors want to illustrate that the results obtained throughout this work are independent of the choice of EoS. The choice of operating conditions of 274.28 K and 1.765 MPa is due to the availability of liquid mole fraction data under similar conditions (Lekvam and Bishnoi, 1997).

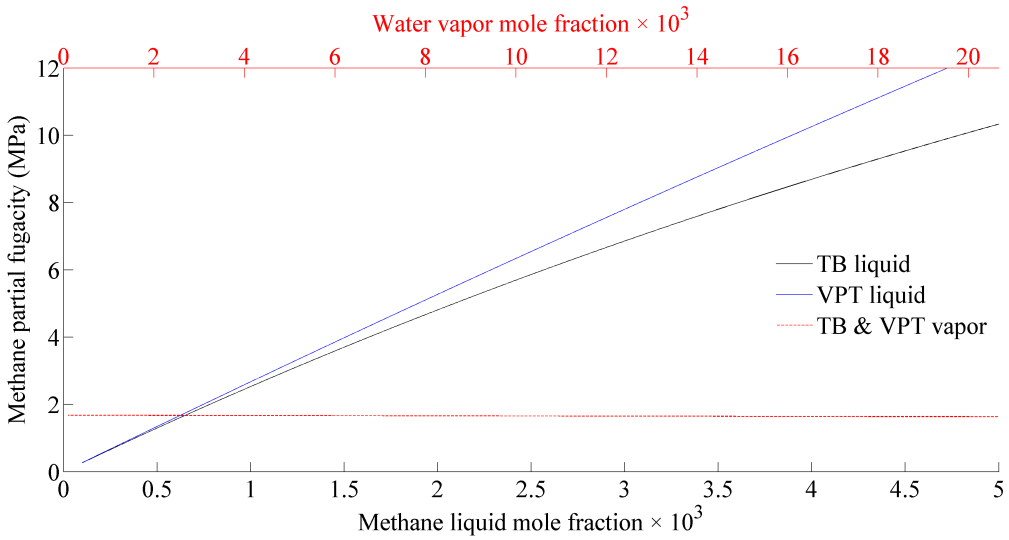

Figure 3.1: Methane partial liquid fugacity (black solid line was modelled with TB EoS (Trebble and Bishnoi, 1987, 1988) while the blue solid line was modelled with VPT EoS with NDD mixing rules (Avlonitis et al., 1994; Patel and Teja, 1982; Teja and Patel, 1981; Valderrama, 1990)) and methane partial vapor fugacity (superimposed red dashed lines for both EoS) for a two-phase methane-water system at 1.765 MPa and 274.28 K. The top x-axis is the composition that can be associated with the vapor fugacity and the bottom x-axis is the composition that can be associated with the liquid fugacity.

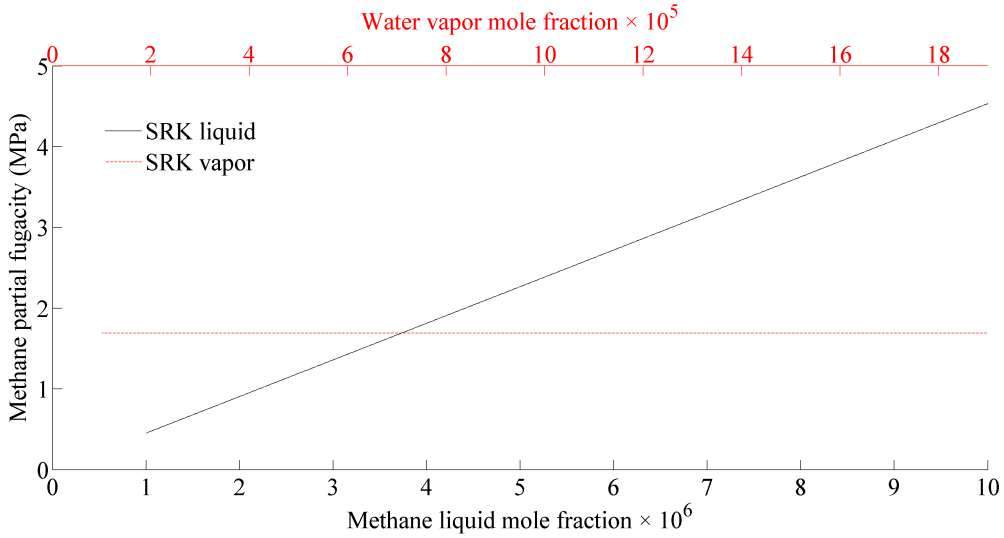

Figure 3.2: Methane partial liquid fugacity (black solid line) and methane partial vapor fugacity (red dashed line) for a two-phase methane-water system at 1.765 MPa and 274.28 K using SRK EoS (Soave, 1972). The top x-axis is the composition that can be associated with the vapor fugacity and the bottom x-axis is the composition that can be associated with the liquid fugacity.

It can be observed in Figure 3.1 that the system modeled by the TB EoS reaches equilibrium where the vapor and liquid partial fugacity lines cross at a methane liquid mole fraction of 7.23×10^{-4} and water vapor mole fraction of 2.65×10^{-4}. This is comparable to the experimental data reported by Lekvam and Bishnoi (Lekvam and Bishnoi, 1997) where the methane liquid mole fraction was 7.35×10^{-4}. The results obtained from the VPT EoS are also displayed in Figure 3.1; the equilibrium liquid composition being 6.24×10^{-4}. For this condition, the TB EoS predicts the liquid mole fraction at equilibrium slightly better than the VPT EoS. Regardless, the VPT EoS predicts the liquid phase composition adequately. Figure 3.1 shows the weak relationship for both EoS between vapor partial fugacity and vapor mole fraction because the slopes are small compared to the liquid phase. Any vapor mole fraction in this graph results in a similar equilibrium fugacity if compared with the liquid fugacity. The same cannot be said about the methane liquid partial fugacity, which has a more significant slope revealing that it is a stronger function of liquid mole fraction. In this case, selecting the wrong methane liquid mole fraction results in a completely different equilibrium fugacity. This signifies that the equilibrium condition is dictated by the liquid mole fraction considerably more than the vapor mole fraction. The same conclusion is observed when using the SRK equation of state in Figure 3.2. The vapor methane partial fugacity is invariant compared to the liquid methane partial fugacity. This equation of state predicts equilibrium vapor methane mole fraction of 3.73×10^{-6}. This is two orders of magnitude smaller than the experimental value and demonstrates that the original SRK equation of state is not suitable for predicting the solubility of gases in water. The objective of using the SRK and VPT equations of state is to show that regardless of the equation of state, compositions have a much greater effect on the liquid partial fugacities than the vapor partial fugacities. Comparison at a different temperature using the experimental data by Servio et al. (Servio and Englezos, 2002) is also performed. The temperature and pressure are 278.65 K and 3.5 MPa, respectively, where liquid mole fraction is 0.00190. The TB EoS predicts a liquid mole fraction of

0.00193 while the VPT EoS predicts 0.00107. As expected the SRK models the liquid composition very different from the experimental data with a value of 8.37 × 10^{-6}. These results demonstrate the same EoS behaviors at a different temperature.

Moving closer to the paper's main case study, carbon dioxide is added to the above analysis in order to model a vapor-liquid carbon dioxide-methane-water system. The results found in Figure 3.3, now with an extra dimension, are analogous to the results from Figure 3.1 and 3.2. The flat plane in Figure 3.3(b) indicates the methane vapor partial fugacity is again a weak function of vapor mole fractions. On the contrary, shown in Figure 3.3(a), the methane liquid partial fugacity is a strong function of liquid mole fractions; its plane is much steeper than its counterpart at any point. The intersection between the two planes shown in Figure 3.3(c) represents the phase equilibrium line. The bottom axis labels on this Figure are omitted to avoid confusion with the different scales. The bottom axis scale for the vapor surface can be taken from Figure 3.3(a) while the ones for the liquid surface can be taken from Figure 3.3(b). The line spans an infinite amount of equilibrium conditions. This can be understood by looking at the phase rule with three components and two phases where three degrees of freedom exist. Consequently, one mole fraction is also fixed in addition to temperature and pressure to completely determine an equilibrium point which lies on the line. The analysis of these models reveals that the liquid mole fractions are vital when predicting equilibrium compositions because liquid fugacities vary more than vapor fugacities and thus have a greater effect on the equilibrium the model predicts.

3.5.2 Interaction parameters sensitivity analysis

The next step in this case study focuses on equilibrium molar composition predictions of the carbon dioxide-methane-water vapor-liquid-hydrate system.

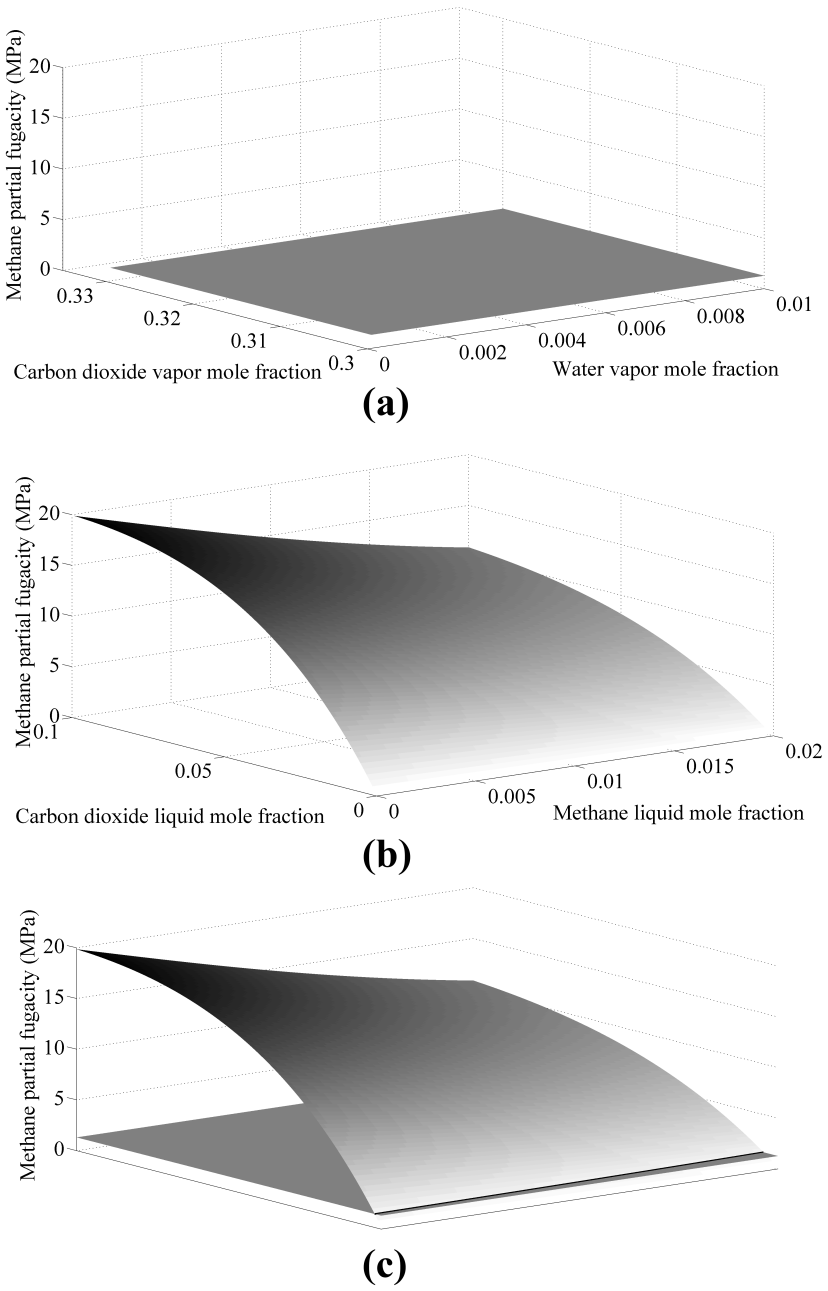

Figure 3.3: Methane partial fugacities for the two-phase carbon dioxide-methane-water system at 2 MPa and 274 K using Trebble-Bishnoi EoS (Trebble and Bishnoi, 1987, 1988): (a) Methane partial liquid fugacity plotted versus liquid mole fractions, (b) Methane partial vapor fugacity plotted versus vapor mole fractions, (c) Figures (a) and (b) superimposed with the same axis respectively. Axis labels are omitted to avoid confusion with the different scales of Figures (a) and (b).

In order to predict equilibrium compositions using an EoS and the model mentioned above, interaction parameters (IPs) are first optimized to fit VLE data. For the carbon dioxide-methane-water system, the IPs for methane-water were previously optimized by Hashemi et al. (Hashemi et al., 2006) for the Trebble-Bishnoi equation of state. The IPs for carbon dioxide-water and carbon dioxide-methane are taken from Trebble and Bishnoi's work (Trebble and Bishnoi, 1988). These IPs were used as a starting point for the analysis. This exercise tests the sensitivity of these parameters to evaluate the accuracy of liquid and vapor equilibrium compositions. Specific modifications of the optimized interaction parameters (+/- 1 %, +/- 10%) are introduced for the methane-water pair within the system. The error between the modeled liquid and vapor mole fractions at equilibrium and experimental data (Bruusgaard et al., 2010a) are reported in Table 3.1. The average absolute relative error (AARE) is calculated for all cases. For the vapor phase, the experimental data available (Bruusgaard et al., 2010a; Bruusgaard and Servio, 2011) reported only the carbon dioxide mole fractions. Water vapor mole fraction can be considered negligible therefore it is reasonable to assume that the AARE for the methane vapor mole fraction will follow the same trend as the AARE for the carbon dioxide vapor mole fraction. For the AARE of carbon dioxide liquid mole fraction, since only the IPs for methane-water are modified, the liquid mole fractions for carbon dioxide are practically unaffected. The authors also introduce modifications to the IPs for the carbon dioxide-water as well as the methane-carbon dioxide pair and found a similar conclusion.

Table 3.1: Behavior of liquid and vapor mole fractions for various methane-water interaction parameters for the carbon dioxide-methane-water vapor-liquid-hydrate equilibrium compared to experimental data (Bruusgaard et al., 2010a). k_a to k_d are the interaction parameters used in the Trebble-Bishnoi equation of state. (Trebble and Bishnoi, 1987, 1988)

Modification (%)	Interaction Parameters of methane-water				AARE (%)	
	k_a	k_b	k_c	k_d	x_{CH_4}	y_{CO_2}
0%	0.4199	-0.1727	-0.0001	-1.2274	8.47	10.88
+1%	0.4241	-0.1744	-0.0001	-1.2397	87.13	11.75
-1%	0.4157	-0.1710	-0.0001	1.2151	29.75	10.88
+10%	0.4619	-0.1900	-0.0001	-1.3501	84.11	11.75
-10%	0.3780	-0.1554	-0.0001	-0.1105	No convergence	

If the parameters are not modified and taken directly from Hashemi (Hashemi et al., 2006), the AARE for methane liquid mole fraction and carbon dioxide vapor mole fraction are 8.47% and 10.88%, respectively, and these errors will serve as a baseline comparison. It is quite clear from the results presented in Table 3.1, regardless of the modification that the AARE for carbon dioxide vapor mole fraction is quite independent of the different interaction parameters, as it never changed by more than 0.87% compared to the baseline. Conversely, the methane equilibrium liquid mole fraction is quite sensitive to changes in IPs as the AARE rose to 87.13%.

From Table 3.1, no proportional relationship between the magnitude of the modification to IPs and the AARE is observed. This is expected since the IPs exist for fitting purposes, and they do not always fit the VLE experimental data smoothly. Consequently, it is reasonable to anticipate large changes in the AARE of liquid mole fractions for relatively small changes in IPs. These results reinforce the principle that liquid equilibrium compositions are more difficult to model

correctly than their gaseous counterparts, this time with respect to interaction parameters. More importantly, it demonstrates the limitations of only reporting vapor equilibrium mole fractions. These results reveal that even if the interaction parameters fit the vapor phase properly, they could be considerably erroneous with respect to liquid compositions.

3.5.3 Interaction parameters optimization analysis

The interaction parameters involved in equations of state for mixtures are found by minimizing the error between the experimental VLE data and the two-phase flash algorithm predictions. These parameters (obtained exclusively from binary experimental data) are then used to solve multi-component and multi-phase equilibrium. A demonstration to show the importance of optimizing these IPs correctly and their sensitivity to liquid phase data compared to vapor phase data is presented below. Once again, the methane-water interaction parameters are used as the example case within the carbon dioxide-methane-water vapor-liquid-hydrate system. The method used for optimization was a combination of Levenberg-Marquardt and stochastic optimization. The interaction parameters were re-optimized from vapor-liquid experimental data of pressure, temperature and mole fractions for both phases (Lekvam and Bishnoi, 1997; Sage and Lacey, 1934). The data's temperature range is 274.19 K to 444.26 K and the pressure range is 0.6 MPa to 68.9 MPa. Three different cases of IPs are regressed. The first case fit the IPs in the two-phase flash to liquid mole fractions only. The second case fit the model to the vapor mole fractions only. Finally, the third case was the one already provided by Hashemi et al. (Hashemi et al., 2006) which was shown to fit both phases of the binary VLE satisfactorily. The first two cases are for demonstration purposes only and in most situations the interaction parameters are optimized for both phases.

Figure 3.4 shows the results for the vapor mole fraction predictions for all cases. As mentioned before, the vapor mole fraction of carbon dioxide is used because of the availability of experimental data points for comparison. As expected, the best fit is with the interaction parameters optimized for the vapor phase as the AARE for carbon dioxide vapor mole fraction is 6.35%. However, the other two optimization schemes give very good results. The AARE for the case where IPs were optimized for the liquid phase is 9.54% and the AARE of the two-phase optimization is 10.37%. This shows that even when the vapor-liquid data is optimized for liquid only, the vapor mole fractions obtained are very close to the experimental data. Although, the model optimized for vapor only seems slightly worse at higher temperatures, the average error at all temperatures is smaller. The same conclusions can also be said of the methane vapor fraction as mentioned in the previous section. The water vapor fraction was not studied because it is not found in appreciable quantities in the vapour phase and is generally not useful in any gas hydrate application.

Figure 3.5 shows the results for the liquid mole fraction predictions, again for all cases. This time, it can be clearly observed that there is a high variability of the liquid phase with respect to the different optimizations. The liquid and the two-phase optimizations give a satisfactory model that fit the experimental data. The vapor optimization gives poor results, and using these values in any application would be inaccurate.

The last two figures clearly show how the vapor phase is not affected significantly by interaction parameters for the carbon dioxide-methane-water gas hydrate system. However, the liquid phase is greatly influenced by the interaction parameters. Because of this strong dependency, liquid mole fractions are difficult to predict using gas hydrate models only fitted to vapour phase data. This makes accurate models and experimental gas hydrate solubility data highly valuable. For these reasons, liquid phase composition predictions should be included when evaluating theoretical models.

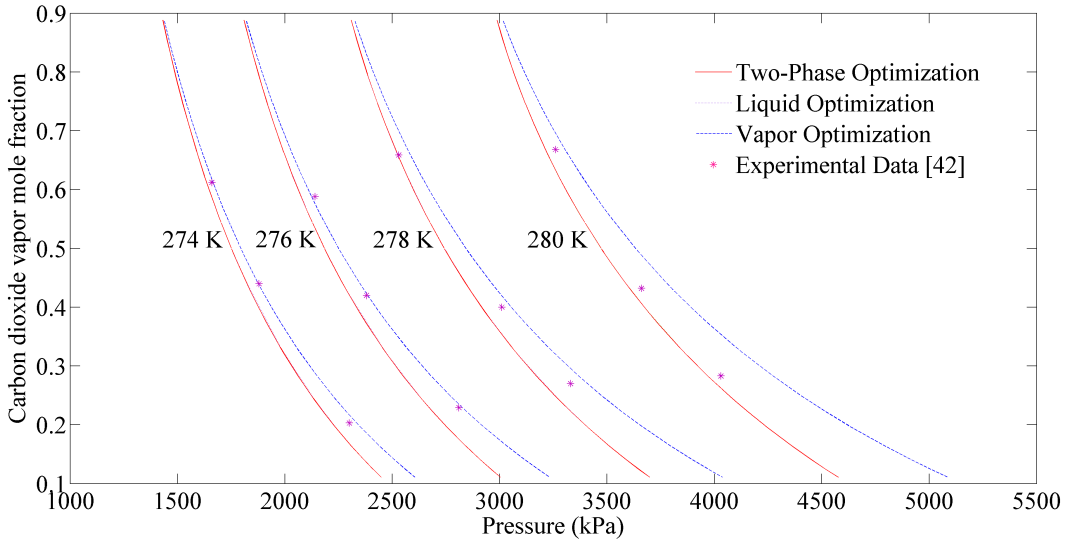

Figure 3.4: Carbon dioxide vapor mole fraction versus pressure at four different temperatures (from left to right: 274 K, 276 K, 278 K, 280 K) for the three different cases of optimizations using Trebble-Bishnoi EoS (Trebble and Bishnoi, 1987, 1988). The red solid line is the two-phase optimization. The purple dotted line is the liquid optimization (hardly visible because it is superimposed by red solid line). The blue dashed line is the vapor optimization. The individual data points represent the experimental data from Bruusgaard et al. (Bruusgaard et al., 2010a).

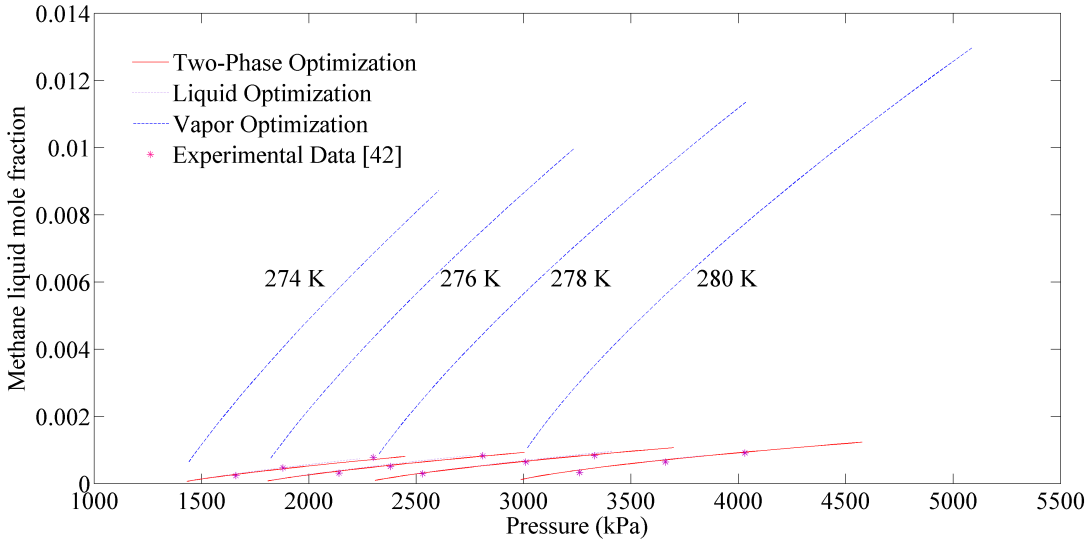

Figure 3.5: Methane liquid mole fraction versus pressure at four different temperatures (from left to right: 274 K, 276 K, 278 K, 280 K) for the three different cases of optimizations using Trebble-Bishnoi EoS (Trebble and Bishnoi, 1987, 1988). The red solid line is the two-phase optimization. The purple dotted line is the liquid optimization (hardly visible because it is superimposed by red solid line). The blue dashed line is the vapor optimization. The individual data points represent the experimental data from Bruusgaard et al. (Bruusgaard et al., 2010a).

3.6 Conclusion

This paper demonstrates that liquid molar compositions cannot be overlooked when modeling three-phase, vapor-liquid-hydrate equilibrium. In gas hydrate systems, the liquid phase contains more non-idealities than the vapor phase which makes predicting liquid compositions a challenge. The liquid phase compositions are also very important for many gas hydrate applications such as defining the driving force in hydrate growth models. Two-phase flash analysis of a methane-water and carbon dioxide-methane-water system shows that a component's partial fugacity is a much stronger function of liquid composition than vapor composition demonstrating that equilibrium conditions have a greater dependency on the liquid phase. This exercise is carried out with three different equations of state (Soave-Redlich-Kwong, Valderrama-Patel-Teja and Trebble-Bishnoi) and they all result in similar trends. A sensitivity analysis on the interaction parameters of the methane-water pair within the carbon dioxide-methane-water three-phase vapor-liquid-hydrate system was performed. The interaction parameters were modified by a certain percentage and used to predict liquid and vapor compositions, which were compared to experimental data. The AAREs for the vapor compositions never rose more than 1%. On the other hand, the AAREs for liquid compositions varied as much as 78.66% from the baseline. These results indicate that gas hydrate models that report the predicted vapor molar composition only, could have erroneous liquid molar compositions. In order to emphasize this last point, hypothetical regressions were simulated where interaction parameters were optimized for three different cases: vapor and liquid data, liquid data only and vapor data only. Using those parameters, both vapor and liquid mole fractions were predicted and compared to experimental data. When the interaction parameters were optimized for liquid data only, the vapor mole fractions were predicted successfully. Conversely, when the interaction parameters were optimized for vapor data only, the liquid mole fraction predictions were orders of magnitude different from experimental data.

Chapter 4

Solubility measurements for the $N_2+CO_2+H_2O$ system under hydrate-liquid-vapor equilibrium[1]

4.1 Preface

The relevance of equilibrium liquid phase characterization to gas hydrate modeling now established, the focus now shifts to the acquisition of experimental solubility data. Due to the fact that most gas hydrate systems are actually comprised of not one but many components, binary mixtures are investigated. The first to be studied is the $N_2+CO_2+H_2O$ system under H-Lw-V equilibrium; a system of importance to flue gas separation and carbon dioxide sequestration studies. With nitrogen favoring sII and carbon dioxide sI, the mixture will naturally have a structure transition, depending on the composition of the gas phase. As three-phase solubility measurements were never experimentally obtained for this mixture, the effect of this transition on solubility trends is presented and explained.

[1]Reprinted with permission from Lang, F. & Servio P., *Solubility Measurements for the $N_2+CO_2+H_2O$ system under hydrate-liquid-vapor equilibrium*, Journal of Chemical Engineering Data, 59 (8), 2547-2550, 2014. DOI: 10.1021/je500340b

4.2 Abstract

Equilibrium liquid and gas mole fraction measurements were taken at H-Lw-V equilibrium for the N_2+CO_2+H_2O system. Experimental conditions ranged from 275.1 to 279.2 K and from 2.7 to 14 MPa. Gaseous mole fractions were compared to literature values in order to validate that equilibrium was reached. The effect of temperature and pressure changes on the solubility of both gas hydrate formers along isotherms is reported. The thermodynamic region associated with a hydrate structure change affected solubility trends.

4.3 Introduction

Gas hydrates are nonstoichiometric crystals that form under favourable thermodynamic conditions of moderate temperatures and high pressures in the presence of water and suitable gas molecules. Methane, ethane, carbon dioxide and nitrogen are common examples of hydrate formers. Gas hydrates are also commonly called clathrates; derived from the latin word clathratus meaning "lattice bars". This lattice, made of water molecules, encapsulates the guest gas. In turn, weak van der Waal forces between the guest and the lattice stabilize the cavity. The combination of various types of these cavities yields different unit cells, which are unique to every hydrate structure. The most common structures are structure I (sI), structure II (sII) and structure H (sH) (Sloan, 1998).

Gas hydrates were discovered in 1810 by Sir Humphry Davy (Davy, 1811). This event spawned a field of research invested into identifying and characterizing this new phenomenon. This academic interest shifted towards industrial applications when it was found in the 1930's that gas hydrates could form inside oil and gas transmission pipelines thereby creating a hazard to flow assurance (Hammerschmidt, 1934). A significant amount of clathrates also exist

as *in situ* natural deposits in permafrost regions and ocean floors in the form of methane hydrates (Kvenvolden, 1988). It was estimated that the amount of carbon content contained within those naturally occurring hydrates is approximately twice the amount of all fossil fuels on earth combined (Kvenvolden, 1988). Currently, a substantial amount of research is focused on efficiently extracting this untapped resource at a feasible cost. Various techniques are being contemplated such as thermal stimulation, depressurization and injection of inhibitors (Sloan, 1998). As these procedures lead to hydrate dissociation, there is a concern that this decomposition could destabilize marine seafloors, potentially causing geological slope failures (Maslin et al., 2010). Carbon dioxide sequestration offers a possible solution to this issue as the enclathrated molecule (methane) could be replaced with carbon dioxide. Consequently, methane gas would be available for extraction while carbon dioxide insertion would maintain the stability of the hydrate layer. Moreover, as carbon dioxide emissions are an ever-growing concern, this method would also mitigate this issue. The efficiency of this exchange phenomenon was significantly improved through the use of a mixture of carbon dioxide and nitrogen (Park et al., 2006b), while a recent field test in Alaska by the National Energy Technology Laboratory (NETL) of the United States Department of Energy (DOE) in partnership with ConocoPhillips, Japan Oil and Metals National Corporation established the feasibility of the process (Parshall, 2012). This same mixture is also of interest as treated gaseous effluents from power plants are composed of CO_2, O_2, and N_2 (Linga et al., 2007). As both O_2 and N_2 form hydrates at similar thermodynamic equilibria, the mixture is often simplified to $CO_2 + N_2$ (Linga et al., 2007). Gas hydrate formation could then be employed to separate the two components for subsequent storage or utilization of CO_2 (Linga et al., 2007).

Hydrates found in nature and in industry typically have more than one type of guest molecule. For this reason, it is important to understand and properly characterize multicomponent hydrate systems and more specifically the

N_2+CO_2 mixture if the outlined technologies are to be successful. Equilibrium conditions for the N_2+CO_2+H_2O system have already been reported in literature (Belandria et al., 2011; Bruusgaard et al., 2008; Seo and Lee, 2003), but the liquid mole fraction at equilibrium has never been experimentally measured. Solubility data for this system were obtained but were the result of indirect measurements through mass balance (Belandria et al., 2011). To the best of our knowledge, this is the first study to report experimental liquid mole fraction data obtained through direct bulk liquid sample extraction at H-Lw-V equilibrium for the multicomponent N_2+CO_2+H_2O system. Experimental liquid compositions data at three-phase equilibrium are relatively scarce in literature even though they are crucial for gas hydrate applications as they define the driving force for hydrate growth (Bergeron and Servio, 2009) and play a major factor in the accurate prediction of hydrate equilibrium conditions (Renault-Crispo et al., 2014). The present study aims at improving the knowledge of the N_2+CO_2+H_2O system under H-Lw-V equilibrium through obtaining experimental solubility measurements.

4.4 Experimental Apparatus

The apparatus used for this work is shown in 4. 1 below. The crystallizer is made of 316 stainless steel and is submerged in a liquid bath containing a 20% ethylene glycol/water mixture. The system temperature is regulated through a VWR AD15R-30 chiller. The crystallizer is equipped with two polycarbonate windows allowing for visual inspection. In addition, a Dyna/Mag mixer from Pressure Products Industries is employed inside the crystallizer in order to reduce mass transfer limitations. All readings are recorded through a National Instruments data acquisition system. The temperatures are measured using Omega RTD probes (± 0.1 K) while the crystallizer's pressure is monitored via

Rosemount pressure transducers with a span of 0-14 MPa and accuracy of ± 0.065% of the given span.

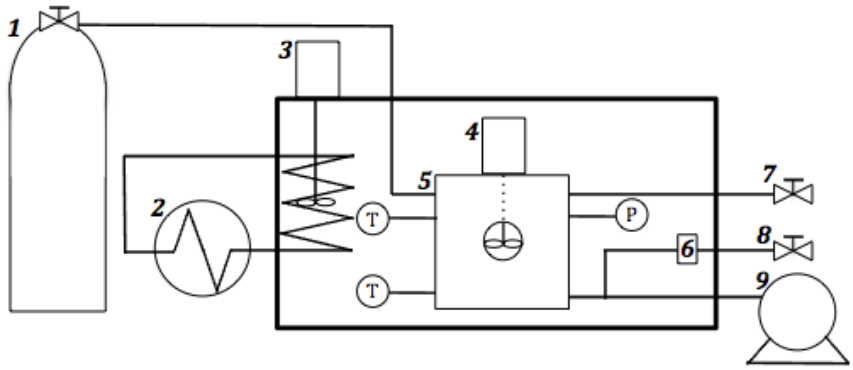

Figure 4.1: Experimental setup: (1) gas cylinder, (2) chiller, (3) liquid bath stirrer, (4) crystallizer stirrer, (5) crystallizer, (6) filter, (7) gas sampling port, (8) liquid sampling port, (9) displacement pump.

The water used underwent reverse osmosis treatment (0.22 μm filter) allowing less than 10 ppb of total organic content while having a conductivity of 10 μS. In order to take samples of both the gas and the liquid phase, two separate lines located at different heights on the crystallizer are connected to two separate globe valves. The liquid line is equipped with a 200 nm Norman 4200 in-line filter to prevent gas hydrate crystal inclusion during liquid phase sampling. A positive displacement pump (Oilphase-DBR, Schlumberger) is used to inject water, which in turn increases the crystallizer's pressure. A digital gasometer (Chandler Engineering) is used to measure the amount of gas stored in liquid samples while a gas chromatograph (Varian CP-3800) is used to analyze gaseous compositions.

4.5 Experimental procedure

The experimental procedure for obtaining liquid and gaseous compositions was based on previous successful sampling techniques for multicomponent systems under H-Lw-V equilibrium (Bruusgaard et al., 2010a). In order to remove any gaseous impurities, the crystallizer was purged three times with the required mixture of N_2+CO_2 (MEGS) at 1 MPa. Once the appropriate temperature is acquired through the chiller, the same gas mixture was fed to the crystallizer followed with the injection of water from the displacement pump until a suitable driving force to enable hydrate formation was obtained. To achieve this, the pressure was set at approximately 1.5 MPa over the known equilibrium pressure (Bruusgaard et al., 2008). The system was left to equilibrate for a period of six hours after hydrate formation was visually observed to ensure stable thermodynamic conditions (temperature and pressure). Samples of the gas and liquid phase were then extracted with previously evacuated sample bombs. Gas mole fractions were directly obtained through gas chromatography by comparing the results with a previously acquired calibration curve. The sample bomb containing the liquid was connected to the gasometer in order to obtain the volumetric amount of gas stored in the liquid phase. The sample bomb was left to warm and depressurize to room temperature and pressure for a period of five hours in order to guarantee that all gas left the liquid phase. Subsequently, the gas accumulated in the gasometer was analyzed through gas chromatography. The amount of moles of N_2 and CO_2 in the gasometer were obtained by :

$$n_i^G = y_i^G \left(p - p_{H_2O}\right) \frac{V}{ZRT} \tag{4.1}$$

where y_i^G, p, p_{H_2O}, V, Z, R, T are respectively the gas mole fraction of component i in the gasometer chamber, atmospheric pressure, vapor pressure of water at room temperature, volume obtained from the gasometer, compressibility factor

for the mixture, universal gas constant and the room temperature. The compressibility factors were calculated using the Trebble-Bishnoi equation of state (Trebble and Bishnoi, 1987, 1988). The amount of moles of N_2 and CO_2 left in the sample bomb (n_i^S) were calculated through known solubility data (Dean, 1992) at room temperature and pressure. By weighing the sample bomb before and after sampling, the equilibrium liquid mole fractions were obtained by :

$$x_i^{EQ} = \frac{n_i^S + n_i^G}{n_{TOT}} \tag{4.2}$$

where x_i^{EQ} is the equilibrium liquid mole fraction of component i, n_i^S the amount of moles left in the sample bomb of component i at room temperature and pressure, n_i^G the amount of moles of component i in the gasometer and n_{TOT} the total amount of moles of all components.

4.6 Results and Discussion

Solubility measurements as well as gas phase equilibrium mole fraction were obtained for the N_2+CO_2+H_2O system under H-Lw-V equilibrium. Operating conditions ranged from 275.1 K to 279.2 K and from 2.7 MPa to 14 MPa. The results are presented in Table 4.1. A minimum of two replicates were conducted for each equilibrium condition. Isotherms of equilibrium gaseous compositions are shown in Figure 4.2 and isotherms of solubility measurements are shown in Figures 4.3 and 4.4. According to Gibbs' phase rule, the experimental system has two degrees of freedom which entails that two intensive properties must be controlled while a third reported in order to ensure that equilibrium was indeed reached (Beltran et al., 2012). In this case, pressure and temperature were controlled while the equilibrium vapor phase compositions were obtained and satisfactorily compared to literature values, as illustrated in Figure 4.2. This comparison confirms that thermodynamic equilibrium was achieved.

Table 4.1: Experimental values of temperature T, pressure p, liquid mole fraction x, and gas mole fraction y for the mixture $N_2(1)+CO_2(2)+H_2O(3)$ at H-Lw-V equilibrium[a]

T/K	p/MPa	x_2	x_1	y_1
275.1	2.7	0.01227	0.00185	0.442
275.1	2.8	0.01205	0.00207	0.487
275.1	2.8	0.01252	0.00182	0.451
275.1	5.6	0.00903	0.00245	0.756
275.1	5.6	0.00913	0.00222	0.745
275.1	9.5	0.00829	0.00610	0.879*
275.1	9.5	0.00565	0.00263	0.875*
275.2	9.5	0.00632	0.00423	0.876*
275.2	9.5	0.00592	0.00255	0.877*
275.2	9.5	0.00566	0.00286	0.882*
277.1	3.2	0.01470	0.00184	0.395
277.2	3.3	0.01503	0.00157	0.389
277.2	3.3	0.01424	0.00198	0.412
277.1	6.1	0.01109	0.00239	0.699
277.1	6.2	0.01139	0.00214	0.690
277.1	13.2	0.00989	0.00657	0.894*
277.1	13.2	0.00777	0.00659	0.897*
277.1	13.3	0.00783	0.00525	0.895*
277.1	13.3	0.00963	0.00658	0.897*
277.1	13.4	0.00855	0.00553	0.896*
279.2	3.9	0.01675	0.00191	0.351
279.2	4.0	0.01638	0.00186	0.379
279.1	7.3	0.01357	0.00224	0.644
279.1	7.3	0.01368	0.00207	0.650
279.1	13.9	0.00910	0.00582	0.843*
279.2	13.9	0.00770	0.00292	0.842*
279.2	14.0	0.00879	0.00603	0.844*

[a]Standard uncertainties u are $u(T)$ = 0.1 K, $u(p)$ = 0.15 kPa, $u(y_1)$ = 0.005 and the combined expanded uncertainty U_c is $U_c(x_1)$ = 0.00014 and $U_c(x_2)$ = 0.00051 (0.95 level of confidence). *Possibility of two types of crystal structure at these conditions (Diamond, 1994; Park et al., 2006; Belandria et al., 2011).

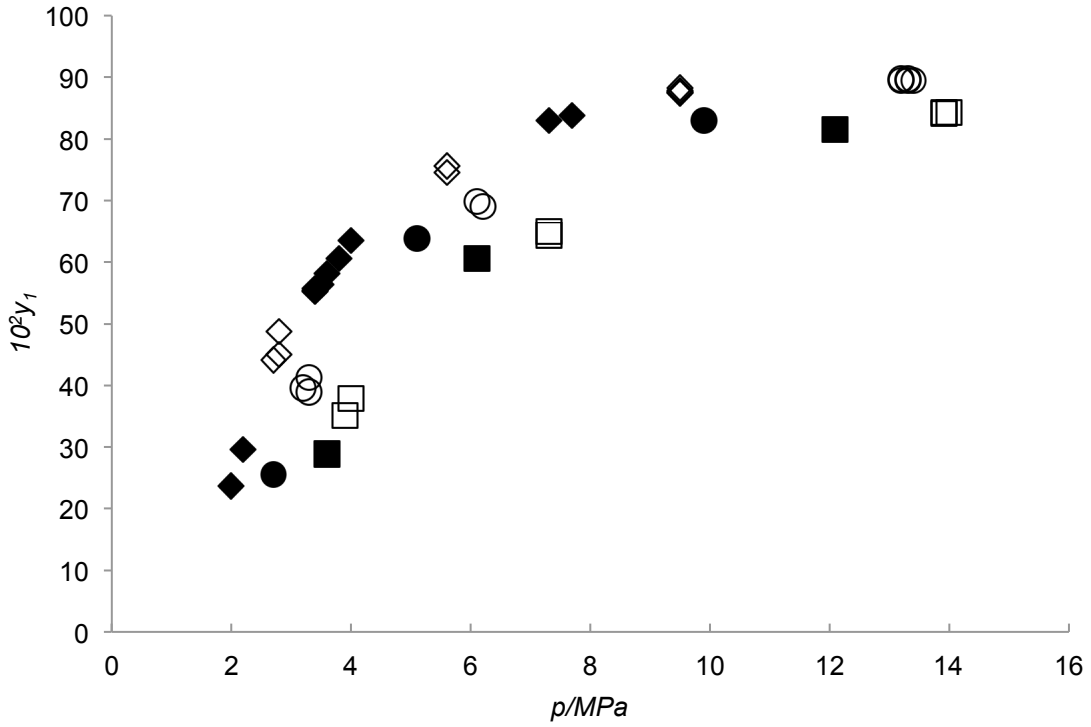

Figure 4.2: Gaseous equilibrium mole fraction of nitrogen under H-Lw-V for the N_2+CO_2+H_2O system. □, this work at 279 K; ■, Bruusgaard *et al.*(Bruusgaard et al., 2008) at 279 K; ○, this work at 277 K; ●, Bruusgaard *et al.*(Bruusgaard et al., 2008) at 277 K; ◇, this work at 275 K; ◆, Bruusgaard *et al.*(Bruusgaard et al., 2008) at 275 K.

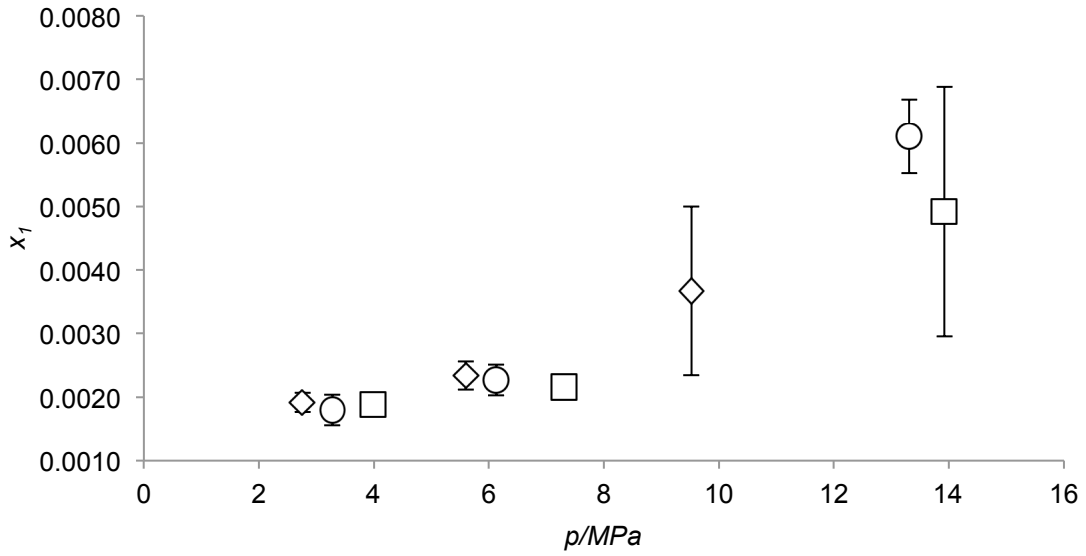

Figure 4.3: Nitrogen solubility under H-Lw-V for the N_2+CO_2+H_2O system. □, this work at 279 K; ○, this work at 277 K; ◇, this work at 275 K.

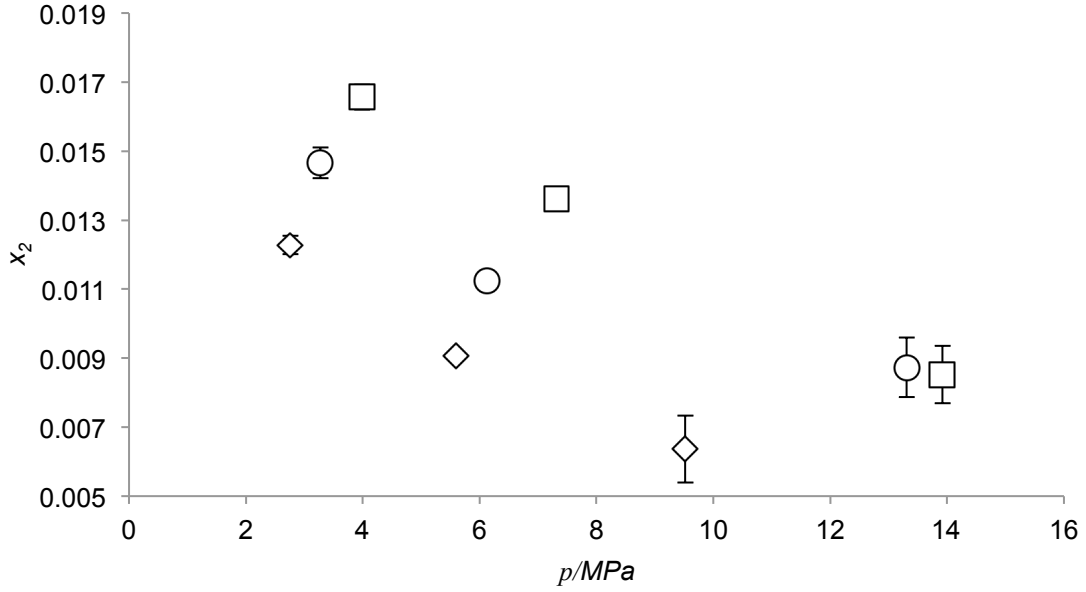

Figure 4.4: Carbon dioxide solubility under H-Lw-V for the N_2+CO_2+H_2O system. □, this work at 279 K; ○, this work at 277 K; ◇, this work at 275 K.

The thermodynamic limits of a binary gas mixture such as CO_2+N_2+H_2O are defined by the equilibrium conditions that each gas hydrate former has as a simple hydrate system. Thermodynamic conditions approaching that of one simple gas hydrate system will result in an increase in gas and liquid mole fraction of that same component. Nitrogen, as a simple gas hydrate system, forms clathrates at higher pressures and lower temperatures than carbon dioxide. Therefore, an increase in pressure and reduction in temperature will increase gas and liquid nitrogen mole fraction. Conversely, the opposite change will increase carbon dioxide solubility and gaseous mole fraction. This trend can be seen in the data presented.

It can be observed from Figures 4.3 and 4.4 that in three instances (275.1 K & 9.5 MPa, 277.1 K & 13.3 MPa, 279.1 K & 13.9 MPa), the reported 95% confidence interval is much larger than in the rest of the data presented. For these three cases, the carbon dioxide gas mole fraction varied from 10.3% to 15.8%; conditions where a structure change is reportedly occurring (Diamond, 1994; Park et al., 2006a; Seo and Lee, 2003). Individually, CO_2 is known to form structure I while N_2 forms structure II (Sloan, 1998). As a mixture, they are known to have the ability to form either structure. It can be deduced that when the gaseous mixture approaches either pure CO_2 or N_2 formation, structure I or II are respectively favoured. The phase boundary between the two structures has been reported to be 85 mol % of N_2 (Diamond, 1994) while later X-Ray and NMR studies claimed that N_2+CO_2 mixture forms structure I from gas compositions of 10 and 20 mol % CO_2 (Seo and Lee, 2003). Subsequent NMR analyses reported that gas compositions of over 10 mol % CO_2 yielded structure I (Park et al., 2006a). Only the three rightmost points on Figure 4.3 and 4.4 are located where this transition could have an effect. The remaining data points are outside this region and are not affected by the phenomenon.

Thermodynamic conditions will dictate which structure will be favoured. For the three cases where a structure change has been reported, only sI or sII or a combination of sI/sII could be present during sampling. This could explain the increased variation in the data under these conditions as this parameter cannot be controlled or measured with our setup. This may also explain why the solubility of carbon dioxide at 277.1 K and 13.3 MPa does not follow the trend of other isotherms, as illustrated by Figure 4.4. To the best of our knowledge, this is the first solubility study conducted at conditions where a structure change occurs.

4.7 Conclusion

Solubility measurements of N_2 and CO_2 at H-Lw-V equilibrium were reported for the N_2+CO_2+H_2O system. The temperatures of the experiments ranged from 275.1 K to 279.2 K while the corresponding equilibrium pressure varied from 2.7 MPa to 14 MPa. Vapor phase compositions were compared to literature values in order to confirm equilibrium. Results showed that along each isotherm, the solubility of nitrogen was found to increase with increasing pressure and decreasing temperatures while the carbon dioxide solubility increased with decreasing pressure and increasing temperatures. It was also observed that solubility measurements located around the conditions where a structure change is reportedly occurring could not be accurately replicated. It is therefore postulated that the structure may have an effect on solubility.

Chapter 5

Solubility measurements for the $CH_4+C_2H_6+H_2O$ system under hydrate-liquid-vapor equilibrium[1]

5.1 Preface

The second mixture to be studied through H-Lw-V experimental solubility measurements is the $CH_4+C_2H_6+H_2O$ system. As both methane and ethane are two major components of natural gas, their combination is highly relevant in both industry and research. A structure transition is also possible but differs from the previous study as both methane and ethane favor sI. Under a certain range of gas compositions, the mixture can also form sII. Experimental solubility measurements were never previously acquired and will further enhance the knowledge of this important system. It will be determined if the structure transition also affects solubility trends and hence establish the previously found phenomenon as a direct result of thermodynamic properties found in each individual structure.

[1]Reproduced in part with permission from Lang, F. & Servio P., *Solubility measurements for the $CH_4+C_2H_6+H_2O$ system under hydrate-liquid-vapor equilibrium*, Journal of Natural Gas Science and Engineering, 26, 130-134, 2015. DOI: 10.1016/j.jngse.2015.06.002

5.2 Abstract

Liquid and gas mole fractions were obtained at three-phase H-Lw-V equilibrium for the CH_4+C_2H_6+H_2O system at experimental conditions ranging from 275.1 to 279.1 K and 0.76 to 2.87 MPa. To ensure the system reached equilibrium while sampling, gaseous mole fractions were compared to literature values and were found to correspond. The solubility of both methane and ethane along isotherms is reported at various pressures. The effect of thermodynamic parameters on equilibrium liquid mole fractions can be observed. Additionally, structure transitions between sI and sII were found to influence solubility trends. While scarce in literature, experimentally obtained liquid mole fractions at three-phase equilibrium conditions provide further insights into multicomponent gas hydrate system properties and establish a solid foundation for future studies.

5.3 Introduction

Gas hydrates or clathrates are crystalline compounds that form in the presence of water and suitable gas molecules such as methane, ethane and carbon dioxide. As they are the result of a phase change, thermodynamics dictate at which conditions (temperature and pressure, for instance) the shift in state occurs. Much like ice, hydrogen bonding between water molecules is predominant in gas hydrates but is structured in repeating, cage-like unit cells that house guest gas molecules. These cavities are then stabilized by weak van der Waal forces exerted between the guest and the lattice. The size of guest molecules is the principal factor in dictating the favoured unit cell. Various different unit cells exits and their different yet specific combination yields different types of structure. The most common are structure I (sI), structure II (sII) and structure H (sH)(Sloan, 1998). The presence of a guest in every cell is not required for these structures to be stable, which explains the nonstoichiometric nature of gas hydrates.

The discovery of gas hydrates is attributed to Sir Humphry Davy, who in 1811 reported that the combination of chlorine gas and water formed a solid body. As an academic field, the onset of gas hydrate research focused on identifying gas molecules that could be enclathrated along with establishing their thermodynamic equilibrium conditions. More than a century after Davy's find, research shifted towards industrial applications, as it was revealed that gas hydrates could form inside natural gas pipelines thereby creating flow assurance issues (Hammerschmidt, 1934). Due to this newfound concern, gas hydrate inhibitor development began. These chemicals either modified thermodynamics conditions rendering hydrate formation impossible or significantly reduced the rate of crystal growth with the goal of reducing the risk of substantial masses in pipelines. As the composition of natural gas includes mostly methane and ethane, these components were at the forefront of gas hydrate research. It was later realized that gas hydrates were not only a nuisance, but also represented a potentially significant energy resource as methane clathrate *in-situ* deposits were located in both permafrost regions and ocean seafloors in considerable quantities (Kvenvolden, 1988). In both zones, hydrocarbons (mostly methane) become enclathrated due to the presence of water and favourable thermodynamic conditions. It is estimated that more carbon based resources exist in hydrate form than in all fossil fuels combined (Kvenvolden, 1988). In order to make gas hydrate extraction economically viable, many countries such as the United States, Japan, India, China, Korea and Germany are deploying significant amount of resources in research and field studies (Makogon, 2010).

In both examples of gas hydrate applications mentioned above, methane is the dominant molecule. The crystal structure will not necessarily be dictated by methane though, but will depend on the presence of other gases as well. For instance, mixtures of methane and ethane were experimentally found to be able to form sII under certain thermodynamic conditions even though both components favour sI in a single component hydrate system (Hendriks et al.,

1996; Subramanian et al., 2000). Consequently, a small addition of ethane to a pure methane system could make a significant impact as the structure transitions from sI to sII. The effectiveness of thermodynamic and kinetic inhibitors for instance, could be greatly reduced if specifically catered towards one type of hydrate structure while another is actually present (Ohno et al., 2009).

Due to its relevance outlined above, the CH_4+C_2H_6+H_2O system must be well understood and characterized. Deaton and Frost investigated H-Lw-V equilibrium for the CH_4+H_2O and C_2H_6+H_2O systems as well the CH_4+C_2H_6+H_2O system during the 1940's (Frost and Deaton, 1946). Servio and Englezeos experimentally obtained methane solubilities in a CH_4+H_2O system with various phases present, including H-Lw-V (Servio and Englezos, 2002) which were modelled later on by Hashemi et al. (Hashemi et al., 2006). Experimental solubilities were also obtained by Song et al (Song et al., 1997) for both the CH_4+H2O and C_2H_6+H_2O system at and near hydrate conditions. The components chosen for this study have already been the subject of numerous studies on gas hydrates but to the best of our knowledge experimental liquid mole fractions for the CH_4+C_2H_6+H_2O system at three-phase H-Lw-V equilibrium were never obtained. The amount of gas stored in the liquid phase at equilibrium, also known as the solubility, is plentiful in literature for two-phase vapour-liquid systems. Conversely, solubility data for three-phase systems (hydrate, liquid and vapor) are relatively scarce considering their versatile applications. In any crystallisation process like that of gas hydrates, growth is bound to the degree of supersaturation, which is the difference between the bulk liquid mole fraction and the solubility. This stresses the importance of solubility as it defines the driving force for hydrate growth thus making hydrate growth rate models and predictions possible (Bergeron and Servio, 2009). Moreover, experimental solubility data is required to correctly assess gas hydrate equilibrium models (Renault-Crispo et al., 2014). Furthermore, it was also demonstrated how strongly hydrate dissociation pressures are linked to gas solubility (Lundgaard

and Mollerup, 1991). The aim of this study is to improve the knowledge of the CH_4+C_2H_6+H_2O system by mapping experimental solubilities at H-Lw-V equilibrium while assessing the effect of structure transitions.

5.4 Experimental Apparatus

The schematic of the apparatus utilized in this study is the same as the one described previously, illustrated in Figure 4.1. The pressurized vessel made of 316 stainless steel is submerged in a bath holding a 20% volume ethylene glycol/water mixture. The vessel temperature is regulated indirectly as the bath temperature is controlled through a VWR AD15R-30 chiller. Two polycarbonate windows allow for visual inspection inside the vessel possible, which is necessary for confirmation of hydrate formation. A Dyna/Mag mixer from Pressure Products Industries mounted atop the vessel is employed to stir the system, which reduces mass and heat transfer limitations. The temperatures are measured using Omega RTD probes (± 0.1 K) while pressure is monitored via Rosemount pressure transducers with a span of 0-14 MPa and accuracy of ± 0.065% of the given span. A National Instruments® data acquisition system is used to record all readings. The water used is treated at McGill University through reverse osmosis using a 0.22 μm filter. This allows less than 10 ppb of total organic content to be present while having a conductivity of 10 μS. In order to sample both the liquid and gas phase, two lines are located at different heights on the crystallizer and connected to two globe valves to maintain pressure. Water is injected into the crystallizer with a positive displacement pump (Oilphase-DBR, Schlumberger), which is also used to increase pressure. The amount of gas dissolved in liquid samples is measured with a digital gasometer (Chandler Engineering) and then subsequently analyzed through gas chromatography (Varian CP-3800) to obtain gaseous compositions.

5.4 Experimental Procedure

The experimental techniques and calculations used in this study were based on previous work that established the necessary steps to experimentally acquire gas and liquid compositions of multicomponent systems under H-Lw-V equilibrium (Bruusgaard et al., 2010a). The temperature of the chiller was set in order to achieve the desired vessel temperature and the system was left to equilibrate. The pressure vessel was initially purged a minimum of three times at approximately 1 MPa with the required mixture of CH_4+C_2H_6 (MEGS) to remove impurities. In order to produce a wide range of equilibrium conditions, multiple loading compositions were necessary. The pressure was increased to approximately 1.5 MPa above the known equilibrium, establishing a driving force. Once hydrate formation was visually confirmed, the system containing approximately 300 cm^3 of water was left to stabilize and reach equilibrium by having pressure and temperature constant for a minimum of six hours. Both gas and liquid samples were then extracted and contained using sample cylinders of approximately 10 cm^3 purchased from Swagelok. As methane/ethane hydrates were buoyant and the liquid sample port located at the bottom of the vessel, no in-line filtration unit was required to prevent the extraction of hydrate crystals. The gas equilibrium mole fraction was obtained by analyzing the gas sample through gas chromatography and comparing directly with a previously acquired calibration curve. The liquid equilibrium mole fraction required more steps, as the mass of the sample cylinder was measured before and after sampling, after which the sample cylinder was connected to the gasometer. The liquid sample was then flashed and left to equilibrate to room pressure and temperature for approximately five hours. The volume of the accumulated gas in the gasometer chamber was displayed digitally while its composition was determined using gas chromatography. By combining the parameters described above, the liquid mole fraction is computed using the ideal gas law. To account for deviations from ideality, compressibility factors are calculated using the Trebble-Bishnoi equation

of state (Trebble and Bishnoi, 1987, 1988). Detailed calculations can be found in a previous work (Lang and Servio, 2014).

5.5 Results and Discussion

Solubility measurements and gas phase equilibrium mole fraction were obtained for the CH_4+C_2H_6+H_2O system under H-Lw-V equilibrium for thermodynamic conditions ranging from 275.1 K to 279.1 K and 0.76 MPa to 2.87 MPa. Since the chosen system has two degrees of freedom as per Gibb's phase rule, two intensive properties must be controlled and a third reported in order to lock the system. In this case, the experimental pressure and temperature were maintained while the gaseous mole fraction acts as the third intensive property as it can be compared to literature. The results presented in Table 5.1 demonstrate that two replicates for each equilibrium condition were acquired. Isotherms of equilibrium gaseous compositions at 275 K, 277 K and 279 K are shown in Figure 5.1 and agree with previous work (Bruusgaard et al., 2010b). It can be observed that increasing the temperature as well as decreasing the pressure reduces the mole fraction of methane in the gas phase. The opposite observation is also true for ethane. This shift essentially moves the operating conditions closer to ethane's three-phase equilibrium and correspondingly further from methane's three phase equilibrium therefore reducing the presence of methane gas at equilibrium.

This analogy can also be used to explain isotherm solubility trends shown in Figures 5.2 and 5.3. Similarly to methane gas mole fraction trends, an increase in temperature or decrease in pressure lowers the amount of methane gas present in water at equilibrium. For all three temperatures, a small but noticeable shift in solubility trends for methane and especially ethane is noticeable in a region where a structure change is known to occur. As a structure change has been

Table 5.1: Experimental Values of Temperature *T*, Pressure *p*, Liquid Mole Fraction *x* and Gas Mole Fraction *y* for the $CH_4(1)+C_2H_6(2)+H_2O(3)$ Mixture at H-Lw-V Equilibrium[a]

T/K	p/MPa	x_1	x_2	y_1
275.1	0.76	0.00011	0.00021	0.363
275.2	0.77	0.00012	0.00022	0.373
275.1	1.14	0.00024	0.00020	0.684
275.1	1.15	0.00022	0.00019	0.687
275.1	1.77	0.00053	0.00010	0.921*
275.1	1.77	0.00053	0.00011	0.920*
275.1	1.53	0.00052	0.00016	0.877*
275.2	1.54	0.00056	0.00018	0.874*
275.1	1.66	0.00055	0.00012	0.904*
275.1	1.68	0.00055	0.00012	0.906*
275.1	1.99	0.00069	0.00009	0.945*
275.1	2.00	0.00069	0.00009	0.945*
277.2	0.96	0.00008	0.00027	0.364
277.2	0.98	0.00012	0.00033	0.391
277.1	1.37	0.00028	0.00022	0.662
277.2	1.36	0.00027	0.00022	0.656
277.1	1.77	0.00055	0.00019	0.835*
277.2	1.77	0.00052	0.00017	0.838*
277.1	2.00	0.00054	0.00012	0.892*
277.1	2.00	0.00055	0.00013	0.893*
277.1	2.13	0.00066	0.00012	0.912*
277.1	2.18	0.00070	0.00011	0.919*
279.1	1.15	0.00009	0.00033	0.318
279.1	1.18	0.00010	0.00033	0.354
279.1	1.55	0.00028	0.00027	0.607
279.1	1.55	0.00026	0.00026	0.608
279.1	2.01	0.00053	0.00022	0.779*
279.1	2.03	0.00052	0.00023	0.783*
279.1	2.30	0.00057	0.00015	0.863*
279.1	2.32	0.00055	0.00016	0.866*
279.1	2.86	0.00079	0.00011	0.932*
279.1	2.87	0.00085	0.00011	0.933*

[a] Standard uncertainties *u* are $u(T)$ = 0.1 K, $u(p)$ = 0.03 MPa, $u(y_1)$ = 0.005 and the combined expanded uncertainty U_c is $U_c(x_1)$ = 0.00000668 and $U_c(x_2)$ = 0.00000620 (coverage factor k = 2). *Possibility of two crystal structure at these conditions.

already reported in literature to have an effect on solubility trends (Lang and Servio, 2014), it is an appropriate explanation for this case. Individually, CH_4 and C_2H_6 each form sI. This explains why as a mixture, high CH_4 or C_2H_6 gaseous concentration leads to sI as simple gas system properties are being approached. Additionally, sII can be formed when gaseous methane mole fraction at equilibrium is between 75% and 99% at 274.2 K (Ballard and Sloan, 2000). These bounds represent the equilibrium conditions of a four-phase (sI-sII-Lw-V) system with one degree of freedom. Consequently, changing one intensive property such as temperature will also modify the conditions necessary for structure transitions (Kwon et al., 2014). Theoretically predicted by Hendriks et al. (Hendriks et al., 1996) and confirmed experimentally through NMR and Raman spectroscopy by Subramanian et al. (Subramanian et al., 2000), this transition can be explained by the type and ratio of cavities present in each structure (Ohno et al., 2009). One unit cell of structure I consists of two 5^{12} and six $5^{12}6^2$ cavities (big cavity/ small cavity ratio of 3) while one unit cell of structure II consists of sixteen 5^{12} and eight $5^{12}6^4$ (big cavity/ small cavity ratio of 0.5). As a larger molecule, ethane prefers bigger cavities present in higher ratio per unit cell in sI. The 5^{12} cavity present in both sI and sII is too small for ethane but can be stabilize by methane, a smaller molecule. As a mixture, these two gases have the ability to form structure II when methane is predominant in the gas phase as a higher ratio of 5^{12} cages in sII favours for the abundant methane molecules while ethane present to a lesser extent, can stabilize the remaining larger $5^{12}6^4$ cavities.

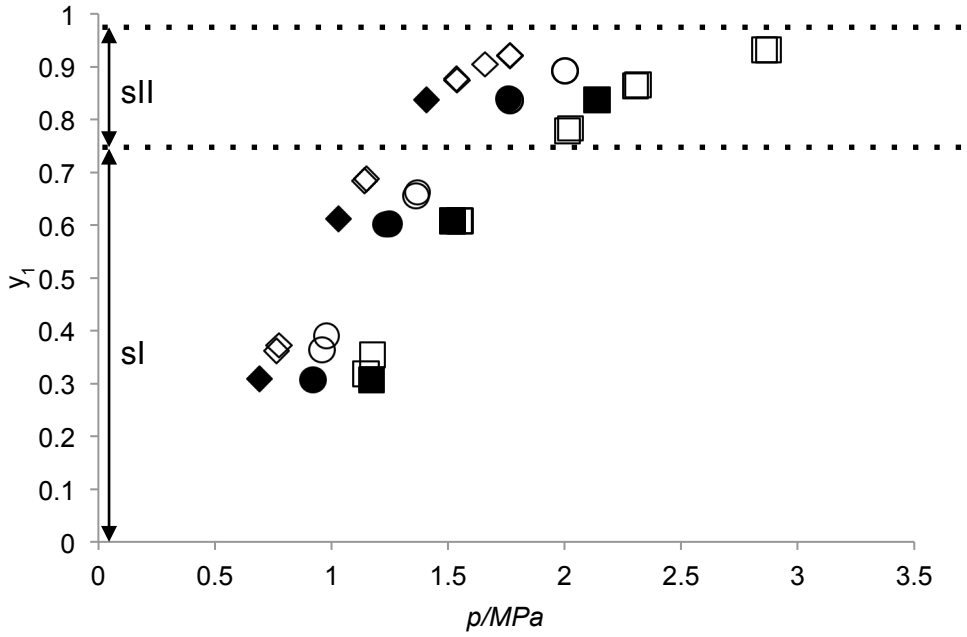

Figure 5.1: Gaseous equilibrium mole fraction of methane under H-Lw-V for the CH_4+C_2H_6+H_2O system: ◇, this work at 275 K; ◆, Bruusgaard et al. at 275 K; ○, this work at 277 K; ●, Bruusgaard et al. at 277 K; □, this work at 279 K; ■, Bruusgaard et al. at 279 K. Structure transitions showed are at 274.2 K (Ballard and Sloan, 2000).

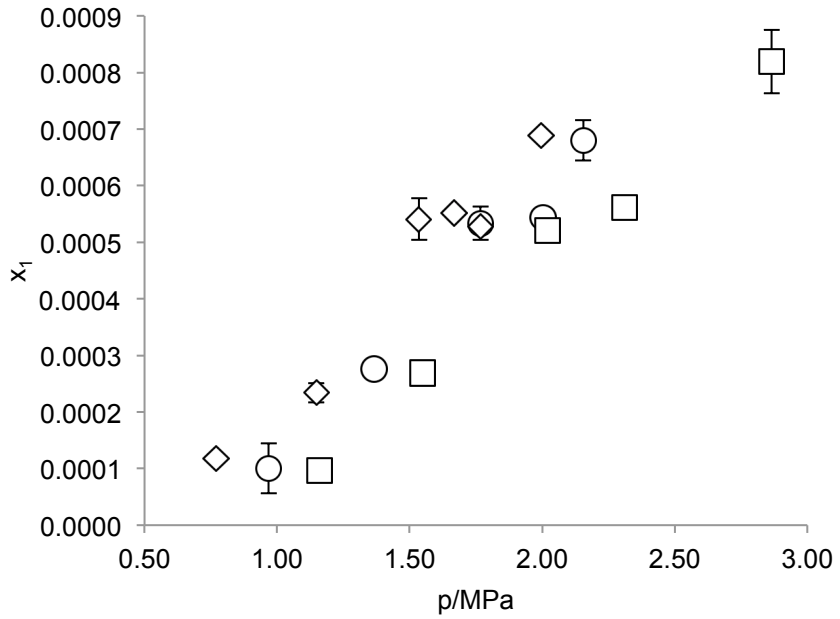

Figure 5.2: Methane solubility under H-Lw-V equilibrium for the CH_4+C_2H_6+H_2O system. ◇, this work at 275 K; ○, this work at 277 K; □, this work at 279 K.

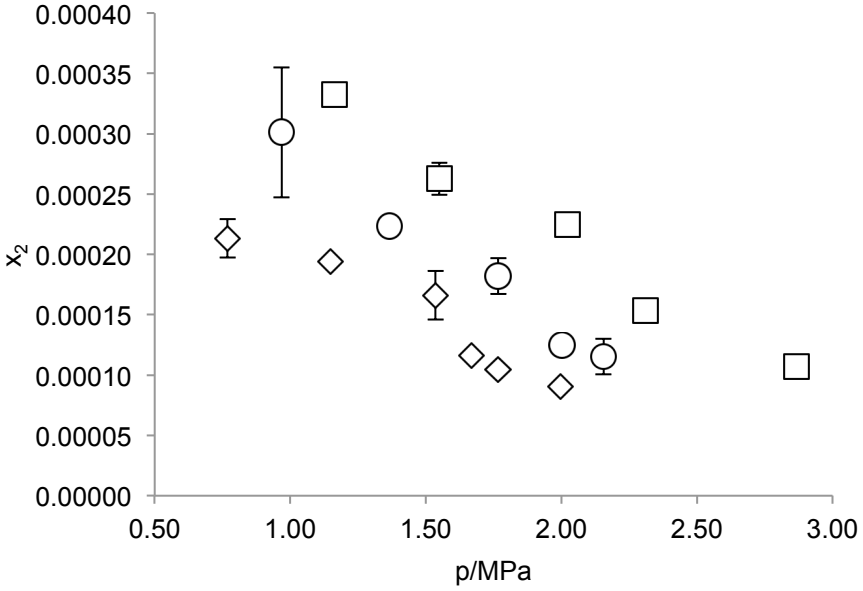

Figure 5.3: Ethane solubility under H-Lw-V equilibrium for the CH_4+C_2H_6+H_2O system. ◇, this work at 275 K; ○, this work at 277 K; □, this work at 279 K

As this structure transition is dictated by gaseous mole fractions, solubility results were plotted against gas phase composition depicted by Figure 5.4 and 5.5. It can be observed more clearly that the structure change coincides with a shift in the trends. It should also be noted that experimental equilibrium conditions close to this transition means that both sI and sII could have been present during sampling. In this case, it is possible that the two structures are at equilibrium or that one of them is in a metastable state. As the type of structures cannot be identified nor controlled with the current setup, this explains why certain solubility measurements localized near the sI-sII equilibrium could not be accurately replicated.

As mentioned earlier, the ratio of enclathrated methane and ethane gas will change depending on the type of structure as each has different cage occupancy. Fundamentally, if the gases mole fractions in the solid phase change, the mole fraction in both the liquid and gas phase should shift accordingly. It should be noted that this fact is not apparent in the obtained gas equilibrium mole fraction results. This is justified by the fact that both methane and ethane are present in extremely low quantities in the liquid phase compared to the gas phase at equilibrium. This would explain why they are more subject to change if a structure transition occurs.

By comparing the trends in Figures 5.4 and 5.5 it can be further observed that the structure transitions did have a more significant effect in the case of ethane. It should be reminded that as an equilibrium property, solubility is going to be affected by compositional changes in other phases. The composition of the hydrate phase, as non-stoichiometric, is often described in terms of cage occupancies; a ratio of filled cavities over the number of available ones. As a bigger molecule, ethane can only stabilize the larger cavity in sI ($5^{12}6^2$) and sII ($5^{12}6^4$). On the other hand, methane can fill the smaller cavity (5^{12}) of both structures while also stabilizing the remaining lager cavities.

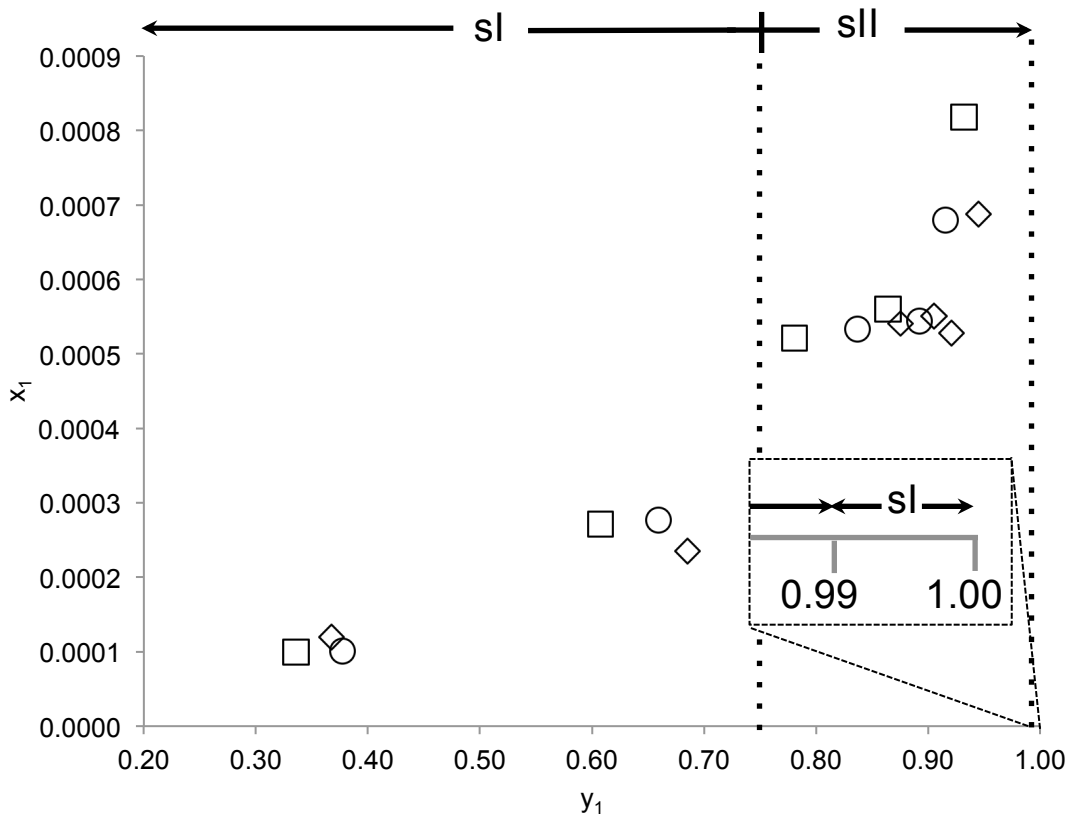

Figure 5.4: Liquid and gaseous mole fraction of methane at H-Lw-V equilibrium for the CH_4+C_2H_6+H_2O system. □, this work at 279 K; ○, this work at 277 K; ◇, this work at 275 K. Structure transitions showed are at 274.2 K (Ballard and Sloan, 2000).

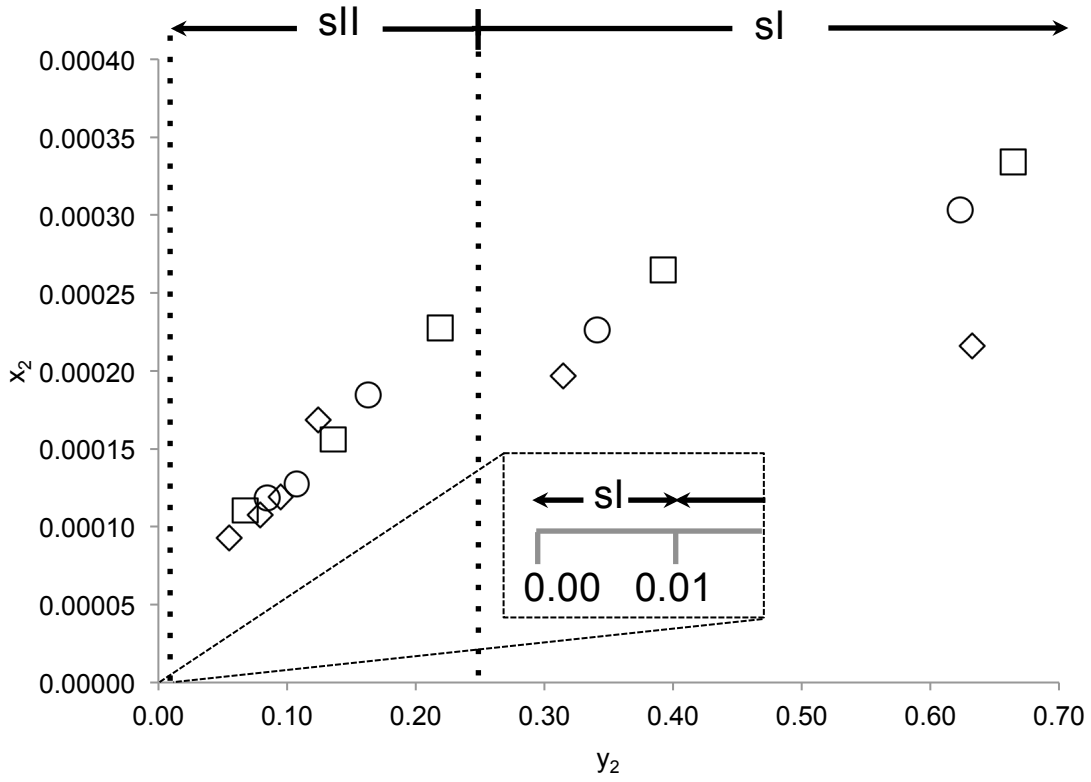

Figure 5.5: Liquid and gaseous mole fraction of ethane at H-Lw-V equilibrium for the CH_4+C_2H_6+H_2O system. ◇, this work at 275 K □; ○, this work at 277 K; this work at 279 K. Structure transitions showed are at 274.2 K (Ballard and Sloan, 2000).

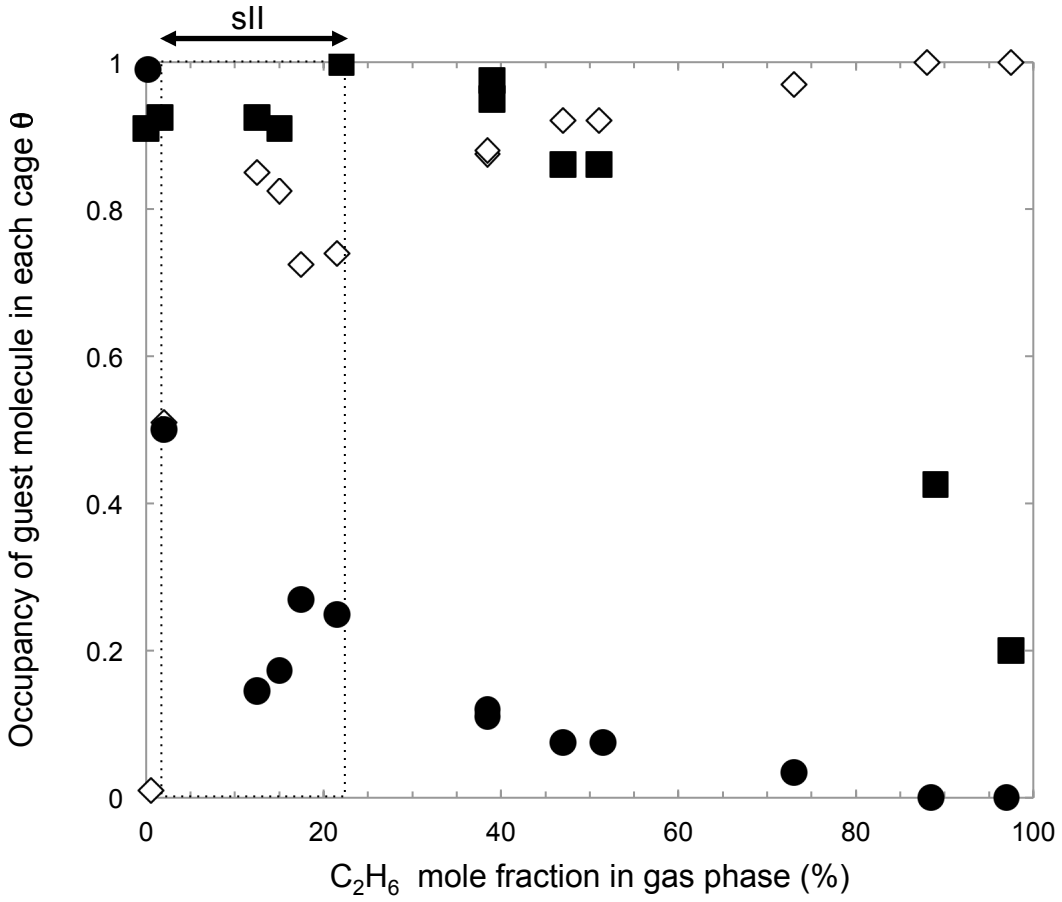

Figure 5.6: Adapted from Uchida et al. (Uchida et al., 2002). Cage occupancies of methane and ethane at 1.5 MPa and 258 K. ◇, cage occupancy of ethane; ■ , cage occupancy of methane in small cavity; ● , cage occupancy of methane in large cavity.

Through Raman spectroscopy, X-ray diffraction and gas chromatography, cage occupancy trends for the methane-ethane gas system were obtained for various gaseous mole fractions (Uchida et al., 2002) as illustrated by Figure 5.6. It was observed that the occupancy trend of methane in the small cage remained constant throughout the region associated with the structure II change. Conversely, the large cage occupancy trends of both methane and ethane see drastic changes over gas mole fractions associated with structure II. As ethane's presence in the hydrate phase is solely dependent on its presence in the large cavity, which is significantly affected by the structure change, this could explain why the ethane solubility trends, in comparison with methane, were more affected.

5.6 Conclusion

Solubility measurements of methane and ethane at H-Lw-V equilibrium were reported for the CH_4+C_2H_6+H_2O system. Experimental conditions ranged from 275.1 K to 279.1 K and 0.76 MPa to 2.87 MPa, respectively. In order to confirm that equilibrium was reached during sampling, gas phase compositions were compared to literature. The solubility trends obtained showed that decreasing pressures and increasing temperatures reduced the solubility of methane while increasing the solubility of ethane. A shift in those trends was observed which was localised near the conditions where structure change occurs. Due to these findings, it is therefore postulated that the type of structure present may have an effect on solubility.

Chapter 6

Bulk liquid and gas mole fraction during growth for the $CH_4+CO_2+H_2O$ system

6.1 Preface

This study shifts the focus from equilibrium to kinetics in order to obtain a broader understanding of multicomponent gas hydrate systems. Phase sampling during kinetic growth has been previously acquired for simple hydrate systems but never for mixtures. The methane and carbon dioxide mixture is chosen, as both components are critical to several gas hydrate applications. The goal of the study is to establish the time dependency of gas and liquid mole fractions once gas hydrate formation has commenced. Furthermore, liquid and gas mole fractions are obtained during the induction period. The addition of these experimental results gathered before the turbidity point will assist in determining the effect of hydrate formation on both the gas and liquid phases. Finally, mole consumption profiles were determined using a suitable equation of state.

6.2 Abstract

Gas and liquid mole fraction were experimentally obtained for the $CH_4+CO_2+H_2O$ system at four different time intervals during crystal growth. In order to validate the procedure, equilibrium mole fractions were also obtained and satisfactorily compared to literature values. Using a 70% CH_4 – 30% CO_2 loading composition in combination with a 1.6 MPa driving force at 274 K, results showed that both the liquid and gas mole fraction of methane and carbon dioxide

were independent of time during the early stages of growth. For comparison purposes, samples were also obtained during the induction period. After the nucleation event, methane liquid mole fractions dropped below induction values while no change was observed for carbon dioxide. It is therefore postulated that methane consumption is favored during the early stages of growth. The rates of crystal growth were acquired and in parallel with all other parameters obtained experimentally, were proven critical to understand multicomponent gas hydrate kinetics.

6.3 Introduction

Gas hydrates are the consequence of a phase change, resulting in a solid state where guest molecules become enclosed by three-dimensional water molecule structures. These cavities form through hydrogen bonding and only interact with their guest through weak van der Waals forces. Molecules capable of forming clathrates include methane, ethane, carbon dioxide, nitrogen as well as volatile liquids like neohexane (Sloan and Koh, 2008). As with any phase transition, thermodynamics dictate favorable conditions, which in the case of gas hydrates, are moderate temperatures and high pressures.

This crystalline compound has been recognized as a potential energy resource due to significant natural deposits in ocean seafloors and permafrost regions containing valuable hydrocarbons such as methane (Makogon, 1965). Conversely, they have also been showed to form inside natural gas pipelines, hindering flow assurance (Hammerschmidt, 1934). Kinetic and thermodynamic inhibitors were as a result, developed to prevent these masses from becoming safety concerns. As such, these inhibitors are applied in environments where not one but many gas components are present stressing the importance of multicomponent gas hydrate systems. Novel technologies are also being developed such as flue gas separation (Kang and Lee, 2000), carbon dioxide

sequestration (Lee et al., 2003; Yamasaki et al., 2000) and transportation of natural gas (Thomas, 2003); all examples of cases where several gas components populate systems.

Analogous to crystallization processes, gas hydrate formation requires the liquid phase to be supersaturated with a guest in order to provoke a nucleation event. Proposed by Bergeron and Servio, the driving force for hydrate growth for simple gas hydrate systems (one guest component) is described as the difference between the bulk liquid mole fraction *(x^B)* and the solubility *(x^{HL})* under two-phase H-Lw equilibrium, both at experimental temperature and pressure (Bergeron and Servio, 2009):

$$\frac{dn}{dt} = \frac{V_L \rho_w}{MW_w} \pi \mu_2 k_r \, (x^B - x^{HL}) \tag{6.1}$$

Where V_L is the volume occupied the solution, ρ_w the density of water, MW_w the molecular weight of water, μ_2 the second moment of the particle distribution (Kane et al., 1974) and k_r the intrinsic rate constant.

For this model to be established, several parameters were obtained experimentally, including bulk liquid mole fractions and mole consumption measurements *(dn/dt)* of systems using gases such as methane and carbon dioxide (Bergeron and Servio, 2009). The goal of this study is to extrapolate this work to multicomponent systems to build the foundation for future multicomponent kinetic models.

As both methane and carbon dioxide have been extensively investigated as simple hydrate systems due to their numerous applications including carbon dioxide sequestration, their mixture is a relevant selection for the proposed work. Kinetic studies on the CH_4+CO_2+H_2O system have already been documented

using gas chromatography, NMR and Raman spectroscopy but never through liquid mole fraction measurements during growth (Horvat et al., 2012; Rovetto, 2008; Uchida et al., 2005). To the best of our knowledge, this work represents the first attempt at characterizing the liquid phase of any multicomponent gas hydrate system through mole fraction measurements during growth. To complete the analysis, the gas phase is analyzed in parallel through gas chromatography. In addition, solubility measurements, bulk liquid phase mole fractions during induction as well as mole consumption trends are obtained.

6.4 Experimental Apparatus

The experimental apparatus used for this study is illustrated below by Figure 6.1. The stainless steel 316 crystallizer is equipped with two polycarbonate windows allowing for visual inspections. To indirectly control its temperature, it is submerged in a bath holding mixture of glycol-water; itself controlled by a Neslab RTE chiller. Three small gas cylinders are submerged which assist in providing isobaric conditions during kinetic experiments. The reservoir, set at a pressure above experimental conditions, provides gas through a Baumann 51000 Low Flow control valve. The two other cylinders serve as biases providing accurate pressure readings for both the reservoir and the crystallizer. To reduce heat and mass transfer limitations inside the crystallizer, magnetic stir bar is used which is spun by rotating magnets. In order for the experimental data to be comparable, only one single gas mixture with mole fractions of 0.70 for methane and 0.30 for carbon dioxide was chosen for the study, purchased from MEGS. Water previously treated by McGill University through reverse osmosis, was injected in the crystallizer with a positive displacement pump (Oilphase-DBR, Schlumberger). Less than 10 ppb of total organic content was present in the liquid while having a conductivity of 10 μS. Temperature and pressure readings were recorded through a National Instruments® data acquisition system. Omega

RTD probes (± 0.1 K) were used for temperature measurements while pressure was monitored via Rosemount pressure transducers with a span of 0-14 MPa and accuracy of ± 0.065% of the given span. Gas and liquid samples were extracted using sample cylinders purchased by Swaglok. In order to prevent the inclusion of hydrate particles during sampling, an in-line Norman filter was installed. Gaseous mole fractions were analyzed through a gas chromatography (Varian CP-3800) while a digital gasometer (Chandler Engineering) was used to evaluate the volumetric amount of gas dissolved in liquid samples.

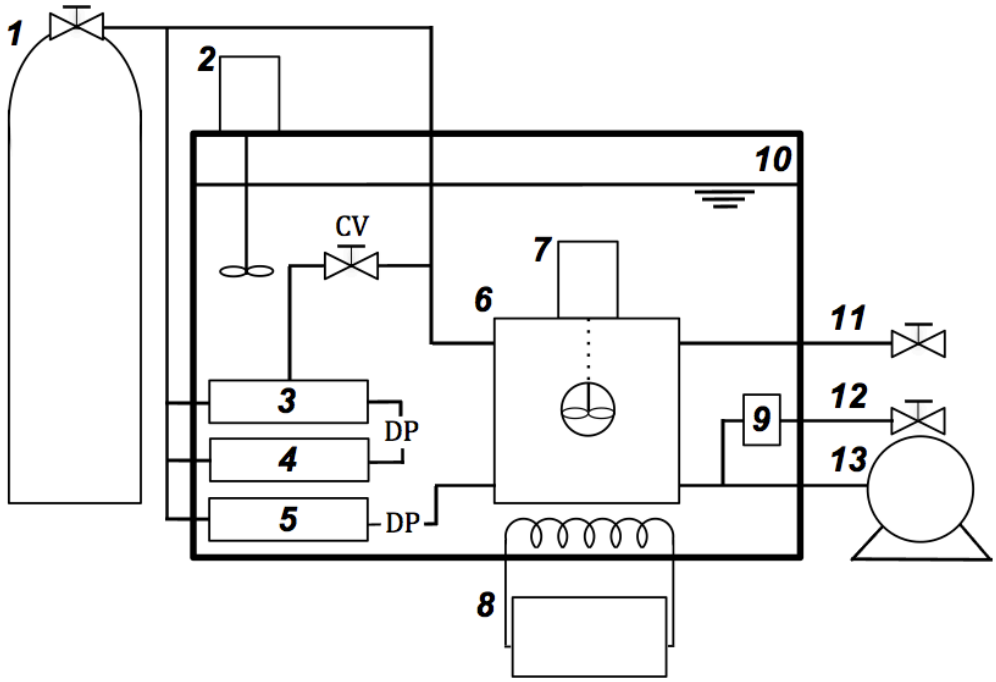

Figure 6.1: Experimental setup: (1) gas cylinder, (2) liquid bath stirrer, (3) reservoir, (4) reservoir bias, (5) crystallizer bias, (6) crystallizer, (7) crystallizer stirrer (8) chiller, (9) filter, (10) bath, (11) gas sampling port, (12) liquid sampling port (13) displacement pump.

6.5 Experimental Procedure

In order to provide insights into multicomponent gas hydrate kinetics, liquid and gas samples were extracted during hydrate growth at 0, 5, 10 and 15 minutes after nucleation. Additional samples were obtained during induction and at equilibrium. Three replicates per conditions were acquired where every single experiment yielded one liquid and one gas sampling. Hence, after each experiment, the crystallizer was emptied and the procedure described below was repeated.

For these results to be comparable and repeatable, experimental conditions during hydrate growth had to be kept constant in order to yield a constant driving force. In simple gas hydrate systems, typically temperature is controlled and pressure is kept constant at a certain value above the three-phase equilibrium line as illustrated by Figure 6.2. However, in a binary system, one more degree of freedom is present. Hence, a three-dimensional plane now represents all equilibrium conditions instead of a simple two-dimensional line, as illustrated by Figure 6.3. This means that in addition of having temperature constant, another variable has to be maintained for the experimental conditions to be locked in the same position above the equilibrium plane.

The gas phase composition was used as the additional intensive property. Although it cannot be used to define the two-phase H-Lw solubility, which would enable mole fraction driving force calculations, in this case it can be used to confirm consistent operating conditions during growth. This explains why gas phase compositions were obtained in parallel with liquid mole fractions measurements. In this work, operating conditions during hydrate growth were maintained at 3.9 MPa, 274 K and gas mole fractions of 0.8 for methane and 0.2 for carbon dioxide. These operating conditions are 1.6 MPa higher than the location on the three-phase equilibrium that shares the same temperature and

gas phase composition as illustrated by Figure 6.3. Solubility measurements were obtained at 274 K and 2.3 MPa. Since these were already experimentally obtained in literature, they served to validate the procedure.

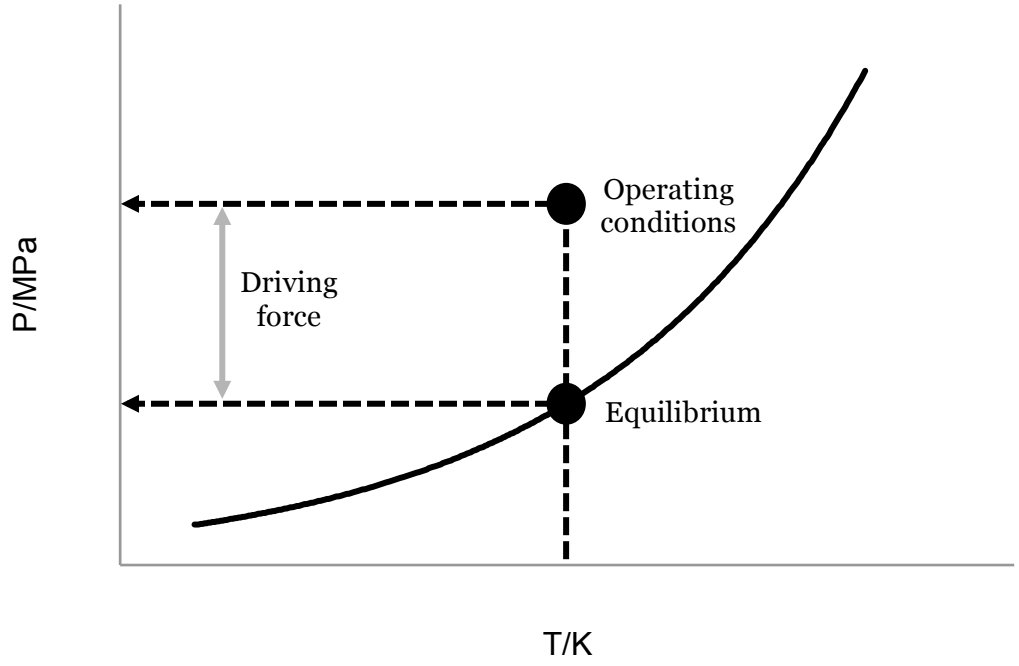

Figure 6.2: Driving force example for simple hydrate system kinetic experiments.

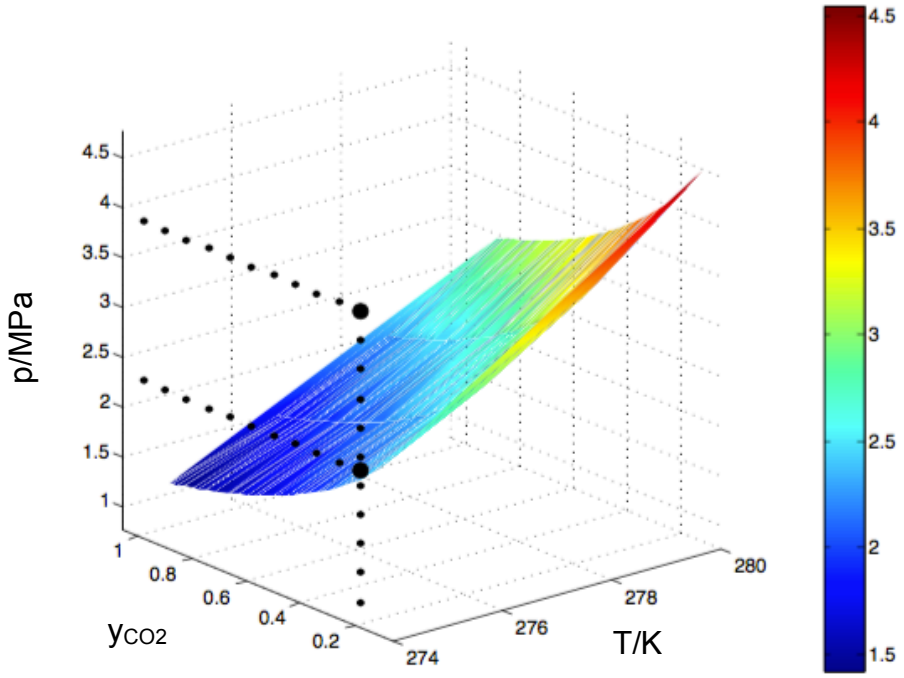

Figure 6.3: Equilibrium plane for the CH_4+CO_2+H_2O system under H-Lw-V equilibrium. This simulation made use of the Trebble-Bishnoi equation of state (Trebble and Bishnoi, 1987, 1988). The upper point represents operating conditions for kinetics run while the other the equilibrium point that shares the same temperature and gas phase composition. Solubility measurements were obtained under theses conditions.

6.5.1 Mole fractions during growth

The crystallizer was first purged of impurities by increasing its internal pressure to about 1 MPa three times with a mixture of 70% methane and 30% carbon dioxide. Approximately 300 cm^3 of purified water was then inserted in the crystallizer. Once the desired temperature of 274 K was achieved, the pressure was increased to 3.9 MPa; a value 1.6 MPa higher than the known equilibrium of 2.3 MPa. The control valve was setup to maintain the same pressure differential throughout the experiment. Once the stirrer inside the crystallizer was activated, the temperature was monitored. A sudden increase revealed the formation of hydrates. Time was then carefully monitored to ensure proper sampling after the turbidity point. As three replicates per time conditions of 0, 5, 10 and 15 minutes after nucleation were performed, a total of twelve separate experiments were undertaken.

The procedure to obtain gaseous and liquid compositions previously described in this thesis in Chapter 4 was followed. Briefly, both gas and liquid samples were collected using sample cylinders of approximately 25 cm^3 purchased from Swaglock. Gas mole fractions were directly obtained from gas chromatography. Liquid sample cylinders were weighted before and after sampling to determine the amount of water present. They were then left to equilibrate to room temperature and pressure while connected to a gasometer. The volumetric amount of gas was recorded and later analyzed through gas chromatography. Combined with an equation of state, these values resulted in the calculation of liquid mole fractions.

6.5.2 Mole fractions during induction

This procedure is identical to the one described above except samples were not taken after nucleation but 50 minutes after the stirred was activated. In cases where the nucleation event occurred before the 50-minute mark, the crystallizer was emptied and the procedure reinitiated. Gas and liquid samples were extracted and analyzed as described in the procedure above. Three replicates were obtained.

6.5.3 Solubility measurements

In this case, the crystallizer was set at the same temperature (274 K) and pressure (3.9 MPa) using the same loading compositions (70% methane and 30% carbon dioxide). However, the control valve was not active and as such, pressure declined from the moment the stirrer was activated until equilibrium was reached. Once temperature and pressure were stable for a minimum of one hour, gas and liquid samples were extracted and analyzed as described above. Two replicates were obtained and the same procedure to obtain liquid and gas mole fractions was followed.

6.6 Results and Discussion

6.6.1 Solubility results

Liquid and gas mole fractions at H-Lw-V equilibrium were experimentally obtained for the methane-carbon dioxide-water system at 274.1 K using a loading composition of 70 % methane and 30% carbon dioxide. As the chosen system has two degrees of freedom per Gibbs phase rule, two intensive properties must be controlled and a third reported to confirm equilibrium. Pressure, temperature and gas phase compositions respectively fill these roles, which can be found in

Table 6.1 below. These parameters have already been reported in literature and were found to agree with the results obtained in this work as illustrated by Figure 6.4, 6.5 and 6.6. This confirms the validity of the procedure for gas and liquid phase sampling that will be subsequently used for kinetic experiments. Furthermore, it establishes the target temperature and gas mole fractions that will be necessary during kinetic experiments in order to claim a pressure differential between the equilibrium and kinetic operating conditions.

Table 6.1: Experimental Values of Temperature *T*, Pressure *p*, Liquid Mole Fraction *x* and Gas Mole Fraction *y* for the CH_4+CO_2+H_2O Mixture at H-Lw-V Equilibrium[α]

T/K	p/MPa	x_{CH4}	x_{CO2}	y_{CO2}
274.1	2.27	0.000757	0.00498	0.198
274.1	2.31	0.000775	0.00467	0.191

[α] Standard uncertainties *u* are *u(T)* = 0.1 K, *u(p)* = 0.03 MPa, $u(y_{CO2})$ = 0.005 and the combined expanded uncertainty U_c is $U_c(x_{CH4})$ = 0.0000502 and $U_c(x_{CO2})$ = 0.0000563 (coverage factor k = 2).

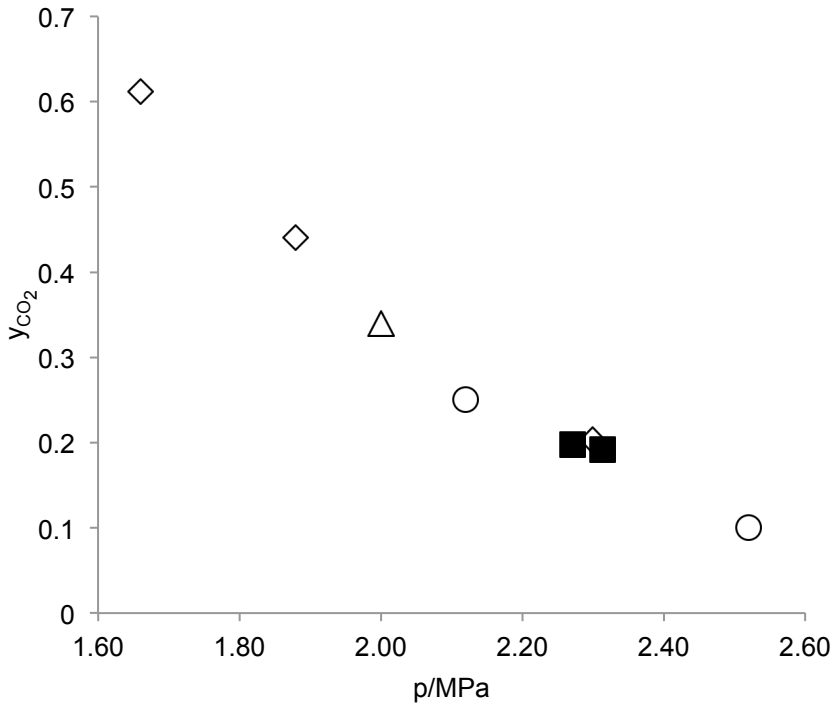

Figure 6.4: H-Lw-V equilibrium for the CH_4+CO_2+H_2O system. ◇, (Bruusgaard et al., 2010a) at 274.0 K and 274.1 K; △, (Seo and Lee, 2001) at 274.2 K; ○, (Adisasmito et al., 1991) at 273.7 K and 273.8 K; ■, this work at 274.1 K.

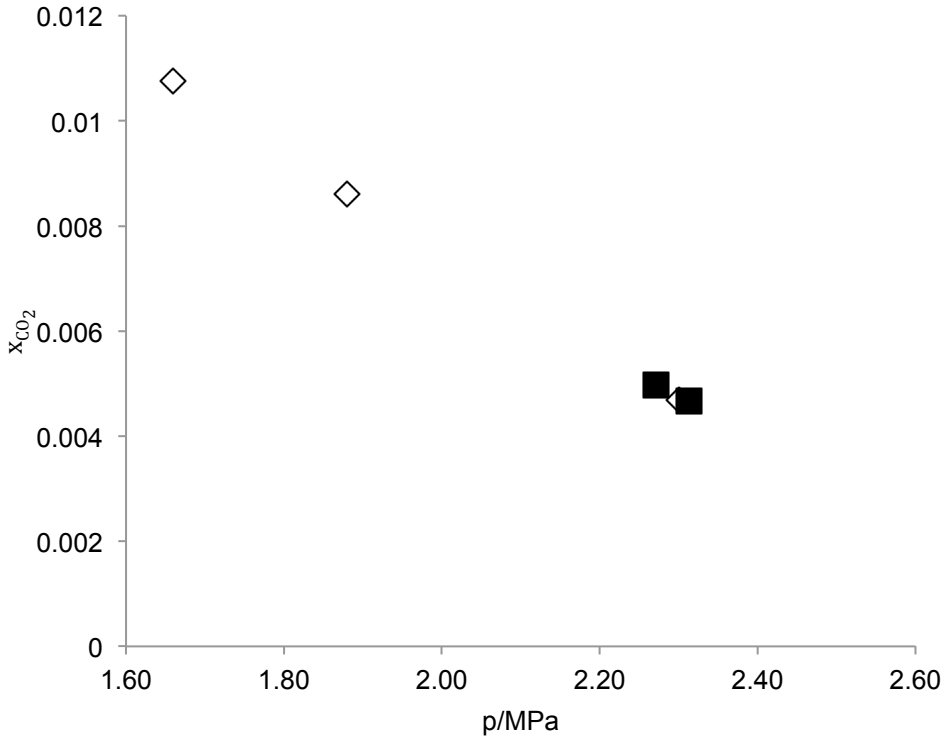

Figure 6.5: Carbon dioxide solubility at H-Lw-V equilibrium for the CH_4+CO_2+H_2O system. ◇, (Bruusgaard et al., 2010a) at 274.0 K and 274.1 K; ■, this work at 274.1 K.

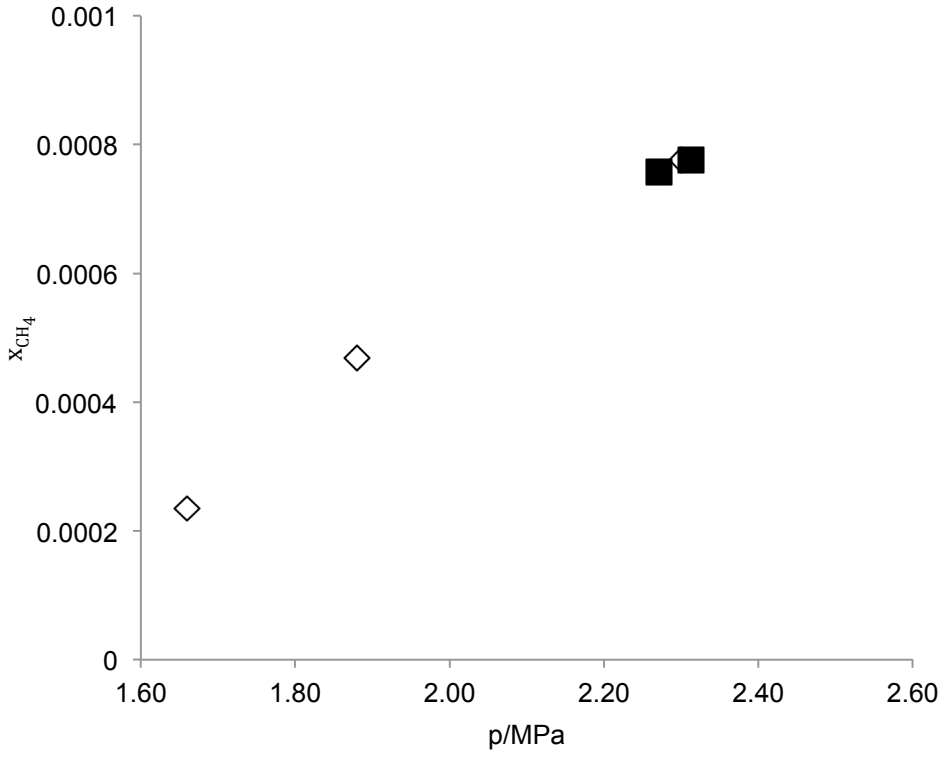

Figure 6.6: Methane solubility at H-Lw-V equilibrium for the CH_4+CO_2+H_2O system. ◇, (Bruusgaard et al., 2010a) at 274.0 K and 274.1 K; ■, this work at 274.1 K.

6.6.2 Gas and liquid mole fractions

Liquid and gas mole fractions were experimentally obtained during induction and growth using a 70% methane - 30% carbon dioxide loading mixture at 274.1 K and pressures approximately 1.6 MPa higher than the values obtained at equilibrium. The results displayed by Table 2 below show three replicates per conditions were performed. Due to the stochastic nature of nucleation, replicates of mole fractions obtained during growth experiments under similar conditions will not necessarily yield the same gas consumption as a result of induction time variations. For both induction and growth experiments, pressure and temperature in Table 2 represents the average pressure maintained by the control valve throughout growth and the temperature during sampling, respectively. The purpose of restricting the experiments to a maximum of fifteen minutes is to ensure negligible heat and mass transfer limitations during growth.

All temperatures during growth are reported above 274.1 K due to hydrate formation being an exothermic process. To ensure this does not have a significant effect, two experiments performed 15 minutes after nucleation are obtained with lower initial temperatures for comparison purposes. It can be observed in Table 2 that the small temperature variation on liquid mole fractions is negligible.

In order to locate the experimental conditions above the equilibrium plane, three intensive properties needs to be reported. Furthermore, to analyze the evolution of the results through time, all these parameters need to be consistent. As pressure and temperature were controlled, it is clear from Table 2 that these properties were independent of time. Conversely, the gaseous mole fractions (displayed by Figure 6.7) could not be controlled and varied on average by 4.4 %. Hence, it can be concluded that all experiments were conducted under similar conditions; at a pressure 1.6 MPa greater than solubility measurements, which share the same temperature and gas mole fraction.

Table 6.2: Experimental Values of Time, Temperature *T*, Pressure *p*, Liquid Mole Fraction *x* and Gas Mole Fraction *y* for the CH_4+CO_2+H_2O mixture during induction (IND) and growth[a].

Time/min	*T/K*	p/MPa	x_{CH_4}	x_{CO_2}	y_{CO_2}
IND	274.0	3.90	0.00119	0.00710	0.185
IND	274.1	3.91	0.00120	0.00699	0.189
IND	274.1	3.90	0.00117	0.00711	0.186
0	274.3	3.90	0.000577	0.00692	0.213
0	274.3	3.91	0.000581	0.00674	0.212
0	274.3	3.92	0.000562	0.00696	0.203
5	274.3	3.90	0.000530	0.00712	0.197
5	274.4	3.91	0.000551	0.00706	0.213
5	274.4	3.91	0.000551	0.00705	0.200
10	274.4	3.90	0.000535	0.00713	0.217
10	274.4	3.90	0.000542	0.00731	0.209
10	274.3	3.89	0.000599	0.00655	0.195
15	274.4	3.91	0.000542	0.00697	0.193
15	274.2	3.91	0.000557	0.00687	0.210
15	274.2	3.91	0.000571	0.00673	0.201

[a] Standard uncertainties *u* are *u(T)* = 0.1 K, *u(p)* = 0.03 MPa, $u(y_{CO_2})$ = 0.005 and the combined expanded uncertainty U_c is $U_c(x_{CH_4})$ = 0.0000693 and $U_c(x_{CO_2})$ = 0.0000789 (coverage factor k = 2).

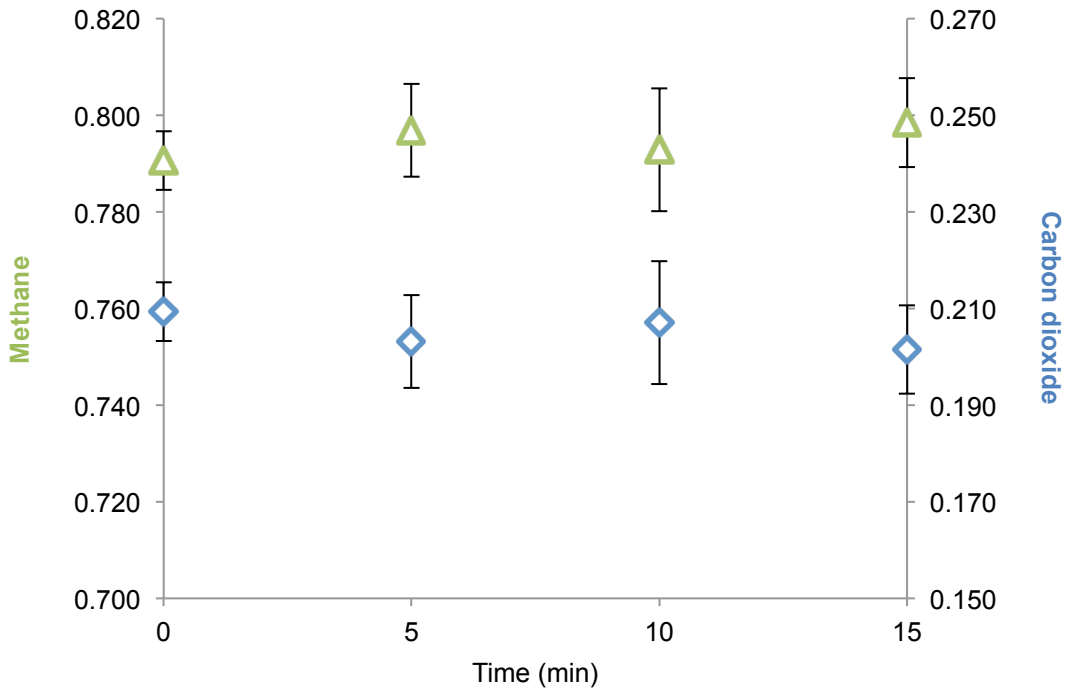

Figure 6.7: Gas phase composition variation with time. Green: methane, left y-axis; Blue: carbon dioxide, right left y-axis.

Methane and carbon dioxide liquid mole fractions during the early stages of growth were already reported in literature for both methane-water and carbon dioxide-water system. It was revealed that in both cases, bulk liquid mole fractions did not change significantly with time in the early stage of growth; thus maintaining a constant driving force ($x^{B} - x^{HL}$) (Bergeron and Servio, 2009). The same observation can be made for the binary mixture as liquid mole fractions of the methane-carbon dioxide-water system displayed by Figure 6.8 and 6.9 show that liquid compositions are independent of time. Methane and carbon dioxide mole fractions vary on average by 3 and 2.3 %, respectively.

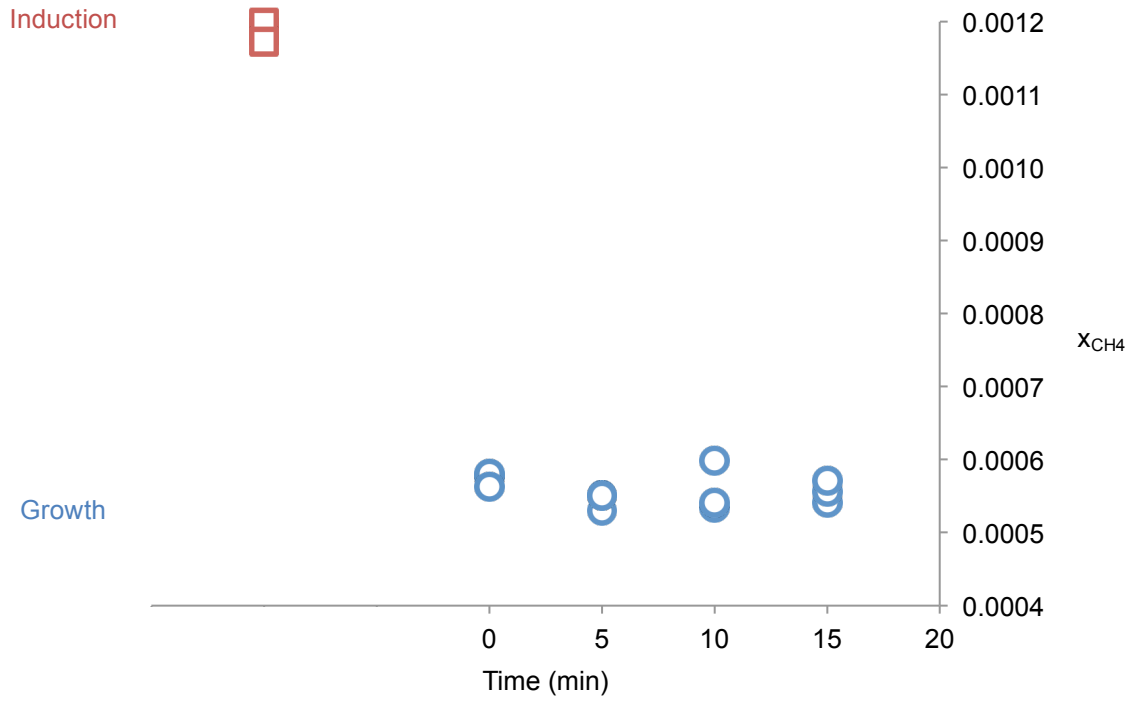

Figure 6.8: Methane bulk liquid mole fraction during induction and growth for the CH_4+CO_2+H_2O system.

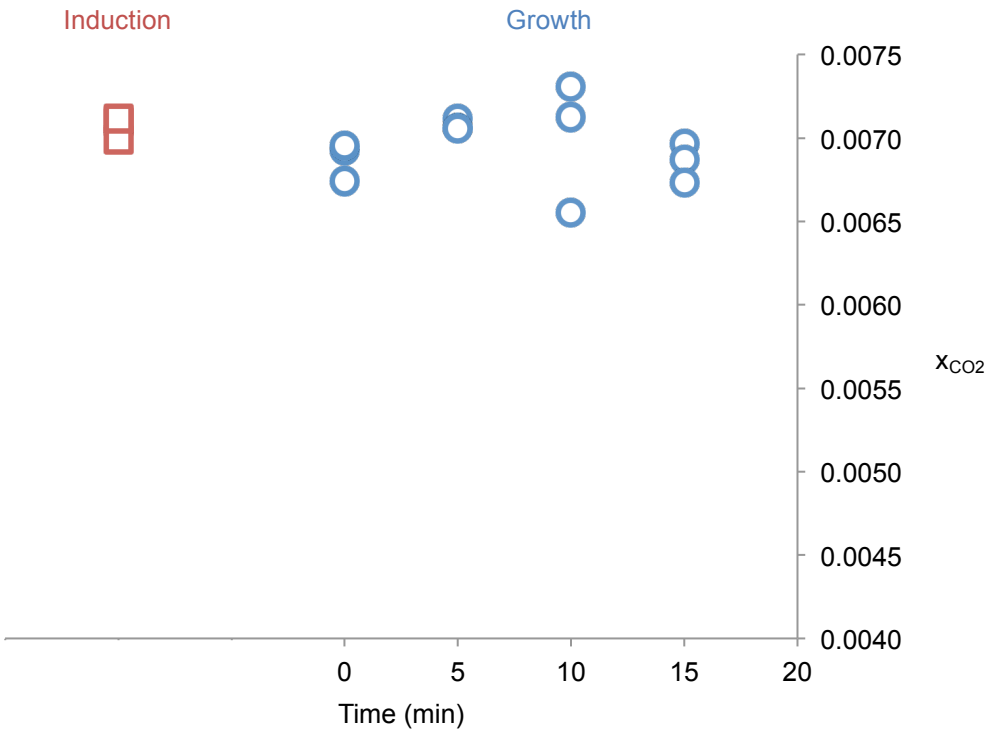

Figure 6.9: Carbon dioxide bulk liquid mole fractions during induction and growth for the CH_4+CO_2+H_2O system.

Comparing bulk liquid mole fractions before (induction) and after nucleation (growth) reveals that carbon dioxide liquid mole fractions remained mostly stable with a 1.7 % reduction on average, while methane experienced a drop of 112.5%. In simple hydrate systems, the gas presence in the liquid phase decreases past the nucleation event due to the fact that hydrate phase requires a significant amount of gas. Hence, these results suggest that carbon dioxide does not participate in the hydrate formation as much as methane during the early stages of growth.

Similar observations were made by Uchida who investigated the evolution of both gas and solid phase for the methane-carbon dioxide-water system through gas chromatography and Raman spectroscopy over multiple gas phase compositions (Uchida et al., 2005). More specifically, it was concluded that in environments where carbon dioxide is abundantly present in the gas phase (y_{CH_4}/y_{CO_2} ratio lower than 0.3), methane only is consumed during hydrate growth. Although work on methane rich mixtures was not experimentally attempted, it was theorized that methane would not be preferentially consumed in the early stages of growth in such cases. As the results obtained in this study were obtained using a y_{CH_4}/y_{CO_2} ratio of 4, it can be concluded that the preferred consumption of methane is possible in both methane and carbon dioxide rich environments. This is also in agreement with another study which established through gas chromatography that methane is preferentially consumed in methane rich environments for $CH_4+CO_2+H_2O$ systems (Horvat et al., 2012).

This short-term kinetic effect could be linked to the formation of cage-like structures during gas dissolution, prior to the nucleation event (Uchida et al., 2005; Uchida et al., 1997). As methane produces more of these structures than carbon dioxide, it can more readily form hydrate structures (Ben-Naim, 1980). Furthermore, since methane preferentially fills the 5^{12} cavity (which is the smallest and simplest of hydrate cavities) in mixtures, it was proposed that the 5^{12}

cage-like structure is the precrystallization state that induces hydrate formation (Uchida et al., 2005). Molecular dynamic simulations support this theory; models generated concluded that regardless of the size the guest, the 5^{12} cage (whether filled or empty) is consistently the dominant cavity through which the critical nucleus is formed (Jacobson et al., 2010).

6.6.3 Molar consumption

Since both pressure and temperature were experimentally maintained, the corresponding two-phase solubility (H-Lw) under growth conditions would be locked for a simple hydrate system. Due to the fact that two gas components populate the system, an additional degree of freedom is present. Hence, the corresponding two-phase solubilities of each gas component could not be kept constant. Because of this, it cannot be deduced that the driving forces for hydrate growth ($x^{B} - x^{HL}$ for both methane and carbon dioxide) are independent of time even if bulk liquid mole fractions were shown to be constant in the previous section.

However, molar consumption of the guest gases can provide meaningful insights into gas hydrate kinetics. This trend can be verified experimentally as pressure changes in the reservoir were monitored throughout the experiment. Given the mole fraction inside the reservoir is known (70-30), the amount of moles consumed can be readily computed using an equation of state. In this case, the Trebble-Bishnoi equation of state for mixtures (Trebble and Bishnoi, 1988) was utilized to compute the overall mole consumption profiles of each of the 15 minutes experiment. Figure 6.10 illustrates the results.

It can be observed that each of the three profiles exhibits a linear relationship with time. The dependency on time for each profile can be linearly regressed with an R-squared value over 99.9 %. The slopes obtained were consistent; the average slope was found to be 2.17×10^{-5} moles/s while having a

standard deviation of 4.83 $\times 10^{-7}$ moles/s. The find of a constant molar consumption combined with the fact that constant bulk liquid mole fractions were present for CH_4+CO_2+H_2O system, yields the conclusion that the combination of all other parameters in a future multicomponent kinetic gas hydrate model would then also have to be independent of time.

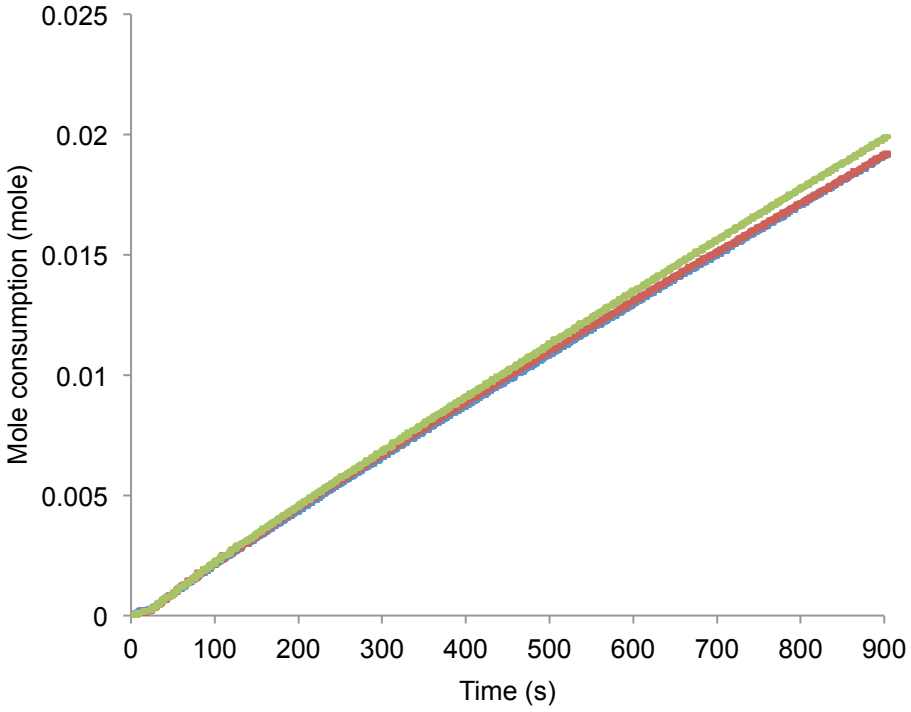

Figure 6.10: Overall mole consumption profiles for the first fifteen minutes of growth for the CH_4+CO_2+H_2O system at 274.1 K and 3.9 MPa.

6.7 Conclusion

Bulk liquid mole fractions were obtained during the early stages of growth for the CH_4+CO_2+H_2O using operating conditions of 274.1 K and 3.9 MPa and a loading composition of 70% CH_4 and 30 % CO_2. It was revealed that liquid and gas mole fractions were relatively stable with time. While the mole fraction of methane reduced significantly past the nucleation event, negligible change was observed for carbon dioxide before and after the turbidity point. This is believed to be a short-term kinetic effect where methane is preferentially consumed at the early stages of growth. Overall crystal growth rates were computed as pressure fluctuations in the reservoir were converted into moles through an equation of state. The obtained growth rates were found linear with time. The fact that experimental conditions, bulk liquid mole fractions as well molar consumption rates during growth were held constant suggests that the combination of all parameters included in a future multicomponent growth model would have to be independent of time as well. These experimental results will serve as the foundation for potential multicomponent kinetic models.

Chapter 7

Thesis conclusion and future work recommendations

7.1 Comprehensive conclusion

The critical role of equilibrium mole fractions in gas hydrate modeling was first established through Chapter 4. Through several two-phase and three-phase simulations, it was clearly illustrated that the assessments of models with vapor phase data only were erroneous. The addition of solvent-solute interactions, in comparison with the gas phase, is the reason behind the complexity of modeling the liquid phase. For this reason, future gas hydrate models should evaluate the accuracy of solubilities and not equilibrium gas mole fractions.

Chapter 5 and 6 focused on the acquisition of experimental solubilities and equilibrium gas mole fractions of the N_2+CO_2+H_2O and CH_4+CO_2+H_2O system. In addition of being both industrially relevant, each system has the ability to form either sI or sII depending on the ratio of gas present. Solubility isotherm trends were obtained for both systems in regions where sI and sII were thermodynamically favorable. It was demonstrated that the structure transition affected solubility isotherm trends. This novel find can be explained by the fact that each structure holds a different ratio of guest component. If different guest mole fractions are present in the solid phase, the mole fractions in the other phases should also be influenced.

Lastly, Chapter 7 concentrated on the kinetics of the CH_4+CO_2+H_2O system in methane rich environments. Gas and bulk liquid mole fractions were obtained during the first fifteen minutes of crystal growth during which experimental conditions were maintained constant. Both methane and carbon dioxide bulk liquid mole fractions were found independent of time. Mole consumption profiles were also obtained and had a linear relationship with time. These two findings are instrumental for future multicomponent gas hydrate models as it is now established that the combination of all other parameters need to be independent of time as well. Additionally, bulk liquid mole fractions were also acquired prior to the nucleation event, during the induction period. Methane bulk liquid mole fractions during the induction period were significantly higher than ones recorded during growth. Conversely, carbon dioxide bulk mole fractions remained relatively constant from induction to growth. This suggests the preferential consumption of methane during the early stages of growth in methane rich environments.

7.2 Future work recommendations

The author recommends the following studies, as they would directly compliment the work presented:

- Model solubility trends for the N_2+CO_2+H_2O and CH_4+C_2H_6+H_2O system in thermodynamic regions favoring sI and sII.

- Acquire bulk liquid mole fractions of systems with structure transition by performing kinetic experiment on the N_2+CO_2+H_2O and CH_4+C_2H_6+H_2O system under conditions favorable to sI and sII.

-Investigate other binary systems to study the preferential consumption of methane.

Bibliography

Aaron, D., and Tsouris, C. (2005). Separation of CO2 from flue gas: a review. *Sep. Sci. Technol.* **40**, 321-348.

Adisasmito, S., Frank, R. J., and Sloan, E. D. (1991). Hydrates of carbon dioxide and methane mixtures. *Journal of Chemical & Engineering Data* **36**, 68-71.

Avlonitis, D., Danesh, A., and Todd, A. C. (1994). Prediction of VL and VLL equilibria of mixtures containing petroleum reservoir fluids and methanol with a cubic EoS. *Fluid Phase Equilibria* **94**, 181-216.

Ballard, A. L., and Sloan, E. D., Jr. (2000). Structural transitions in methane + ethane gas hydrates. Part II: modeling beyond incipient conditions. *Chem. Eng. Sci.* **55**, 5773-5782.

Belandria, V., Eslamimanesh, A., Mohammadi, A. H., and Richon, D. (2011). Gas Hydrate Formation in Carbon Dioxide + Nitrogen + Water System: Compositional Analysis of Equilibrium Phases. *Industrial & Engineering Chemistry Research* **50**, 4722-4730.

Beltran, J. G., Bruusgaard, H., and Servio, P. (2012). Gas hydrate phase equilibria measurement techniques and phase rule considerations. *J. Chem. Thermodyn.* **44**, 1-4.

Benesh M.E. (1942) The use of gas hydrates in improving the load factor of gas supply systems, United States Patent Office, 2270016

Ben-Naim, A. (1980). "Hydrophobic Interactions," Plenum Press, New York.

Bergeron, S., Beltrán, J. G., Macchi, A., and Servio, P. (2010). Theoretical pressure dependency of carbon dioxide solubility under hydrate–liquid water equilibrium. *The Canadian Journal of Chemical Engineering* **88**, 307-311.

Bergeron, S., Beltrán, J. G., and Servio, P. (2009). Reaction rate constant of methane clathrate formation. *Fuel* **89**, 294-301.

Bergeron, S., and Servio, P. (2008). Reaction rate constant of CO2 hydrate formation and verification of old premises pertaining to hydrate growth kinetics. *AIChE Journal* **54**, 2964-2970.

Bergeron, S., and Servio, P. (2009). CO2 and CH4 mole fraction measurements during hydrate growth in a semi-batch stirred tank reactor and its significance to kinetic modeling. *Fluid Phase Equilib.* **276**, 150-155.

Bishnoi, P. R., Gupta, A. K., Englezos, P., and Kalogerakis, N. (1989). Multiphase equilibrium flash calculations for systems containing gas hydrates. *Fluid Phase Equilib.* **53**, 97-104.

Bishnoi, P. R., and Natarajan, V. (1996). Formation and decomposition of gas hydrates. *Fluid Phase Equilibria* **117**, 168-177.

Brewer, P. G., Friederich, G., Peltzer, E. T., and Orr, F. M. (1999). Direct Experiments on the Ocean Disposal of Fossil Fuel CO2. *Science* **284**, 943-945.

Bruusgaard, H., Beltran, J. G., and Servio, P. (2008). Vapor-Liquid Water-Hydrate Equilibrium Data for the System N2 + CO2 + H2O. *J. Chem. Eng. Data* **53**, 2594-2597.

Bruusgaard, H., Beltran, J. G., and Servio, P. (2010a). Solubility measurements for the CH4 + CO2 + H2O system under hydrate-liquid-vapor equilibrium. *Fluid Phase Equilib.* **296**, 106-109.

Bruusgaard, H., Carbone, A., and Servio, P. (2010b). H-LW-V Equilibrium Measurements for the CH4 + C2H6 + H2O Hydrate Forming System. *J. Chem. Eng. Data* **55**, 3680-3683.

Bruusgaard, H., and Servio, P. (2011). Prediction of methane and carbon dioxide solubilities for the CH4+CO2+H2O system under hydrate-liquid-vapor equilibrium. *Fluid Phase Equilibria* **305**, 97-100.

Chazallon, B., and Kuhs, W. F. (2002). In situ structural properties of N2-, O2-, and air-clathrates by neutron diffraction. *J. Chem. Phys.* **117**, 308-320.

Clennell, M. B., Hovland, M., Booth, J. S., Henry, P., and Winters, W. J. (1999). Formation of natural gas hydrates in marine sediments: 1. Conceptual model of gas hydrate growth conditioned by host sediment properties. *Journal of Geophysical Research: Solid Earth* **104**, 22985-23003.

Davidson, D. W., Handa, Y. P., Ratcliffe, C. I., Tse, J. S., and Powell, B. M. (1984). The ability of small molecules to form clathrate hydrates of structure II. *Nature* **311**, 142-143.

Davy, H. (1811). The Bakerian Lecture: On Some of the Combinations of Oxymuriatic Gas and Oxygene, and on the Chemical Relations of These Principles, to Inflammable Bodies. *Philosophical Transactions of the Royal Society of London* **101**, 1-35.

Dean, J. A. (1992). "Lange's Handbook of Chemistry, Fourteenth Edition," McGraw-Hill.

Deaton, W. M., and Frost, E. M., Jr. (1946). Gas hydrates and their relation to the operation of natural-gas pipe lines. *U.S. Bur. Mines, Monograph* **8**, 101 pp.

Diamond, L. W. (1994). Salinity of multivolatile fluid inclusions determined from clathrate hydrate stability. *Geochimica et Cosmochimica Acta* **58**, 19-41.

Englezos, P. (1993). Clathrate hydrates. *Industrial and Engineering Chemistry Research* **32:7**, 1251-1274.

Englezos, P., Kalogerakis, N., Dholabhai, P. D., and Bishnoi, P. R. (1987). Kinetics of formation of methane and ethane gas hydrates. *Chem. Eng. Sci.* **42**, 2647-58.

Eslamimanesh, A., Babaee, S., Gharagheizi, F., Javanmardi, J., Mohammadi, A. H., and Richon, D. (2013). Assessment of clathrate hydrate phase equilibrium data for CO2 + CH4/N2 + water system. *Fluid Phase Equilibria* **349**, 71-82.

Eslamimanesh, A., Mohammadi, A. H., Richon, D., Babaee, S., and Javanmardi, J. (2012a). Experimental data assessment test for composition of vapor phase in equilibrium with gas hydrate and liquid water for carbon dioxide + methane or nitrogen + water system. *Ind. Eng. Chem. Res. Industrial and Engineering Chemistry Research* **51**, 3819-3825.

Eslamimanesh, A., Mohammadi, A. H., Richon, D., Naidoo, P., and Ramjugernath, D. (2012b). Application of gas hydrate formation in separation processes: A review of experimental studies. *J. Chem. Thermodyn.* **46**, 62-71.

Frost, E. M., Jr., and Deaton, W. M. (1946). Gas hydrate composition and equilibrium data. *Oil Gas J.* **45**, 170-8.

Gaudette, J., and Servio, P. (2007). Measurement of Dissolved Propane in Water in the Presence of Gas Hydrate. *Journal of Chemical & Engineering Data* **52**, 1449-1451.

Gudmundsson. J.S. and Borrehang, A. (1996). Available from http://www.ipt.ntnu.no/~ngh/library/paper2.html

Gupta, A. K., Bishnoi, P. R., and Kalogerakis, N. (1991). A method for the simultaneous phase equilibria and stability calculations for multiphase reacting and nonreacting systems. *Fluid Phase Equilib.* **63**, 65-89.

Hammerschmidt, E. G. (1934). Formation of gas hydrates in natural gas transmission lines. *Ind. Eng. Chem.* **26**, 851-5.

Handa, Y. P. (1990). Effect of hydrostatic pressure and salinity on the stability of gas hydrates. *The Journal of Physical Chemistry* **94**, 2652-2657.

Harrison, W. J., Wendlandt, R. F., and Dendy Sloan, E. (1995). Geochemical interactions resulting from carbon dioxide disposal on the seafloor. *Applied Geochemistry* **10**, 461-475.

Hashemi, S., Macchi, A., Bergeron, S., and Servio, P. (2006). Prediction of methane and carbon dioxide solubility in water in the presence of hydrate. *Fluid Phase Equilib.* **246**, 131-136.

Hashemi, S., Macchi, A., and Servio, P. (2007). Gas Hydrate Growth Model in a Semibatch Stirred Tank Reactor. *Industrial & Engineering Chemistry Research* **46**, 5907-5912.

Hendriks, E. M., Edmonds, B., Moorwood, R. A. S., and Szczepanski, R. (1996). Hydrate structure stability in simple and mixed hydrates. *Fluid Phase Equilib.* **117**, 193-200.

Henry, P., Thomas, M., and Clennell, M. B. (1999). Formation of natural gas hydrates in marine sediments: 2. Thermodynamic calculations of stability conditions in porous sediments. *Journal of Geophysical Research: Solid Earth* **104**, 23005-23022.

Herri, J. M., Bouchemoua, A., Kwaterski, M., Fezoua, A., Ouabbas, Y., and Cameirao, A. (2011). Gas hydrate equilibria for CO2–N2 and CO2–CH4 gas mixtures—Experimental studies and thermodynamic modelling. *Fluid Phase Equilibria* **301**, 171-190.

Holder, G. D., Corbin, G., and Papadopoulos, K. D. (1980). Thermodynamic and molecular properties of gas hydrates from mixtures containing methane, argon, and krypton. *Industrial and Engineering Chemistry Fundamentals* **19**, 282-286.

Holder, G. D., and Hand, J. H. (1982). Multiple-phase equilibria in hydrates from methane, ethane, propane and water mixtures. *AIChE Journal* **28**, 440-447.

Holder, G. D., and Manganiello, D. J. (1982). Hydrate dissociation pressure minima in multicomponent systems. *Chemical Engineering Science* **37**, 9-16.
Horvat, K., Kerkar, P., Jones, K., and Mahajan, D. (2012). Kinetics of the formation and dissociation of gas hydrates from CO2-CH4 mixtures. *Energies* **5**, 2248-2262.
Jacobson, L. C., Hujo, W., and Molinero, V. (2010). Nucleation Pathways of Clathrate Hydrates: Effect of Guest Size and Solubility. *The Journal of Physical Chemistry B* **114**, 13796-13807.
Jeffrey, G. A. (1984). Hydrate inclusion compounds. Vol. 1, pp. 135-90. Academic.
Kane, S. G., Evans, T. W., Brian, P. L. T., and Sarofim, A. F. (1974). Determination of the kinetics of secondary nucleation in batch crystallizers. *AIChE Journal* **20**, 855-862.
Kang, S.-P., and Lee, H. (2000). Recovery of CO2 from Flue Gas Using Gas Hydrate: Thermodynamic Verification through Phase Equilibrium Measurements. *Environ. Sci. Technol.* **34**, 4397-4400.
Karaaslan, U., and Parlaktuna, M. (2002). A New Hydrate Inhibitor Polymer. *Energy Fuels* **16**, 1387-1391.
Kim, Y. S., Ryu, S. K., Yang, S. O., and Lee, C. S. (2003). Liquid Water−Hydrate Equilibrium Measurements and Unified Predictions of Hydrate-Containing Phase Equilibria for Methane, Ethane, Propane, and Their Mixtures. *Industrial & Engineering Chemistry Research* **42**, 2409-2414.
Koh, C. A., Sloan, E. D., Sum, A. K., and Wu, D. T. (2011). Fundamentals and applications of gas hydrates. *Annual review of chemical and biomolecular engineering* **2**, 237-57.
Koh, C. A., Westacott, R. E., Zhang, W., Hirachand, K., Creek, J. L., and Soper, A. K. (2002). Mechanisms of gas hydrate formation and inhibition. *Fluid Phase Equilibria* **194–197**, 143-151.
Kontogeorgis, G. M., Folas, G. K., Muro-Suñé, N., von Solms, N., Michelsen, M. L., and Stenby, E. H. (2007). Modelling of associating mixtures for applications in the oil & gas and chemical industries. *Fluid Phase Equilibria* **261**, 205-211.
Kvenvolden, K. A. (1988). Methane hydrate. A major reservoir of carbon in the shallow geosphere? *Chem. Geol.* **71**, 41-51.
Kwon, M., Lee, J.-W., and Lee, H. (2014). Temperature-Dependent Structural Transitions in Methane-Ethane Mixed Gas Hydrates. *J. Phys. Chem. C* **118**, 28906-28913.
Lang, F., and Servio, P. (2014). Solubility Measurements for the N2 + CO2 + H2O System under Hydrate-Liquid-Vapor Equilibrium. *J. Chem. Eng. Data* **59**, 2547-2550.
Lee, H., Seo, Y., Seo, Y.-T., Moudrakovski, I. L., and Ripmeester, J. A. (2003). Recovering methane from solid methane hydrate with carbon dioxide. *Angew. Chem., Int. Ed.* **42**, 5048-5051.
Lekvam, K., and Bishnoi, P. R. (1997). Dissolution of methane in water at low temperatures and intermediate pressures. *Fluid Phase Equilibria* **131**, 297-309.

Li, X. S., Wu, H. J., Li, Y. G., Feng, Z. P., Tang, L. G., and Fan, S. S. (2007). Hydrate dissociation conditions for gas mixtures containing carbon dioxide, hydrogen, hydrogen sulfide, nitrogen, and hydrocarbons using SAFT. *The Journal of Chemical Thermodynamics* **39**, 417-425.

Linga, P., Kumar, R., and Englezos, P. (2007). Gas hydrate formation from hydrogen/carbon dioxide and nitrogen/carbon dioxide gas mixtures. *Chem. Eng. Sci.* **62**, 4268-4276.

Lu, W., Chou, I. M., and Burruss, R. C. (2008). Determination of methane concentrations in water in equilibrium with sI methane hydrate in the absence of a vapor phase by in situ Raman spectroscopy. *Geochimica et Cosmochimica Acta* **72**, 412-422.

Lundgaard, L., and Mollerup, J. M. (1991). The influence of gas phase fugacity and solubility on correlation of gas-hydrate formation pressure. *Fluid Phase Equilib.* **70**, 199-213.

Makogon, Y. F. (1965). Hydrate Formation in the Gas-Bearing Beds Under Permafrost Conditions. *Gazovaia Promyshlennost* **5**, 14-15.

Makogon, Y. F. (1988). Natural gas hydrates - the state of study in the U.S.S.R. and perspective for its use. Third Chemical Congress of North America, Toronto, Ont. June 5-10.

Makogon, Y. F. (2010). Natural gas hydrates - a promising source of energy. *J. Nat. Gas Sci. Eng.* **2**, 49-59.

Maslin, M., Owen, M., Betts, R., Day, S., Jones, T. D., and Ridgwell, A. (2010). Gas hydrates: past and future geohazard? *Philos. Trans. R. Soc., A* **368**, 2369-2393.

Michelsen, M. L., and Mollerup, J. (2007). "Thermodynamic Models: Fundamentals and Computational Aspects," 2nd/Ed. Tie-Line Publications.

Mork, M., and Gudmundsson, J. S. (2002). Hydrate formation rate in a continous stirred tank reactor - experimental results and bubble-to-crystal model. *4th International Conference on Gas Hydrates - Yokohama*, 813-818.

Mullin, J. W. (2001). "Crystallization," Butterworth-Heinemann, Oxford; Boston.

Nagata, I., and Kobayashi, R. (1966). Prediction of Dissociation Pressures of Mixed Gas Hydrates from Data for Hydrates of Pure Gases with Water. *Industrial & Engineering Chemistry Fundamentals* **5**, 466-469.

Natarajan, V., Bishnoi, P. R., and Kalogerakis, N. (1994). Induction phenomena in gas hydrate nucleation. *Chem. Eng. Sci.* **49**, 2075-87.

Ohno, H., Strobel, T. A., Dec, S. F., Sloan, E. D., Jr., and Koh, C. A. (2009). Raman Studies of Methane-Ethane Hydrate Metastability. *J. Phys. Chem. A* **113**, 1711-1716.

Park, J., Seo, Y.-T., Lee, J.-w., and Lee, H. (2006a). Spectroscopic analysis of carbon dioxide and nitrogen mixed gas hydrates in silica gel for CO2 separation. *Catalysis Today* **115**, 279-282.

Park, Y., Kim, D.-Y., Lee, J.-W., Huh, D.-G., Park, K.-P., Lee, J., and Lee, H. (2006b). Sequestering carbon dioxide into complex structures of naturally occurring gas hydrates. *Proc. Natl. Acad. Sci. U. S. A.* **103**, 12690-12694.

Parrish, W. R., and Prausnitz, J. M. (1972). Dissociation Pressures of Gas Hydrates Formed by Gas Mixtures. *Industrial & Engineering Chemistry Process Design and Development* **11**, 26-35.
Parshall, J. (2012). Production Method for Methane Hydrate Sees Scientific Sucess. *Journal of Petroleum Technology* **64**, 50-51.
Patel, N. C., and Teja, A. S. (1982). A new cubic equation of state for fluids and fluid mixtures. *Chemical Engineering Science* **37**, 463-473.
Pellenbarg, R. E., and Max, M. D. (2000). Introduction, Physical Properties, and Natural Occurrences of Hydrate. *In* "Natural Gas Hydrate in Oceanic and Permaforst Environments", pp. 1-8. Kluwer Academic Publishers, Dordrecht.
Peng, D.-Y., and Robinson, D. B. (1976). A new two-constant equation of state. *Ind. Eng. Chem., Fundam.* **15**, 59-64.
Renault-Crispo, J.-S., Lang, F., and Servio, P. (2014). The importance of liquid phase compositions in gas hydrate modeling: Carbon dioxide-methane-water case study. *J. Chem. Thermodyn.* **68**, 153-160.
Ripmeester, J. A., Tse, J. S., Ratcliffe, C. I., and Powell, B. M. (1987). A new clathrate hydrate structure. *Nature* **325**, 135-136.
Rovetto, L. J., Dec, S. F., Koh, C. A., & Sloan E. D. (2008). NMR studies on CH4 + CO2 binary gas hydrates dissociation behavior. *In* "6th International Conference on Gas Hydrates", Vancouver, British Columbia, Canada.
Sage, B. H., and Lacey, W. N. (1934). Phase Equilibria in Hydrocarbon Systems I Methods and Apparatus. *Industrial & Engineering Chemistry* **26**, 103-106.
Seo, Y., Lee, H., and Ryu, B.-J. (2002). Hydration number and two-phase equilibria of CH4 hydrate in the deep ocean sediments. *Geophysical Research Letters* **29**, 85-1-85-4.
Seo, Y.-T., Kang, S.-P., Lee, H., Lee, C.-S., and Sung, W.-M. (2000). Hydrate phase equilibria for gas mixtures containing carbon dioxide: A proof-of-concept to carbon dioxide recovery from multicomponent gas stream. *Korean Journal of Chemical Engineering* **17**, 659-667.
Seo, Y.-T., and Lee, H. (2001). Multiple-Phase Hydrate Equilibria of the Ternary Carbon Dioxide, Methane, and Water Mixtures. *J. Phys. Chem. B* **105**, 10084-10090.
Seo, Y.-T., and Lee, H. (2003). Structure and Guest Distribution of the Mixed Carbon Dioxide and Nitrogen Hydrates As Revealed by X-ray Diffraction and 13C NMR Spectroscopy. *The Journal of Physical Chemistry B* **108**, 530-534.
Servio, P., and Englezos, P. (2001). Effect of temperature and pressure on the solubility of carbon dioxide in water in the presence of gas hydrate. *Fluid Phase Equilib.* **190**, 127-134.
Servio, P., and Englezos, P. (2002). Measurement of Dissolved Methane in Water in Equilibrium with Its Hydrate. *J. Chem. Eng. Data* **47**, 87-90.
Skovborg, P., and Rasmussen, P. (1994). A mass transport limited model for the growth of methane and ethane gas hydrates. *Chem. Eng. Sci.* **49**, 1131-43.
Sloan, E. D. (1998). "Clathrate Hydrates of Natural Gases," Marcel Dekker, New York.

Sloan, E. D. (2003). Fundamental principles and applications of natural gas hydrates. *Nature* **426**, 353-363.
Sloan, E. D., and Koh, C. A. (2008). "Clathrate hydrates of natural gases," CRC Press, Boca Raton, FL.
Soave, G. (1972). Equilibrium constants from a modified Redlich-Kwong equation of state. *Chemical Engineering Science* **27**, 1197-1203.
Someya, S., Bando, S., Chen, B., Song, Y., and Nishio, M. (2005). Measurement of CO2 solubility in pure water and the pressure effect on it in the presence of clathrate hydrate. *International Journal of Heat and Mass Transfer* **48**, 2503-2507.
Song, K. Y., Feneyrou, G., Fleyfel, F., Martin, R., Lievois, J., and Kobayashi, R. (1997). Solubility measurements of methane and ethane in water at and near hydrate conditions. *Fluid Phase Equilib.* **128**, 249-260.
Subramanian, S., Kini, R. A., Dec, S. F., and Sloan, E. D., Jr. (2000). Evidence of structure II hydrate formation from methane + ethane mixtures. *Chem. Eng. Sci.* **55**, 1981-1999.
Taylor, F. W. (1991). The greenhouse effect and climate change. *Reports on Progress in Physics* **54**, 881-918.
Teja, A. S., and Patel, N. C. (1981). The applications of a generalized equation of state to the correlation and prediction of phase equilibria. *Chemical Engineering Communications* **13**, 39-53.
Tester, J. W. M. M. (1997). "Thermodynamics and its applications," Prentice Hall PTR, Upper Saddle River, N.J.
Thomas, S. (2003). Review of ways to transport natural gas energy from countries which do not need the gas for domestic use. *Energy Energy* **28**, 1461-1477.
Thomas, S., and Dawe, R. A. (2003). Review of ways to transport natural gas energy from countries which do not need the gas for domestic use. *Energy (Amsterdam, Neth.)* **28**, 1461-1477.
Trebble, M. A., and Bishnoi, P. R. (1987). Development of a new four-parameter cubic equation of state. *Fluid Phase Equilib.* **35**, 1-18.
Trebble, M. A., and Bishnoi, P. R. (1988). Extension of the Trebble-Bishnoi equation of state to fluid mixtures. *Fluid Phase Equilib.* **40**, 1-21.
Uchida, T., Ikeda, I. Y., Takeya, S., Kamata, Y., Ohmura, R., Nagao, J., Zatsepina, O. Y., and Buffett, B. A. (2005). Kinetics and Stability of CH4–CO2 Mixed Gas Hydrates during Formation and Long-Term Storage. *ChemPhysChem* **6**, 646-654.
Uchida, T., Takagi, A., Mae, S., and Kawabata, J. (1997). Dissolution mechanisms of CO2 molecules in water containing CO2 hydrates. *Energy Conversion and Management* **38, Supplement**, S307-S312.
Uchida, T., Takeya, S., Kamata, Y., Ikeda, I. Y., Nagao, J., Ebinuma, T., Narita, H., Zatsepina, O., and Buffett, B. A. (2002). Spectroscopic Observations and Thermodynamic Calculations on Clathrate Hydrates of Mixed Gas Containing Methane and Ethane: Determination of Structure, Composition and Cage Occupancy. *J. Phys. Chem. B* **106**, 12426-12431.

Valderrama, J. O. (1990). A generalized Patel-Teja equation of state for polar and nonpolar fluids and their mixtures. *J. Chem. Eng. Japan / JCEJ JOURNAL OF CHEMICAL ENGINEERING OF JAPAN* **23**, 87-91.

Van Denderen, M., Ineke, E., and Golombok, M. (2009). CO2 removal from contaminated natural gas mixtures by hydrate formation. *Industrial and Engineering Chemistry Research* **48**, 5802-5807.

van der Waals, J. H., and Plawtteeuw, J. C. (1959). Clathrate Solutions. *Advances in Chemical Physics* **2**, 1-55.

Vysniauskas, A., and Bishnoi, P. R. (1983). A kinetic study of methane hydrate formation. *Chem. Eng. Sci.* **38**, 1061-72.

Yamasaki, A., Wakatsuki, M., Teng, H., Yanagisawa, Y., and Yamada, K. (2000). A new ocean disposal scenario for anthropogenic CO2: CO2 hydrate formation in a submerged crystallizer and its disposal. *Energy (Oxford)* **25**, 85-96.

Yang, S. O., Cho, S. H., Lee, H., and Lee, C. S. (2001). Measurement and prediction of phase equilibria for water + methane in hydrate forming conditions. *Fluid Phase Equilibria* **185**, 53-63.

Yang, S. O., Yang, I. M., Kim, Y. S., and Lee, C. S. (2000). Measurement and prediction of phase equilibria for water+CO2 in hydrate forming conditions. *Fluid Phase Equilibria* **175**, 75-89.